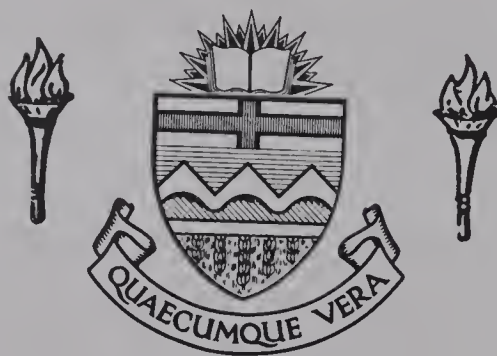


For Reference

NOT TO BE TAKEN FROM THIS ROOM

Ex LIBRIS
UNIVERSITATIS
ALBERTAENSIS



High Level

BOOK BINDERY LTD.

10372 - 60 Ave., Edmonton

"THE HIGHEST LEVEL OF
CRAFTSMANSHIP"

THE UNIVERSITY OF ALBERTA

ORIFICE FLOWS OF FIBRE SUSPENSIONS

by



THADDEUS EUGENE KIZIOR

A THESIS

SUBMITTED TO THE FACULTY OF GRADUATE STUDIES AND RESEARCH

IN PARTIAL FULFILMENT OF THE REQUIREMENTS

FOR THE DEGREE OF MASTER OF SCIENCE

IN CHEMICAL ENGINEERING

DEPARTMENT OF CHEMICAL AND PETROLEUM ENGINEERING

EDMONTON, ALBERTA

SPRING, 1972

Thesis
1972
72

UNIVERSITY OF ALBERTA
FACULTY OF GRADUATE STUDIES AND RESEARCH

The undersigned certify that they have read, and recommend to the Faculty of Graduate Studies and Research for acceptance a thesis entitled "Orifice Flows of Fibre Suspensions" submitted by Thaddeus Eugene Kizior in partial fulfilment of the requirements for the degree of Master of Science in Chemical Engineering.

ABSTRACT

The utility of simple particle suspensions in modelling complex fluids has motivated considerable study in fundamental suspension behaviour. Unfortunately, most of these studies have been restricted to examining suspension behaviour in simple shear flows, neglecting the behaviour in extensional flows.

The orifice jet thrust technique was used to experimentally investigate the behaviour of fibre suspensions in extensional flows. Fibres with axis ratios of 85 to 340 were suspended in 60% and 66-2/3% sugar solutions at concentration levels of 0.1% and 0.2%. Thrust reduction was observed for suspensions with shear viscosities similar to the shear viscosity of the suspending medium. The thrust reduction, which may be viewed as an increase in elongational viscosity, became more pronounced with increasing axis ratio and/or fibre concentration as predicted by the specific elongational viscosity theory of Takserman-Krozer and Ziabicki.

An unusual behaviour, indicated by apparently steady-state pressure and thrust readings suddenly changing to new steady-state readings, was observed during some of the experiments. This occurred for both the suspensions and the Newtonian suspending medium.

ACKNOWLEDGEMENTS

I wish to express my gratitude and appreciation to:

- The National Research Council of Canada for the financial support which made this study possible,
- Dr. F. A. Seyer for his capable guidance and assistance,
- Dr. B. Hlavacek for his assistance with the theory and the interpretation of the results,
- the staff of the Chemical and Petroleum Shops for their assistance in building the equipment,
- my colleagues for their helpful suggestions,
- Mrs. Betty Boon for the excellent typing.

I am especially grateful to my wife, Sylvia, for her understanding and moral support.

TABLE OF CONTENTS

	Page
ABSTRACT	i
LIST OF TABLES	v
LIST OF FIGURES	vii
NOMENCLATURE	ix
I INTRODUCTION	
1.1 General	1
1.2 Rheological Properties of Elongated Particle Suspensions	3
1.2.1 Viscous Behaviour	3
1.2.2 Elastic Behaviour	7
1.2.3 Behaviour of Elongated Particle Suspensions in Extensional Flows	9
II THEORY	
2.1 General	14
2.2 Orifice Jet Thrust Measurements	16
2.2.1 Kinematics of Orifice Flows	16
2.2.2 Analysis of Orifice Jet Thrust	22
III EXPERIMENTAL EQUIPMENT AND PROCEDURE	
3.1 General	27
3.2 Experimental Apparatus	27
3.2.1 Spring System	27
3.2.2 Orifice Plate and Reservoir	32
3.2.3 Transducers and Mountings	33
3.2.4 Pumps	35

	Page
3.2.5 Experimental Fluids	36
3.3 Experimental Procedure	39
3.3.1 Suspension Preparation	39
3.3.2 Calibration	39
3.3.3 Data Collection	41
IV DISCUSSION OF RESULTS	
4.1 Viscoelastic Behaviour	42
4.2 Newtonian Behaviour	42
4.3 Fibre Suspension Behaviour	48
4.3.1 Thrust Measurements	48
4.3.2 Prediction of Elongational Viscosity	59
4.4 Unusual Behaviour	64
V CONCLUSIONS AND RECOMMENDATIONS	
5.1 Conclusions	67
5.2 Recommendations	68
BIBLIOGRAPHY	71
APPENDICES	
A Calibrations	
B Thrust Measurements	
C Sample Calculations and Least-Squares Fits	
D Elongational Viscosity Calculations	

LIST OF TABLES

	Page
1.1 Influence of Fibre Flexibility on Viscosity Behaviour	6
3.1 Experimental Fluids	37
A-1 Zenith Pump Flowrate Calibration	A-2
A-2 Instron Flowrate Calibration	A-4
A-3 Pressure Transducer Calibration	A-6
A-4 Pressure Transducer Calibration	A-7
A-5 Thrust Calibration for Test No. 1	A-15
A-6 Thrust Calibration for Test No. 2	A-16
A-7 Thrust Calibration for Test No. 3	A-17
A-8 Thrust Calibration for Test No. 4	A-18
A-9 Thrust Calibration for Test No. 5	A-19
A-10 Thrust Calibration for Test No. 6	A-20
A-11 Thrust Calibration for Test No. 7	A-21
A-12 Thrust Calibration for Test No. 8	A-22
A-13 Thrust Calibration for Test No. 9	A-23
A-14 Thrust Calibration for Test No. 10	A-24
A-15 Thrust Calibration for Test No. 11	A-25
A-16 Thrust Calibration for Test No. 12	A-26
A-17 Thrust Calibration for Test No. 13	A-27
A-18 Thrust Calibration for Test No. 14	A-28
A-19 Thrust Calibration for Test No. 14	A-29
A-20 Thrust Calibration for Test No. 15	A-30
A-21 Thrust Calibration for Test No. 16	A-31

	Page
B-1 Results for Test No. 1	B-2
B-2 Results for Test No. 2	B-3
B-3 Results for Test No. 3	B-4
B-4 Results for Test No. 4	B-5
B-5 Results for Test No. 5	B-6
B-6 Results for Test No. 6	B-7
B-7 Results for Test No. 7	B-8
B-8 Results for Test No. 8	B-9
B-9 Results for Test No. 9	B-10
B-10 Results for Test No. 10	B-11
B-11 Results for Test No. 11	B-12
B-12 Results for Test No. 12	B-13
B-13 Results for Test No. 13	B-14
B-14 Results for Test No. 14	B-15
B-15 Results for Test No. 15	B-17
B-16 Results for Test No. 16	B-19
D-1 Least-Squares Coefficients of Reliable Thrust-Velocity Data	D-5
D-2 "Representative" and Theoretical Elongational Viscosities	D-6

LIST OF FIGURES

	Page
1.1 Elongational Viscosity Behaviour of Elongated Ellipsoids	11
2.1 Velocity Field for Viscoelastic Flow Through an Orifice	17
2.2 Velocity Field for Newtonian Flow Through an Orifice	21
3.1 Schematic of Experimental Apparatus	28
3.2 Top View of Thrust Device	29
3.3 Side View of Undercarriage of Spring Table	30
3.4 Schematic of Pressure Transducer Hook-Up	34
4.1 Thrust-Velocity Curves for Water, Separan AP30 Solutions and the Most "Elastic" Suspension	43
4.2 Thrust-Velocity Curves for Water and Sugar Solutions	44
4.3 Normalized Thrust for Tests 12 and 15	47
4.4 Normalized Thrust for Tests 9 and 16	50
4.5 Normalized Thrust for Test 10	51
4.6 Normalized Thrust for Test 11	52
4.7 Normalized Thrust for Test 13	53
4.8 Normalized Thrust for Test 14	54
4.9 Normalized Thrust for Test 3	55
4.10 Effect of AR on $\langle TN \rangle$	57
4.11 Effect of C on $\langle TN \rangle$	58
4.12 Comparison of Contraction Coefficients	60
4.13 Comparison of Theoretical and "Representative" Elongational Viscosities	63
4.14 Typical Recorder Trace of "Unusual Behaviour"	65

	Page
A-1 Zenith Gear Pump Flowrate Calibration	A-3
A-3 Pressure Transducer Calibration	A-8
A-4 Pressure Transducer Calibration	A-9
A-5 Pressure Transducer Calibration	A-10
A-6 Thrust Calibration Scheme	A-12
C-1 Unconstrained Representation of Test 13	C-7
C-2 Constrained Representation of Test 13	C-8

NOMENCLATURE

a_i	arbitrary constant
A	coefficient vector of a_i
A_2	cross-sectional area of a well-developed jet
AR	axis ratio of a particle defined as the ratio of particle length to particle diameter
B	least-squares coefficient defined by Equation (A-6)
C	fibre concentration
C_c	contraction coefficient defined by Equation (C-1)
d	particle diameter
d_{ij}	deformation rate tensor
D	rotational diffusion constant defined by Equation (D-1)
H	length of hypotenuse in force triangle defined in Appendix A
k	constant defined by Equation (2.2.12)
k_1, k_2	functions defined by Equation (2.2.13)
k'_1, k'_2	functions defined by Equation (2.2.14)
$[k_1], [k_2]$	least-squares coefficients defined by Equation (4.2.1)
$[k'_1], [k'_2]$	least-squares coefficients defined by Equation (4.2.3)
$[k'_{2R}]$	constrained least-squares coefficient defined by Equation (4.3.10)
K	parameter defined by Equations (D-4)
l	particle length
M	parameter defined by Equations (D-4)
n	number of arbitrary data points

N	parameter defined by Equations (D-4)
p	isotropic pressure
P	measured pressure
Q	volumetric flowrate
r	distance from apex of cone
R_o	orifice radius
S_{ij}	deviatoric stress tensor
T	thrust of orifice jet
T	absolute temperature
TN	normalized thrust defined by Equation (4.2.2)
$\langle TN \rangle$	averaged normalized thrust defined by Equation (4.2.3)
$\langle \frac{T}{\pi R_o^2} \rangle$	averaged thrust per unit orifice area defined by Equation (4.2.1)
\mathcal{V}	volume of one particle
v_i	instantaneous velocity component
V_2	average velocity of a well-developed jet
V_o	average velocity at the orifice
VP	recorder signal of pressure
$VSTAR$	variable defined by Equation (A-5)
VT	recorder signal of thrust
W	energy dissipated by a single particle in an extensional flow field
x	arbitrary independent variable
x_i	arbitrary data point
X	arbitrary matrix of the data points, x_i
y	arbitrary dependent variable

y_i	arbitrary data point
Y	arbitrary vector of the data points, y_i
z	arbitrary variable defined by Equation (C-5)

Greek Symbols

α	parameter defined by Equation (1.2.8)
α_0	particle orientation coefficient
α_1	particle interaction coefficient
$\bar{\alpha}_0', \bar{\alpha}_0'', \bar{\beta}_0', \bar{\beta}_0''$	parameters defined by Equations (D-5)
δ_{ij}	Kronecker delta
$\dot{\epsilon}$	elongational deformation rate
η	elongational viscosity of suspension
η_0	elongational viscosity of suspending medium
η_{sp}	specific elongational viscosity defined by Equation (1.2.6)
r	Boltzmann constant
λ	parameter defined by Equations (D-6)
μ	shear viscosity of suspension
μ_0	shear viscosity of suspending medium
μ_r	relative shear viscosity defined by Equation (1.2.1)
μ_{sp}	specific shear viscosity defined by Equation (1.2.4)
ν	intrinsic viscosity defined by Equation (1.2.9)
ρ	density
σ	parameter defined by Equations (D-6)
τ_{ij}	total stress tensor

CHAPTER I

INTRODUCTION

1.1 GENERAL

The rheological behaviour of solid-liquid suspensions has enjoyed considerable engineering interest in a wide variety of applications. One field of major importance involves pipeline transport of solids. Fairly recent endeavours involving suspensions are concerned with modelling of viscoelastic fluids (33,34,39,40) and of blood (15). An important property of many suspensions is the phenomenon of drag reduction in pipe flows. This phenomenon alone has promoted considerable investigation. An extensive review of this subject is presented by Kerekes (21) who also discusses the probable mechanisms for drag reduction in suspension flows.

The prime difficulty in the handling of suspensions has been in uniformly dispersing the solid particles (1,21). Since common industrial slurries involve some heavy particulate (such as sand) and a convenient suspending medium (such as water), sedimentation is an enormous problem. Even in cases where sedimentation is not a serious problem, as, for example, in wood pulp flows, plugging at constrictions is common. From an experimental point of view, since most rheological studies involve bulk measurements, particle coagulation (or concentration gradients) nullify the often necessary assumption of material homogeneity. In this context, it is not surprising that many rheological studies of suspensions have not been entirely successful.

Although drag reduction studies have been successful in terms of relating drag reduction to suspension properties, the mechanism of drag reduction has been a controversial subject (21). Basically, the controversy has been one of evaluating the importance of the elastic contribution to drag reduction. Resolution of this problem is complicated by a lack of sufficient knowledge on the elastic properties of suspensions. Clearly, a better understanding of this problem, and, in fact, many of the problems associated with drag reducing polymers (33,34,39,40) can, perhaps, be explained on the basis of the elastic behaviour of suspensions of relatively simple shapes (29,33,34,39,40).

A particular limitation of most rheological measurements is that extensional flows or "stretching" deformations of the material elements have largely been ignored (25). Rapid extensional deformations, which are often accompanied by shearing deformations, are widespread in practice; as, for example, in extrusion, rolling or pressing operations, and flows through contractions or around submerged objects (24). Metzner (24) points out that the extensional deformations in Newtonian flows contribute relatively minor resistance when compared to the resistances proffered by the shearing deformations. Viscoelastic materials, on the other hand, exhibit very large resistances to rapid stretching deformations (23,24, 25,26,37). Hence, it has been suggested explicitly by Metzner (24) and less explicitly by others (23,26,37) that rapid extensional flows of viscoelastic media may be approximated by considering only the stretching deformations and completely ignoring the shearing deformations. Significantly, this results in a tremendous

simplification in a number of important problems (24). In cases where slow extensional deformations prevail for viscoelastics, or rapid deformations occur in fluids of a low level of elasticity, it is expected that both stretching and shearing deformations must be considered in a complete analysis of the problem.

Although viscoelastic behaviour has been observed in shearing flows of fibrous suspensions (7,8,10,29), the elastic effect has generally been small (10) and complicated by time-dependence and/or network formation as well as particle migration away from a wall (10,29). Suspension behaviour in extensional flows has not yet been experimentally considered. The purpose of this study, therefore, is to experimentally consider the behaviour of fibre suspensions in extensional flows. This analysis will benefit from a brief discussion on the available rheological properties of homogeneous suspensions.

1.2 RHEOLOGICAL PROPERTIES OF ELONGATED PARTICLE SUSPENSIONS

1.2.1 Viscous Behaviour

Most rheological studies of suspensions have dealt specifically with determining shear viscosities. Predictive viscosity theories for suspensions of simple particle shapes have been given by, Einstein (11) for spheres, Jeffery (19) and Guth (29) for rigid ellipsoids and Burgers (29) for rigid ellipsoids and rigid cylinders. As noted by Blakney (6), all of these theories can be expressed by:

$$\mu_r = \frac{\mu}{\mu_0} = 1 + \alpha_0 C \quad (1.2.1)$$

where μ_r is the relative viscosity, μ the viscosity of the suspension, μ_0 the viscosity of the suspending medium, C the volumetric concentration of particles and α_0 a function of particle orientation. Agreement with experiment has been good for all particle shapes so long as they are non-deformable (29) and very dilute (6).

Experimentally, it has been found that the linear viscosity function given by Equation (1.2.1) no longer applies when a critical concentration limit has been reached. This critical limit has been defined by Mason (10) such that for

$$C(AR)^2 < 1.5 \quad (1.2.2)$$

where AR is the axis ratio of the particle (ratio of length to diameter), particle interactions are negligible. The limit given in Equation (1.2.2) is defined by the minimum swept out volume required by a rotating elongated particle (21). Beyond this limit, the dependence of viscosity on concentration and particle properties is quite complex. However, three broad categories based on fibre aggregation have been proposed (10,21):

- i) dilute region where single particles are free to rotate at will and any collisions are random,
- ii) critical concentration region where particle-particle collisions are numerous, but network formation is almost entirely absent,
- iii) concentrated region where particle-particle contact is so prevalent that a more or less continuous network is formed.

In the concentrated region, the suspension exhibits distinct non-Newtonian properties.

Viscosity measurements for rods in the critical concentration region have been substantial (6,7,8,21,29), but attempts to correlate these measurements by a 2-parameter equation have had limited success (29). The 2-parameter viscosity equation is given by

$$\left(\frac{\mu_{sp}}{C}\right) = \alpha_0 + \alpha_1 C \quad (1.2.3)$$

where

$$\mu_{sp} = \left(\frac{\mu - \mu_0}{\mu}\right) C \rightarrow 0 \quad (1.2.4)$$

α_1 is defined as the particle interaction coefficient and μ_{sp} is the specific viscosity. Nawab and Mason (29) found that Equation (1.2.3) could be successfully used to correlate experimental data so long as the particles remained rigid. Their study is of particular importance since they found that fibre suspensions began to exhibit a shear-thinning behaviour when fibre deformations became apparent. A qualitative summary of the observations of Nawab and Mason (29) is given in Table (1.1). It should be noted that the available viscosity data for suspensions are, generally, from a rheological standpoint, limited due to the narrow range of shear rates studied.

Concentrated suspensions have escaped reliable viscosity determination due to their "unusual" behaviour of time dependence and particle migration (10,21,29). As a result, the most successful measurements involving these suspensions have been non-rheological;

TABLE 1.1

INFLUENCE OF FIBRE FLEXIBILITY ON VISCOSITY BEHAVIOUR

<u>AR</u>	<u>C (vol %)</u>	<u>Fibre Behaviour in Rotation</u>	<u>Viscosity Behaviour</u>	<u>Other Remarks</u>
43.2	0.467-1.34	rigid, straight	Newtonian	
75	0.305-0.895	rigid, straight	Newtonian	
113	0.203-0.570	rigid, some fibres curved	Newtonian	
173	0.222-0.473	large fraction curved, slight springiness	slightly shear- thinning	Weissenburg Effect first noticed
240	0.077-0.177	large fraction curved, increased springiness	i) more pronounced shear-thinning ii) slightly time dependent	More pronounced Weissenburg Effect
356	0.048-0.163	large fraction curved, springy and flexible rotations	pronounced shear- thinning and time dependence	Pronounced Weissenburg Effect increasing with time

for example, head-flow studies. Bugliarello and Daily (8) discuss, in detail, the behaviour of "network" suspensions and conclude that present continuum models do not adequately describe concentrated suspension behaviour.

1.2.2 Elastic Behaviour

The two-phase approach to molecular theories on viscoelastic behaviour are based on the "deformability" of a macromolecular system. Elastic properties in the whole fluid can be related to the deformation and subsequent restoration forces of a macromolecular system. The macromolecule has been considered from basically two points of view:

i) Simple particle approach

The fluid is considered as a suspension of simple-shaped, elastically deformable particles. When the fluid is subject to a stress, the particles deform and orient themselves in such a way that the elastic forces in the particles and the forces originating from the orientation of deforming particles in the suspending medium, will come to equilibrium with the external stress. The bulk elastic properties of the whole fluid can be described in terms of the restoration forces within the particles and their subsequent re-orientation (12,13,33).

ii) Complex particle approach

The fluid is considered as a suspension of complex, chain-like particles. When the fluid is at rest, the orientation of the particles, though physically unknown, can be related to an

equilibrium of the intermolecular and intramolecular forces and the random forces of Brownian motion. This relation gives an "average" orientation. When the fluid is subject to a stress, the change in the "average" orientation can be predicted on the basis of the nature of the stress. The bulk elastic properties of the whole fluid can be described in terms of the change in orientation of the macromolecular chain (27,39,40). The restoration forces are considered to be those of brownian motion (18).

Although the relative merits of the two approaches outlined above are beyond the scope of this study, the principles involved may be useful in providing an explanation for the origin of elasticity. Both simple particle and complex particle approaches consider an increase in resistance to a stress due to the presence of particles. This increase in resistance can be regarded effectively as an increase in fluid viscosity and is, by necessity, present in any suspension, elastic or not. The elastic properties of the fluid, on the other hand, arise from the restoration forces which are a consequence of an elastic deformation. At this point, it is not important whether the restoration forces are pre-defined (simple particle approach) or related to Brownian motion (complex particle approach) only that they are not negligible when compared to the viscous forces. It is apparent that the fluid will exhibit only a viscous response to a deformation if the restoration forces are comparatively small

Application of the simple particle approach to a dilute suspension of fibres appears to be reasonable enough since fibres are

relatively simple particles. Nawab and Mason (29) indicated qualitative experimental support to this approach by observing the "Weissenberg Effect" in Couette flows of deformable fibres (see Table 1.1).

Although the "Weissenberg Effect" did not occur until fibre deformations became apparent, the particles were concentrated enough to form networks so that it was not possible to attribute the elasticity solely to the recoverable deformation of single particles. Indeed, the elastic counter-rotation observed by Bugliarello and Daily (8) was directly attributed to a "network relaxation" effect. Also, the available data on normal stresses developed in shear flows of fairly concentrated suspensions (10) have shown the elastic effects to be small. These observations are consistent with the complex particle approach in suggesting low levels of elasticity due to the minor importance of Brownian motion on large particles. In summary, the elastic effects exhibited by fibre suspensions in simple shear flows are generally small and may be of little importance in practical situations. The larger effects expected in stretching deformations clearly underline the importance of extensional flows.

1.2.3 Behaviour of Elongated Particle Suspensions in Extensional Flows

Recently, Takserman-Krozer and Ziabicki (39,40) analyzed, theoretically, the behaviour of rigid ellipsoids in a parallel velocity gradient (extensional flow). This analysis, which may represent a viscoelastic model in steady extensional flows, led to the definition of a specific elongational viscosity

$$\eta_{sp} = \left(\frac{C}{\dot{\epsilon}^2 \eta_0 \bar{v}} \right) \left(\overline{\frac{dW}{dt}} \right) \quad (1.2.5)$$

where

$$\eta_{sp} = \frac{\eta - \eta_0}{\eta_0} \quad (1.2.6)$$

η is the elongational viscosity of the suspension, η_0 the elongational viscosity of the suspending medium, C the volumetric concentration of ellipsoids, $\dot{\epsilon}$ the elongational deformation rate, \bar{v} the volume of one ellipsoid and $\left(\overline{\frac{dW}{dt}} \right)$ the average rate of energy dissipation per particle, which is determined from

$$\left(\overline{\frac{dW}{dt}} \right) = f(AR, \alpha, \eta_0) \quad (1.2.7)$$

where

$$\alpha = \frac{\dot{\epsilon}}{D} \quad (1.2.8)$$

and D is the rotational diffusion constant (34). The intrinsic elongational viscosity, ν , defined by

$$\nu = \left(\frac{\eta_{sp}}{C} \right)_{C \rightarrow 0} \quad (1.2.9)$$

and, for elongated ellipsoids, is depicted in Figure (1.1) as a function of AR with α as a parameter. The limiting cases defined by $\alpha = 0$ and $\alpha = \infty$ are physically attributable to particle orientation in an extensional flow field. In the case of $\alpha = 0$, the particles retain a completely random orientation throughout the flow field as a

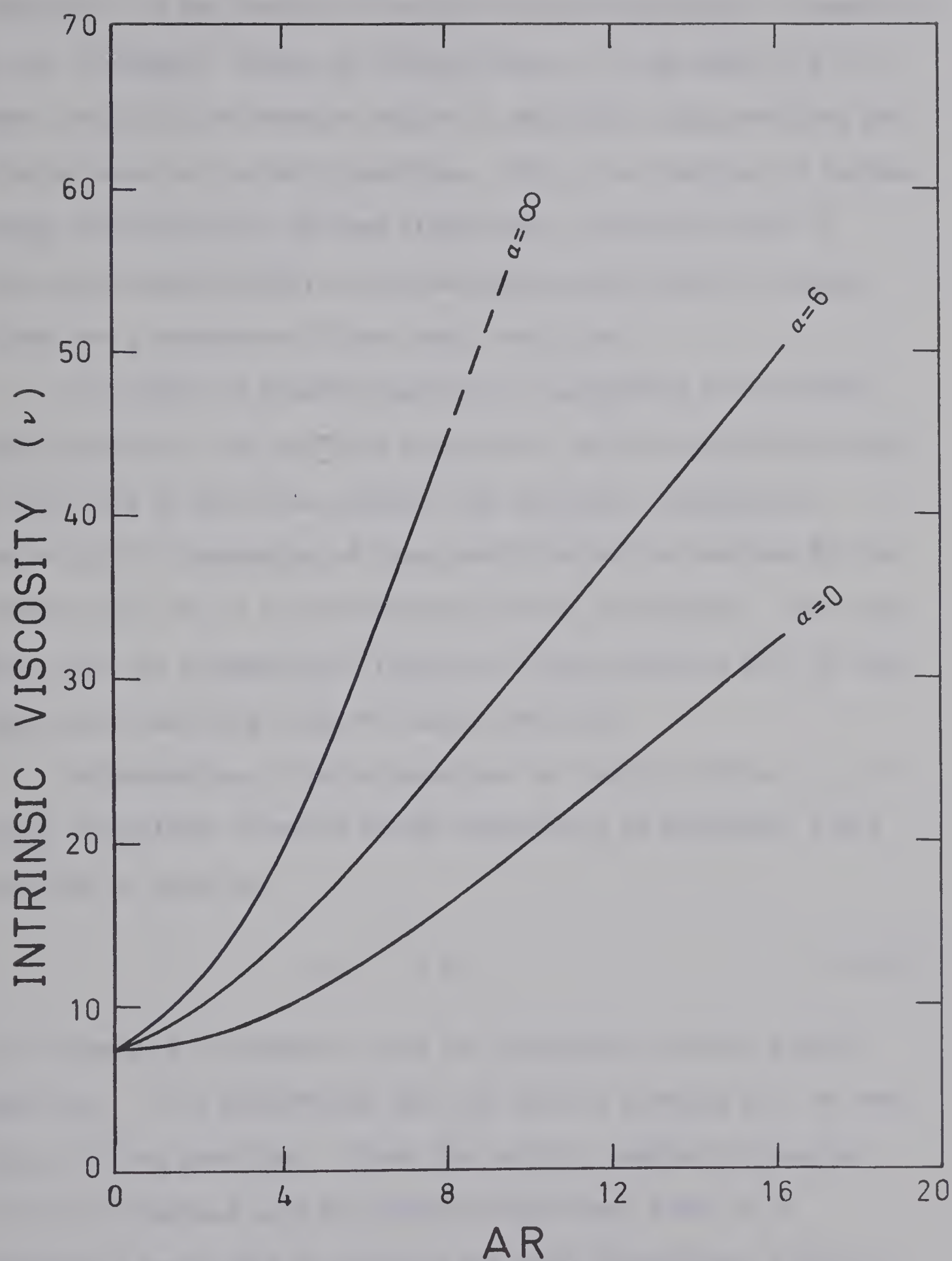


FIGURE (1.1) ELONGATIONAL VISCOSITY
BEHAVIOUR OF ELONGATED
ELLIPSOIDS

consequence of the forces of Brownian motion being large in comparison to the alignment forces of the flow field. In the case of $\alpha = \infty$, where the effect of brownian motion is negligible, the particles are oriented parallel to the streamlines. This is a condition of maximum energy dissipation (or maximum elongational viscosity) which is approached asymptotically as the deformation rate tends to large values for a suspension of very small particles.

The effect of brownian motion on a suspension of relatively large particles, such as fibre suspensions, will be negligible except in the limit of zero flow. Hence, the intrinsic elongational viscosity of a suspension of large particles will be defined by the limiting case of $\alpha = \infty$ for extensional flows of interest. This suggests that the elongational viscosity of long particles will be very high, but essentially free of elastic behaviour.

Determination of the elongational or tensile stress, τ_{11} , in purely extensional flows of dilute suspensions of elongated, rigid particles is given by

$$\tau_{11} = \eta \dot{\epsilon}_{11} \quad (1.2.10)$$

and independent of whether or not the suspension exhibits elastic behaviour. It is significant that the tensile stresses will be very large for long particles. Since the analysis leading to Equation (1.2.10) is defined only for purely elongational flow, it is necessarily restricted to relating the total elongational stress to the elongational deformation rate and applicable only to purely

extensional flows or those which may be reasonably approximated as purely extensional. Solution to the general flow problem requires a description of the continuum behaviour through the use of a constitutive equation which relates the material functions, τ_{ij} , to the kinematic variables, d_{ij} .

It is apparent that the development of Takserman-Krozer and Ziabicki may be useful in defining a "better" constitutive relation. However, since this study is concerned with the behaviour of fibre suspensions in extensional flow, where it is possible to relate elongational stress to elongational deformation rate, the definition of a "better" constitutive relation is left to other investigators.

CHAPTER II

THEORY

2.1 GENERAL

Unlike measurements of shear stresses, the measurement of normal stresses involves the total stress, τ_{ij} , which includes the isotropic stress, $p\delta_{ij}$, as well as the deviatoric stress, S_{ij} (27). Since the meaning of $p\delta_{ij}$ is not fundamentally clear for visco-elastics (24,25,27), it is often convenient to remove the influence of p from normal stress measurements. This is commonly achieved by presenting results in terms of stress differences, for example (27):

$$\tau_{11} - \tau_{22} = -p + S_{11} - (-p + S_{22}) = S_{11} - S_{22} \quad (2.1.1)$$

When knowledge of the total stress is required, it is necessary to make some assumptions about p (24,26,27).

Although measurements have been made of normal stresses developed in very slow elongational flows (3,24,25) and, more recently, in rapid elongational flows (25), most measurements have involved normal stresses developed in simple laminar shear flows (hereinafter referred to as SLSF). Normal stresses developed in SLSF of polymeric solutions can be measured by a variety of techniques (27). The cone and plate instrument (26,27) is very popular due to the superior flow kinematics and to the absence of crude assumptions necessary to complete an analysis (27). Another popular system is the capillary jet (26,27), which is capable of producing first normal stress data at relatively high shear rates. These techniques, however,

are practically restricted to normal stress measurements of fairly elastic polymeric solutions of moderate concentrations (26,27).

In the case of highly concentrated solutions or polymer melts, for example, the instabilities which develop in the cone and plate geometry limit normal stress measurements to uninterestingly low deformation rates (26). Similarly, the capillary jet technique is unwieldy with such materials and subject to flows of low Reynolds number where end effect corrections may be appreciable (2,14,16,17, 26,28). At the other extreme of very dilute elastic solutions, or even moderate concentrations of slightly elastic solutions, the low levels of normal stresses developed in SLSF become difficult to measure with any degree of resolution (26).

Metzner, Uebler, and Chan Man Fong (26) made use of the well-known Maxwell model (27) in an attempt to predict normal stresses in the entrance region of long circular ducts. Although unsuccessful quantitatively, they were able to suggest that sensitive measurements of normal forces could be realized by the measurement of the thrust, or, equivalently, the expansion of orifice jets. This suggestion was made on the basis of some important observations, namely:

- i) In the flow of elastic fluids through a contraction, the kinematics, immediately upstream of the contraction, are essentially those of a purely elongational flow (41).
- ii) The magnitude of the normal stresses developed in these converging flows were shown to be large.

- iii) The rate of elongational deformation, $\dot{\epsilon}$, in these converging flows appeared to be guided by the constancy of the dimensionless elongation rate, $\theta_{f1} \dot{\epsilon}$ (37). Here, θ_{f1} represents the relaxation time of the fluid (35,36,37).

The orifice jet thrust device was employed by Metzner and Metzner (25) who demonstrated the sensitivity of this device to low levels of elasticity as well as the high tensile stresses developed in rapid elongational flows of viscoelastic media.

2.2 ORIFICE JET THRUST MEASUREMENTS

2.2.1 Kinematics of Orifice Flows

Metzner and Metzner (25) have defined the velocity field for a viscoelastic fluid upstream of a sharp-edged circular orifice as depicted in Figure (2.1). The only upstream fluid which passes through the orifice is confined to the conical region bounded by the dashed lines, with the fluid outside this conical region recirculating within the large toroidal vortices indicated. The kinematics of this velocity field may be described in a spherical coordinate system having its origin at the apex of the cone formed by converging streamlines. In this coordinate system, the physical components of velocity may be approximated by the equations (25)

$$v_r = \frac{Q}{2\pi r^2 (1 - \cos \phi)}$$

$$v_\theta = v_\phi = 0 \quad (2.2.1)$$

where Q denotes the volumetric flowrate, ϕ the half-angle of the cone

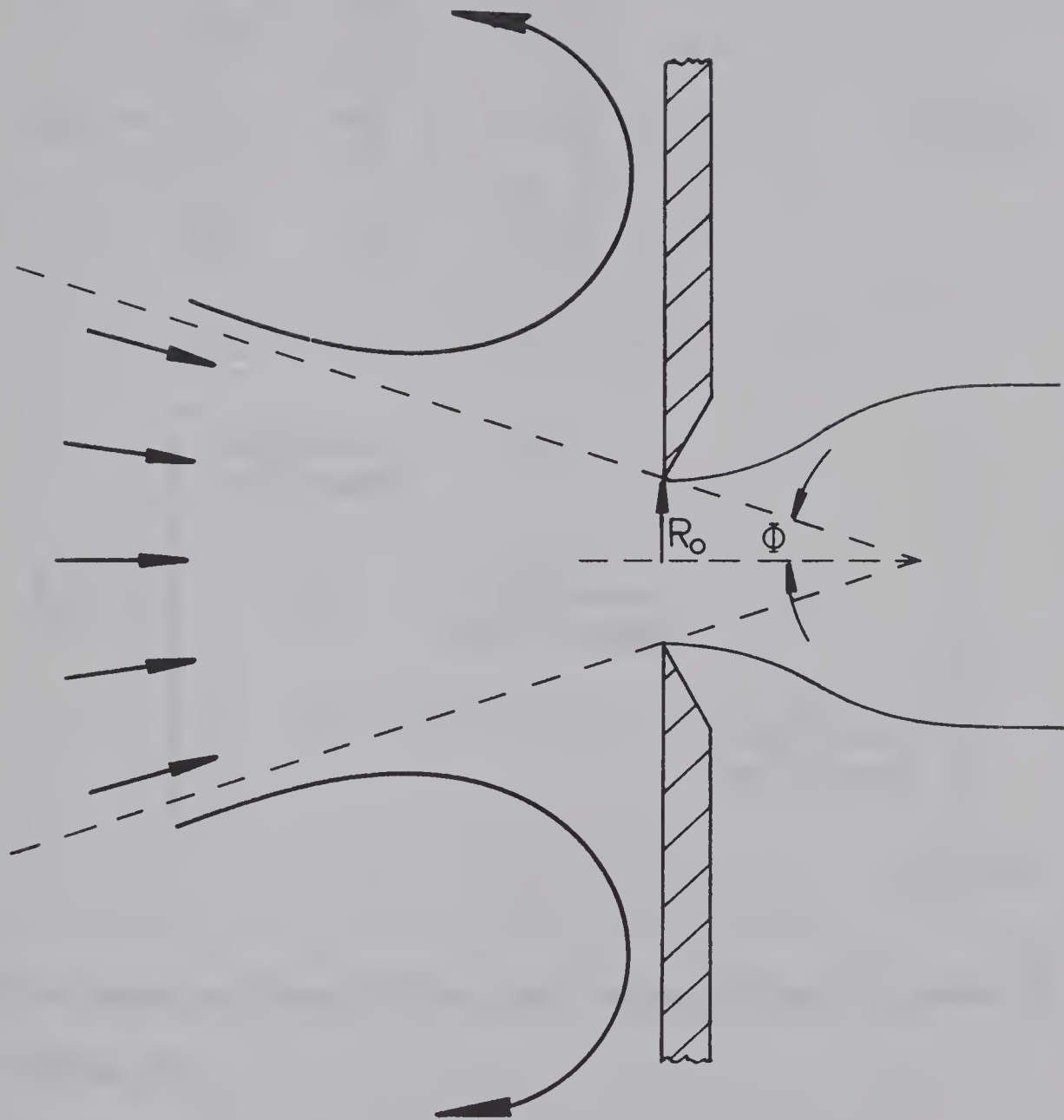


FIGURE (2.1)
VELOCITY FIELD FOR VISCOELASTIC
FLOW THROUGH AN ORIFICE

and r the distance from the apex of the cone.

Equations (2.2.1) may be used to evaluate the physical components of the deformation rate tensor

$$d_{ij} = \begin{bmatrix} \frac{\partial v_r}{\partial r} & 0 & 0 \\ 0 & \frac{v_r}{r} & 0 \\ 0 & 0 & \frac{v_r}{r} \end{bmatrix} \quad (2.2.2)$$

or

$$d_{ij} = \begin{bmatrix} \frac{Q}{\pi r^3(1-\cos\phi)} & 0 & 0 \\ 0 & \frac{Q}{2\pi r^3(1-\cos\phi)} & 0 \\ 0 & 0 & \frac{Q}{2\pi r^3(1-\cos\phi)} \end{bmatrix} \quad (2.2.3)$$

The deformation rates, at the orifice, can now be defined in terms of the orifice radius, R_0 :

$$d_{11} = \frac{-Q \sin^3 \phi}{\pi R_0^3(1-\cos\phi)} \quad (2.2.4)$$

$$d_{22} = d_{33} = \frac{Q \sin^3 \phi}{2\pi R_0^3(1-\cos\phi)}$$

The only variable in Equations (2.2.4) which may be difficult to determine experimentally is Φ . Since the dependence of Φ on Q and R_0 , among other things, is unknown, it is immediately apparent that Φ cannot be measured in a separate (independent) experiment unless dimensional similarity is preserved. In this light, the observations of previous investigators are worth consideration.

Under the experimental conditions studied by Uebler (41), the full cone angle, 2Φ , was found to be about 30° and independent of flowrate. More recent evidence (24,25) however, suggests that Φ decreases with:

- i) increasing flowrate,
- ii) decreasing orifice size, and
- iii) increasing elasticity (an indirect observation based on the constancy of the dimensionless elongational rate, $\theta_{f1}\dot{\epsilon}$) (24,25,26).

Uebler's work also indicated that the converging flows of visco-elastic media were essentially free of shearing deformations (25,26,41) as implied by Equations (2.2.1). Moreover, Metzner and Metzner qualitatively indicate that the absence of shearing deformations becomes more apparent with decreasing Φ . These observations show that experimental knowledge of Φ is essential to accurately predict deformation rates. Additionally, in the orifice jet thrust investigation of fluids of a low level of elasticity, the constancy of $\theta_{f1}\dot{\epsilon}$ implies that Φ will be large. Consequently, measurements of the velocity field may be required to accurately predict deformation rates and to determine whether or not shearing deformations are

properly negligible.

Available observations on Newtonian flow through a contraction (41) indicate that the fluid which passes through the contraction is bounded by the geometry of the reservoir. The toroidal vortices common to flows of viscoelastic media in similar geometries are absent in the Newtonian case (26). When the contraction is a sharp-edged circular orifice in a flat plate, one would expect the upstream velocity field to be as depicted in Figure (2.2). This velocity field may be approximated (in spherical coordinates) by modifying Equations (2.2.1) to

$$v_r(\phi) = \frac{Q}{2\pi r^2(1-\cos\phi)} \cdot f(\phi) \quad (2.2.5)$$

$$v_\theta = v_\phi = 0$$

where $f(\phi)$ will be a maximum at $\phi = 0$ and identically zero at $\phi = 90^\circ$. This simply indicates that the flow is not purely elongational and the deformation rate tensor will have non-zero non-diagonal elements. Since $\phi = 90^\circ$, the elongational deformation rates will be larger than those for viscoelastics. Exact numerical solutions to velocity fields upstream of a contraction are available, but restricted to flows of low Reynolds number (9,42). Although Equations (2.2.5) are a rather poor representation of the velocity field depicted in Figure (2.2), they will serve, nevertheless, to define a maximum conceivable deformation rate for orifice flows.

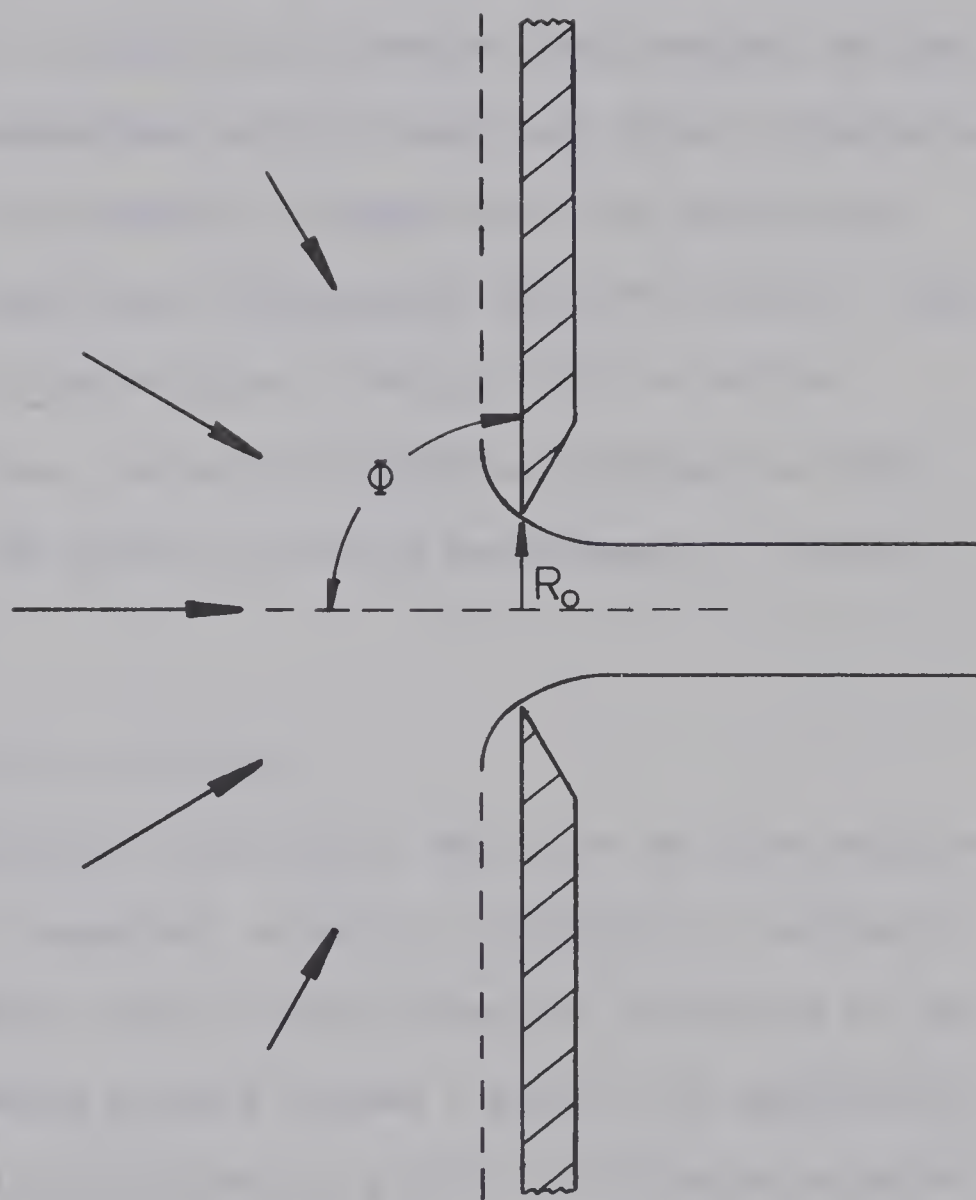


FIGURE (2.2)
VELOCITY FIELD FOR NEWTONIAN
FLOW THROUGH AN ORIFICE

In view of the presence of elasticity in dilute fibre suspensions (10,29), one would expect the velocity field description upstream of an orifice to be bounded by the extremes describing very viscoelastic and Newtonian orifice flows. Again, the implied constancy of $\theta_{f1}\dot{\epsilon}$ suggests that, if elasticity is present, the expected deformation rates for fibre suspensions will be lower than those of Newtonians. In any event, there is no evidence to suggest that the deformation rates will be higher than those of Newtonians in orifice flows. Since no data are available to describe the velocity field in orifice flows of fibre suspensions, reliable elongational deformation rates cannot be predicted. The need for velocity measurements is clearly indicated.

2.2.2 Analysis of Orifice Jet Thrust

In the interpretation of the stress levels of the flow depicted in Figure (2.1), it is convenient to employ a cylindrical coordinate system, r, θ, z , with the z -axis directed along the centerline of the velocity field. A momentum balance between a section far upstream of the orifice and the fully-developed jet yields the following equation for thrust (25):

$$T = \int_A (\rho v_z^2 - \tau_{11}) dA \quad (2.2.6)$$

in which T denotes the (measured) total thrust, ρ the fluid density, v_z the axial component of velocity and τ_{11} the total axial stress in the fluid at the orifice. If the velocity profile is flat (cylindrical coordinates), then τ_{11} is independent of radial position, and

Equation (2.2.6) may be simplified by replacing v_z by V_o and removing the integral, giving

$$T = (\rho V_o^2 - \tau_{11})\pi R_o^2 \quad (2.2.7)$$

where V_o is the average velocity at the orifice. Since the radial stress, τ_{22} , is zero in the well-developed jet (25), Equation (2.2.7) may be expressed in terms of stress differences (25) as

$$\begin{aligned} T_{11} = S_{11} - S_{22} &= \rho V_o^2 - T/\pi R_o^2 \\ &= \rho \left(\frac{Q}{\pi R_o^2} \right)^2 - \frac{T}{\pi R_o^2} \end{aligned} \quad (2.2.8)$$

showing the measurement of thrust, T , as a function of flowrate, Q , relates the normal stress difference, $S_{11} - S_{22}$, to the elongational deformation rate defined by Equation (2.2.4).

If η is required, then the total stress, τ_{11} , is utilized rather than the stress difference. Hence, noting that

$$\tau_{11} = \eta \dot{\epsilon} \quad (2.2.9)$$

and, approximately, that

$$\dot{\epsilon} = \frac{V_o \sin^3 \phi}{R_o (1 - \cos \phi)} \quad (2.2.10)$$

Equation (2.2.7) may be written as a second-order polynomial in V_o , namely

$$\frac{T}{\pi R_o^2} = \rho V_o^2 - \eta \frac{\sin^3 \phi}{R_o (1 - \cos \phi)} V_o \quad (2.2.11)$$

The elongational viscosity of viscoelastics can be determined from experimental measurements of T , V_o , and ϕ . The form of Equation (2.2.11) suggests a simple least-squares approach to data smoothing provided that the term $\frac{\sin^3 \phi}{(1-\cos \phi)}$ remains essentially constant over the range of an experiment. The least-squares approach will be used, in fact, to interpret data.

The orifice jet thrust of an ideal flow can be described by a momentum balance as determined by Equation (2.2.6). In this case, the axial stress, τ_{11} , will be zero. Noting the presence of a vena contracta a short distance downstream of the orifice, the thrust will be related to the velocity at the vena contracta, V_2 , rather than on the average velocity at the orifice, V_o . Hence, assuming incompressible flow, the thrust is given by

$$\begin{aligned} \frac{T}{\pi R_o^2} &= \rho V_2^2 \\ &= \frac{\pi R_o^2}{A_2} \rho V_o^2 = k \rho V_o^2 \end{aligned} \quad (2.2.12)$$

where A_2 is the cross-sectional area of the jet at the vena contracta. The value of k has been determined from ideal flow theory to be 1.64 (5,22,25).

Since orifice flows of viscous Newtonians are not ideal, unusual thrust reduction may result as a consequence of profile relaxation and surface tension effects which are common to capillary flows at low Reynolds numbers (2,14,16,17,28). The thrust reduction may also be affected by the large tensile stresses developed immediately

upstream of the orifice. This suggestion, however, hints of clairvoyance since Newtonian liquids have no memory for previous deformations (24,25). Hence, the thrust per unit orifice area for a Newtonian orifice jet can be described in terms of the orifice velocity, V_o , as

$$\frac{T}{\pi R_o^2} = k_1 \rho V_o^2 - k_2 V_o \quad (2.2.13)$$

where k_1 and k_2 may both be functions of velocity, viscosity, surface tension, orifice size and k_2 may also be a function of deformation rate. As a first approximation, it is assumed that k_1 and k_2 are constants, independent of velocity.

Noting that Equations (2.2.11) and (2.2.13) are of the same form (i.e. both in terms of V_o^2 and V_o) and that the kinematics of orifice flows of fibre suspensions are expected to lie somewhere between the extremes of very viscoelastic and purely Newtonian, the thrust equation for suspension flow may be simply written without resorting to a differential momentum balance. Since the coefficient, k_1 , in the V_o^2 term of Equation (2.2.13) arises from the non-flatness of the Newtonian velocity profile at the orifice, one would expect this coefficient to be smaller for fibre suspensions due to an expected decrease in Φ . The term involving V_o in Equation (2.2.11) is an axial stress term and hence necessary in the fibrous case. Similarly, the term involving V_o in Equation (2.2.13) is a consequence of "unusual behaviour" (which also may be regarded as an axial stress) and is, therefore, important in the fibrous case. Thus, the orifice jet thrust of a fibrous flow will be

$$\frac{T}{\pi R_o^2} = k_1' \rho V_o^2 - k_2' V_o \quad (2.2.14)$$

where k_1' and k_2' are functions similar to k_1 and k_2 respectively, and k_2' will reflect the increase in the axial stress (or elongational viscosity) due to the presence of fibres.

Although Equations (2.2.13) and (2.2.14) both appear amenable to a polynomial least-squares regression of the thrust data, a "good" statistical correlation does not necessarily imply that k_1 and k_2 (or k_1' and k_2') represent the absolute magnitude of the actual physical phenomena. A relative trend may be indicated by the coefficients if a "physical reason" supports the constancy and numerical magnitude of k_1 (or k_1') over the range of an experiment. Hence, in order to properly compare the elongational or "elastic" behaviour of a fibre suspension to a Newtonian, it is necessary to compare experimental results for a Newtonian and a suspension which have approximately the same shear viscosity and, possibly, equal surface tensions.

CHAPTER III

EXPERIMENTAL EQUIPMENT AND PROCEDURE

3.1 GENERAL

The orifice jet thrust technique, noted for its sensitivity to low levels of elasticity (25,26), was chosen for this study. Sugar solutions were chosen as a suspending medium for the fibres. Since fibres disperse easily in a medium of low viscosity and particle aggregation and settling are minimal in a medium of high viscosity, suspension preparation was simplified by first dispersing the fibres in water, then adding sugar to increase the viscosity of the suspending medium.

The experimental program consisted of measuring thrust, pressure and flowrate for orifice flows of two sugar solutions and nine different suspensions of fibres in sugar solutions. Originally, there was an intention to make velocity measurements upstream of the orifice by a photographic technique similar to those used by a number of others (32,35,41). However, velocity measurements were abandoned due to the translucence of the suspensions used. The thrust device and ancillary equipment are represented schematically in Figure (3.1) and, in some detail, in Figures (3.2), (3.3) and (3.4).

3.2 EXPERIMENTAL APPARATUS

3.2.1 Spring System

Basically, the system consisted of the orifice device supported by two 32 inch flat, parallel springs clamped firmly at each end. The spring leaves were 1/16 inch thick x 2 inches wide 304 stainless

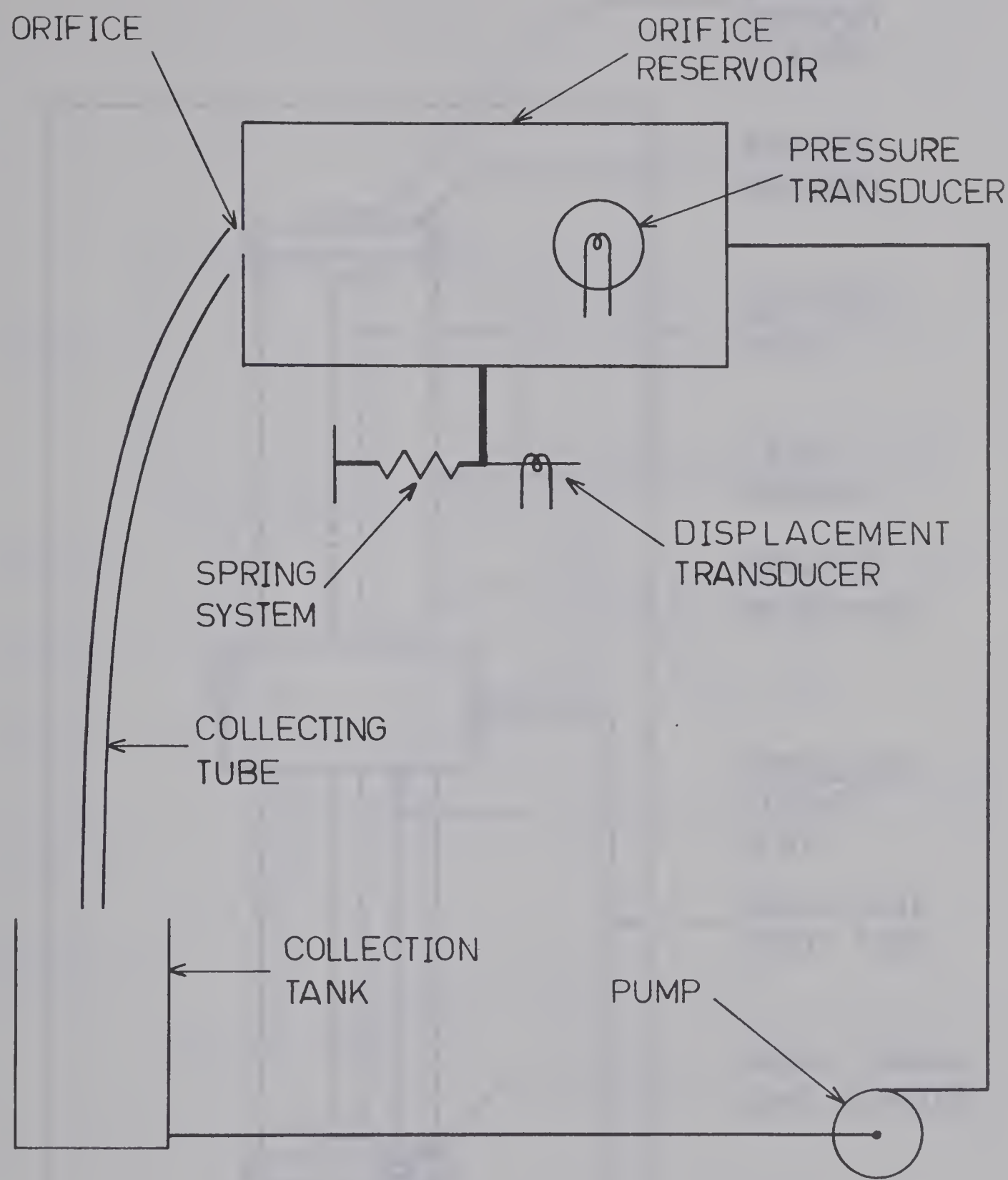


FIGURE (3.1)
SCHEMATIC OF EXPERIMENTAL APPARATUS

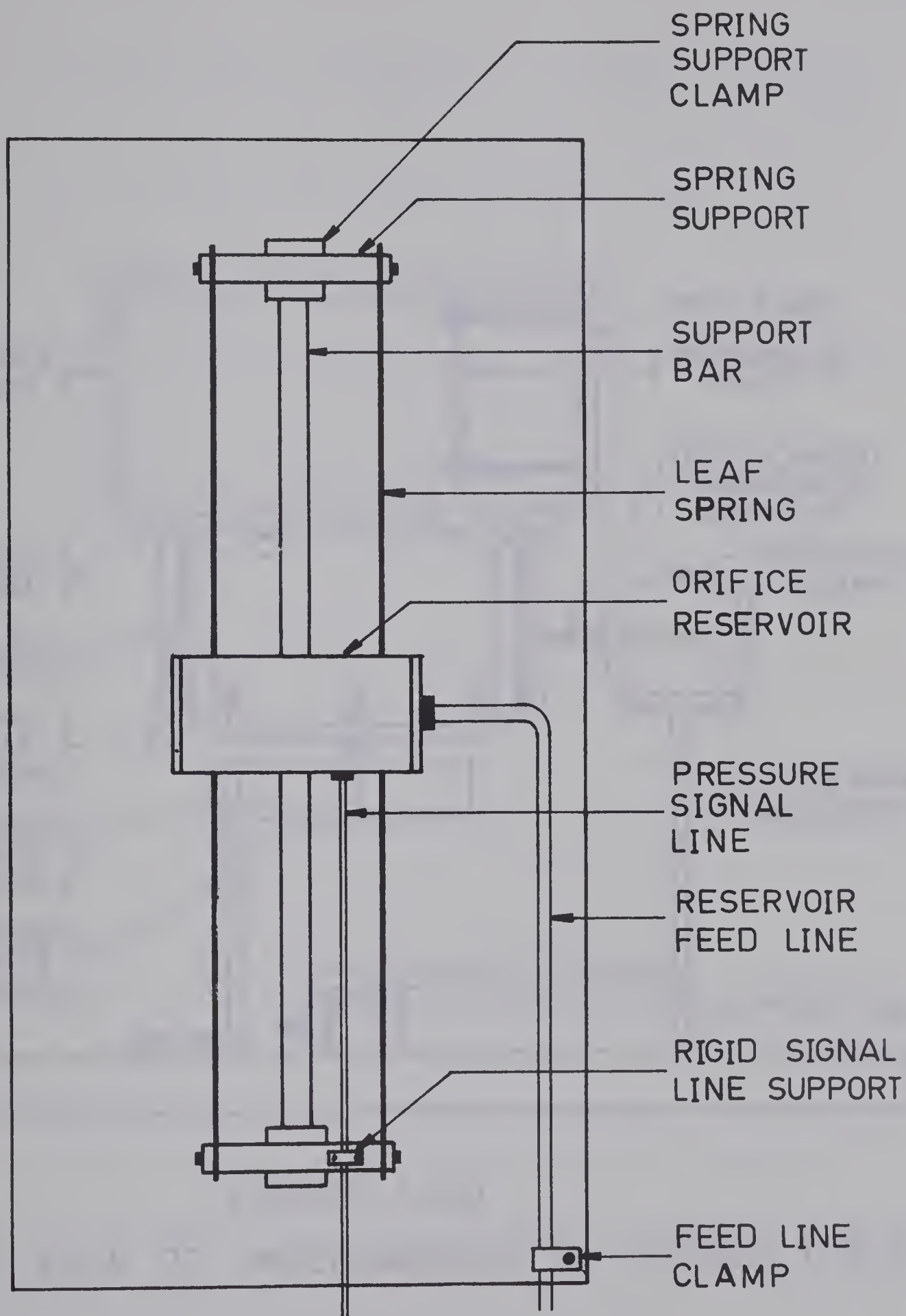


FIGURE (3.2)
TOP VIEW OF THRUST DEVICE

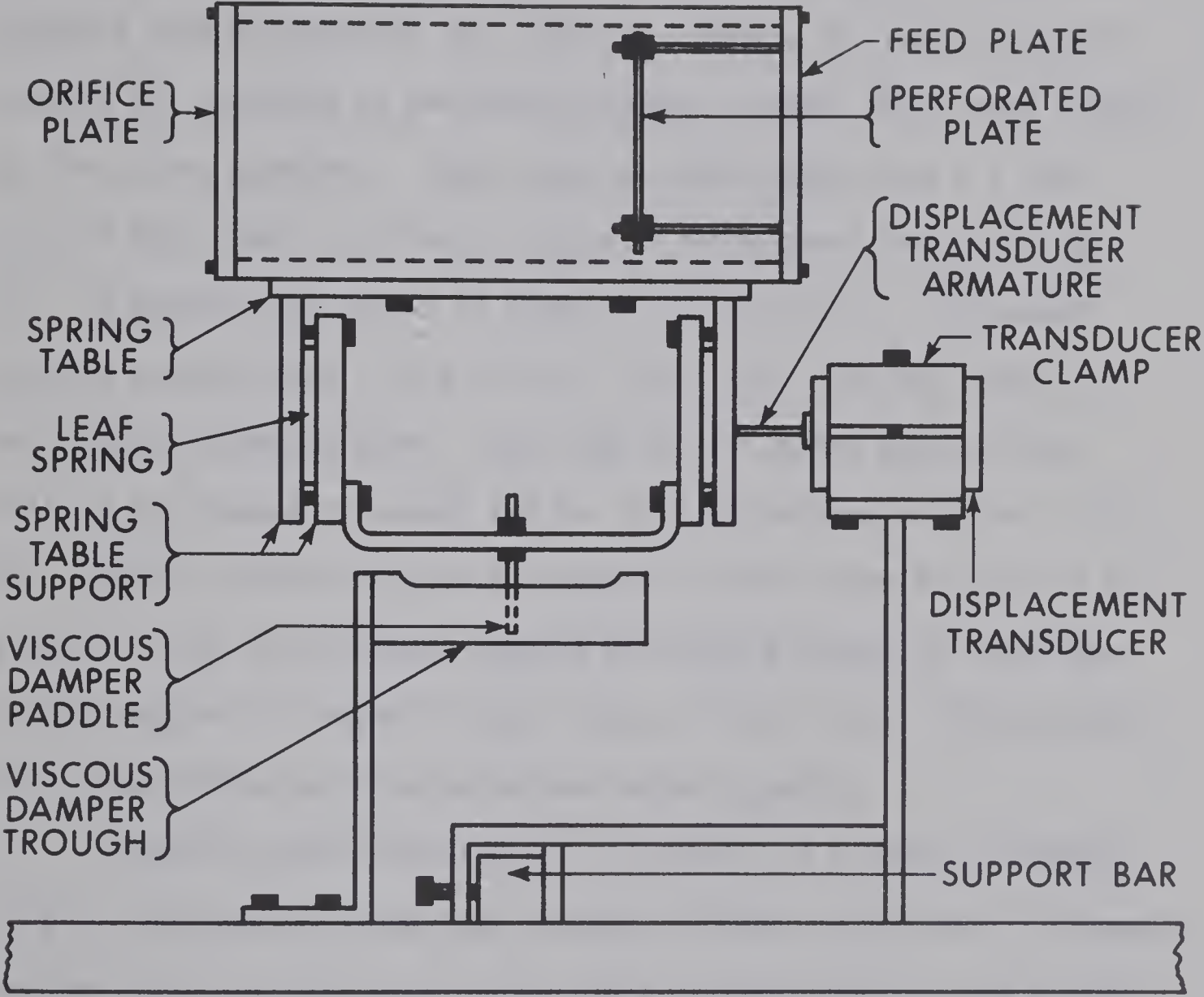


FIGURE (3.3)

SIDE VIEW OF UNDERCARRIAGE OF SPRING TABLE

steel, and, when clamped to the supports, could leave a maximum of 31 inches of unclamped length. The two 5-3/4 inches wide by 6-3/4 inches high rectangular spring supports, shown in Figure (3.2), were milled from a 1 inch cold roll mild steel plate. The spring supports were attached to the 1 inch x 1 inch x 34 inch mild steel support bar by means of the spring support clamps, which were welded to the spring supports. Each clamp was fabricated from a 2 inch cube of mild steel and fixed rigidly to the support bar by two No. 10 - 24 machine set screws as shown in Figure (3.2). The support bar was bolted rigidly to a 20 inch x 40 inch x 3/4 inch thick rectangular aluminum base. Each side of the spring supports was drilled and tapped to accept two No. 10 - 24 machine bolts on 2-1/2 inch centres with the top hole located 1/2 inch below the top of the support. This facilitated clamping the spring leaves to the sides of the supports by means of four 1 inch x 3-1/2 inch x 1/4 inch flat mild steel plates which were bolted to the supports.

A small table of mild steel, 1/4 inch x 3 inches x 7 inches in size, was mounted above the springs, halfway along their unclamped length, with the long axis of the table perpendicular to the spring face. As shown in Figure (3.3), the spring table was attached to the springs by means of spring table supports. Each of the two spring table supports consisted of two lengths of 3/4 inch half-rounds whose rounded surfaces clamped a spring leaf between them. The longer, 3-1/4 inch, half-rounds were rigidly bolted to the spring table.

The viscous damper depicted in Figure (3.3) consisted of a round paddle, which was rigidly fixed to the spring table supports by

means of a $3/4$ inch x $3/16$ inch thick mild steel strap, and immersed in a trough of S.A.E. 140 gear oil. The trough was a fabricated 4 inch x 1 inch I.D. cylinder with enclosed ends and a cutout top to accommodate the paddle. The trough was rigidly attached to the aluminum base by means of $1-1/4$ inch x $1/4$ inch mild steel strap.

The entire apparatus was enclosed by a 19 inch x 39 inch x 18 inch x $1/4$ inch thick plexiglass box with a removable top. Small openings were provided for the transducer leads and the feed tubing. A large hole ($2-1/2$ inch ϕ) was cut opposite the orifice plate to accommodate a short length of 2 inch I.D. Tygon tubing which served to collect the fluid leaving the orifice.

3.2.2 Orifice Plate and Reservoir

The orifice reservoir, which was bolted to the spring table, was fabricated from $3/8$ inch plexiglass. Sheets of the material were glued and screwed together to form a 4 inch x 4 inch x 8 inch open box. The orifice plate was fabricated from $1/4$ inch brass plate and bolted to one end of the open box. A sharp-edged orifice, bevelled 30° normal to the plate, was located in the centre of the plate. A feed plate, also fabricated from $1/4$ inch brass plate, served as the other end of the open plexiglass box. The feedplate originally held a thin, brass, perforated flow-distributor plate 2 inches into the box by means of four long bolts. Owing to fibres being trapped in the perforations, this was later abandoned in favour of a 2 inch x 2 inch x $1/4$ inch thick unperforated teflon plate. The centre of the feed plate was drilled and tapped to accept the O-ring side of a $5/8$ inch

0-ring seal x 3/8 inch swagelok fitting. The swagelok fitting held a fabricated 3/8 inch copper tubing elbow to which was clamped the 3/8 inch heavy-wall Tygon feed tubing.

3.2.3 Transducers and Mountings

One side of the orifice reservoir was drilled and tapped to accept the 0-ring side of a 3/8 inch 0-ring seal by 1/4 inch swagelok fitting. Instrument tubing connected the swagelok fitting with the Validyne DP75 differential pressure transducer, manufactured by Validyne Engineering Corporation of Northridge, California. The negative side of the transducer was open to the atmosphere while the positive side was connected to the tee and valve arrangement depicted schematically in Figure (3.4). The rigid signal line support, shown in Figure (3.2), rigidly fixed the instrument tubing to the spring support and served to isolate accidental movements of the externally located transducer from the calibrated spring system. The calibration vessel, which was connected to the transducer with instrument tubing, served a two-fold purpose; namely, to calibrate the transducer (as discussed later) and to bleed the transducer and signal lines prior to an experimental run.

Spring displacement was measured by a Boulton Paul model F51M zero-resistance displacement transducer, manufactured by Boulton Paul Aircraft Ltd. of Wolverhampton, England. The armature of the transducer was attached to the rear spring table support, normal to the plane of the spring leaves. The transducer coil was held by a 1-1/4 inch x 1-1/4 inch x 1-1/2 inch brass prism which was bored out and

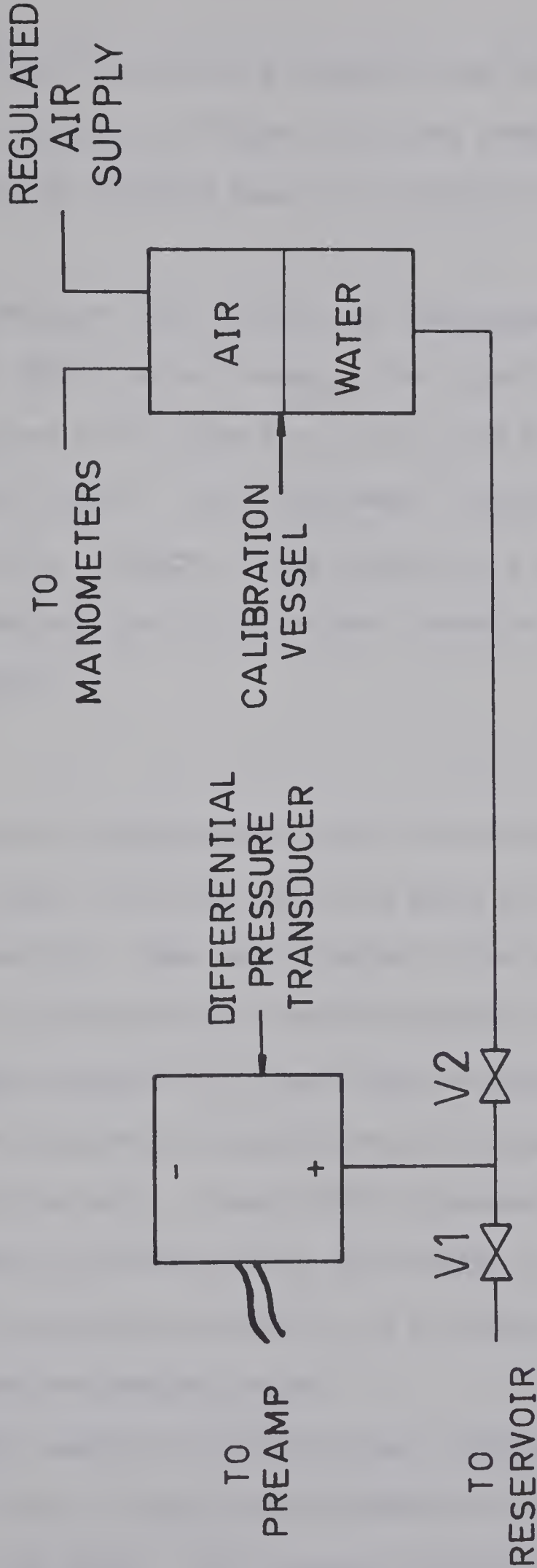


FIGURE (3.4)

SCHEMATIC OF PRESSURE TRANSDUCER HOOK-UP

slit along the bore to serve as a clamp for the cylindrical transducer housing. As shown in Figure (3.3), the transducer clamp was rigidly fixed to the aluminum base via 1-1/4 inch x 1/4 inch mild steel strap.

Both transducers were excited and demodulated by Hewlett-Packard Sanborn 8805A Carrier Preamps. The circuit of the pressure transducer required an RC circuit to correct the phase shift between input and output signals. The displacement transducer required no signal conditioning. Outputs of the preamps were monitored by a two-channel Dynagraph type RS strip-chart recorder manufactured by Beckman Instruments.

3.2.4 Pumps

The original pumping system used in this study was a pair of Zenith type 5, model B-4391 gear metering pumps with teflon seals, connected in parallel. Power was supplied to the pumps by a 1-hp. 220V, 3600 rpm. synchronous motor manufactured by Gill Electric Motors (GEL) of Brighton, England. The pump speed was regulated by a 60-speed epicentric transmission manufactured by Sangamo Controls Ltd. of Bognor Regis, England. Although this system was able to deliver 20 cc/sec., which was sufficient for this study, a problem with fibre plugging and the eventual availability of an Instron tester made way for a more convenient pumping system.

The latter pumping in this study was supplied by a single-acting, 6 inch I.D. x 20 inch stroke hydraulic cylinder powered by an Instron model TTBM tester. This system provided the ideal conditions

of steady, positive displacement and pre-calibrated flow.

3.2.5 Experimental Fluids

The fluids used in this study are classified in Table (3.1) along with the corresponding test numbers. The suspending medium (for the fibres) was a solution of Alberta beet sugar in water.

A 60% (by weight) sugar solution served as the suspending medium for tests 2 to 5, where the short fibres were used. However, an attempt to obtain thrust measurements for the longest fibres suspended in the 60% solution was aborted due to fibre aggregation in the orifice reservoir. It was found, by trial and error, that a 66 2/3% sugar solution would suspend even the longest fibres used in this study without noticeable fibre aggregation. Hence, a 66 2/3% sugar solution suspended the fibres in the latter tests (tests 8 to 16).

The viscosity of the 66 2/3% sugar solution was sampled and found to be 1.7 poise at $22 \pm 1^\circ\text{C}$. This agrees quite favourably with the handbook value (43) of 1.8 poise at 22°C . The shear viscosities of the suspensions, however, were not measured since the effect of shear viscosity was originally considered to be of minor importance. Moreover, at the concentration levels of this study, the change in shear viscosity, due to the presence of fibres, was small (less than 50%) (29) compared to the 150% change between the 60% and 66 2/3% sugar solutions which resulted in an almost negligible difference in thrust reduction (see Figure (4.2)).

TABLE (3.1)
EXPERIMENTAL FLUIDS

Test No.	Suspending Fluid*	Fibre Axis Ratio	Fibre Concentration (Wt.%) (Vol.%)		Measured Density (gm./cc.)
1	A	-	0.00	0.00	1.28
2	A	85	0.05	0.045	?
3	A	85	0.10	0.090	?
4	A	85	0.15	0.135	?
5	A	85	0.20	0.180	?
6	A	-	0.00	0.00	?
7	C	-	0.00	0.00	1.00
8	B	85	0.30	0.278	1.32
9	B	170	0.10	0.0926	1.32
10	B	170	0.20	0.185	1.32
11	B	255	0.10	0.0926	1.32
12	B	-	0.00	0.000	1.32
13	B	340	0.10	0.0926	1.32
14	B	85	0.20	0.185	1.32
15	B	-	0.00	0.000	1.32
16	B	170	0.10	0.0926	1.32

* Suspending Fluid A: 60% Sugar Solution

Suspending Fluid B: 66-2/3% Sugar Solution

Suspending Fluid C: 0.10% Separan AP30 Solution

ORIFICE DIAMETER

Tests 1 to 4 = 0.0846 cm.

Tests 5 to 16 = 0.1477 cm.

As indicated by Table (3.1), suspension densities were not measured in tests 2 to 6. At this point in the study, it was found that evaporation, during suspension preparation over two or three days at high temperature, caused a water loss of up to 40%. The amount of water lost, which was unknown in tests 2 to 6, represented a change in suspension density, which, in turn, classified these tests as unreliable. Since the thrust reduction, due to the presence of fibres, was relatively small (see Chapter IV), it is emphasized that a small (and unknown) change in suspension density will significantly affect the absolute thrust reduction. In tests 8 to 16, the suspension densities were adjusted (by adding water) to the required specification (see comments in following sections).

The fibres used in this study were purchased, precut, from Microfibres Inc. of Pawtucket, Rhode Island. All fibres were 1.5 denier viscose rayon cut to lengths of 0.05 inch, 0.10 inch, 0.15 inch, and 0.20 inch. Sample measurements of dry fibre diameter, with the aid of a measuring microscope, yielded a remarkably constant value of 15 ± 0.25 microns. Examination of the fibres, with a microscope, after a run, revealed no evidence of frilibration or swelling. Vernier caliper measurements of a sample of 0.05 inch fibres showed the stated lengths to be accurate within limits of this measurement. The density of the fibres was determined by immersing fibres in various measured mixtures of carbon tetrachloride and alcohol until no gravitational gradient was observed. The density thus determined was found to be 1.425 gm/cc.

3.3 EXPERIMENTAL PROCEDURE

3.3.1 Suspension Preparation

Sugar solutions were prepared by weighing the ingredients, and stirring and heating the solution to expel the suspended air bubbles. The solution was then cooled while mixing continuously. When the solution cooled to room temperature, it was weighed to determine the evaporation loss and sufficient water was added to make up this loss^{*}.

In preparation of fibre suspensions, the required, weighed amounts of fibres and water were first vigorously mixed to disperse the individual particles. The sugar was added after dispersion was assumed to be complete. The heating, cooling and checking procedure was then followed as outlined above^{*}.

The partially degraded polymer solution used in test 7 of this study was obtained as a sample from a large batch which had been prepared for pipeline tests (32).

3.3.2 Calibration

Flow calibration was a relatively simple procedure for both pumping systems, since the flowrates could be easily related to known pump speeds. The calibration was accomplished by weighing the fluid collected over a period of about 2 minutes. Flow calibration data are presented in Appendix A.

Calibration of the pressure transducer was accomplished

^{*} Evaporation losses were adjusted only in tests 8 to 16.

through the use of the scheme represented in Figure (3.4). The calibration vessel was a cylindrical bomb (closed at both ends) which was half-filled with water. An opening in the top of the bomb could be connected to either a mercury manometer or a water manometer, depending upon the desired calibration range. A line from the bottom of the vessel to valve, V2, provided the pressure signal to the transducer. Prior to a calibration, valve V1, was closed, V2 was opened, and the transducer bled and zeroed. Calibration was performed by pressurizing the bomb to various levels and reading a manometer and corresponding signal on the recorder. Calibration data are presented in tabular and graphic form in Appendix A.

The thrust calibration was accomplished by attaching one end of a thin cotton thread to the rear spring table support and the other end to an external support located behind and above the thrust apparatus in a plane perpendicular to the axis of the springs. Balance weights were attached, by a short length of thread, to this thread, near the thrust apparatus and an arbitrary weight attached by a length of thread to the original thread, farther away from the thrust device. The arbitrary weight was immersed in a container of water to damp oscillations. The original thread was adjusted such that the thread coming from the spring table support was level (perpendicular to the plane of the springs). A measurement of the hypotenuse formed and the horizontal distance between the known and arbitrary weights enabled solving the "force-triangle" for the horizontal force on the springs. A 30 cm. stainless steel machinist rule, with 1 mm. graduations, was used to measure the hypotenuse and horizontal distances.

The force calibrations were used directly instead of relating them to spring displacement. Since the spring calibration was sensitive to the way the pressure and feed lines were connected, it varied from test to test. Hence, a spring calibration was performed for each test. Calibration data, their least-squares equations, and a brief discussion on the errors involved are presented in Appendix A.

3.3.3 Data Collection

The equipment was assembled, pressure transducer bled, and both transducers zeroed. An experimental test was performed through the flowrates as given in the data (Appendix B). The pressure and thrust recorded for each flowrate, as well as the orifice size, are also presented in Appendix B. Upon completion of a test, the thrust calibration was performed. All tests were performed at a temperature of $22^{\circ} \pm 1^{\circ}\text{C}$.

Orifice "plugging" was observed when the orifice jet ceased and the pressure signal rose monotonically (to the point, often, where the plexiglass reservoir burst). In cases where the reservoir did not burst, the "plugging" problem was relieved by carefully reaming the orifice with a short length of thin wire. Tests where "plugging" occurred were invariably unsuccessful as a result of either a broken reservoir, or a calibration change in the spring system. Hence, all tests where "plugging" occurred were deemed unreliable.

CHAPTER IV

DISCUSSION OF RESULTS

4.1 VISCOELASTIC BEHAVIOUR

Thrust measurements of the 0.10% Separan AP30 solution are presented here to demonstrate the sensitivity of the orifice jet thrust device and to compare with previous results. Figure (4.1) depicts the results of test 7 as well as the results of Metzner and Metzner (25) for water and 0.083% Separan AP30 solution. The results of test 13 are also presented to show the relatively low level of "elasticity" developed in the most "elastic" suspension used in this study. The results of test 7 are generally in good agreement with Metzner and Metzner for a similar concentration of polymer.

4.2 NEWTONIAN BEHAVIOUR

Anticipation of unusual thrust reduction (or, effectively non-ideal flow) in orifice flows of viscous Newtonians motivated orifice jet thrust measurements for a Newtonian fluid of approximately the same shear viscosity as the fibre suspensions. Thus, it was possible to determine any change in elongational viscosity resulting from the fibres. As shown in Figure (4.2), the thrust per unit area of the Newtonian suspending medium deviated to lower values, at lower velocities, than those of water (25). It is known that surface tension becomes important in viscous capillary flows at low velocities and tends to significantly reduce thrust (2,14,16,17,28). Surface tension may also tend to reduce the thrust in viscous orifice flows in addition to the thrust reduction caused by the axial stress (see

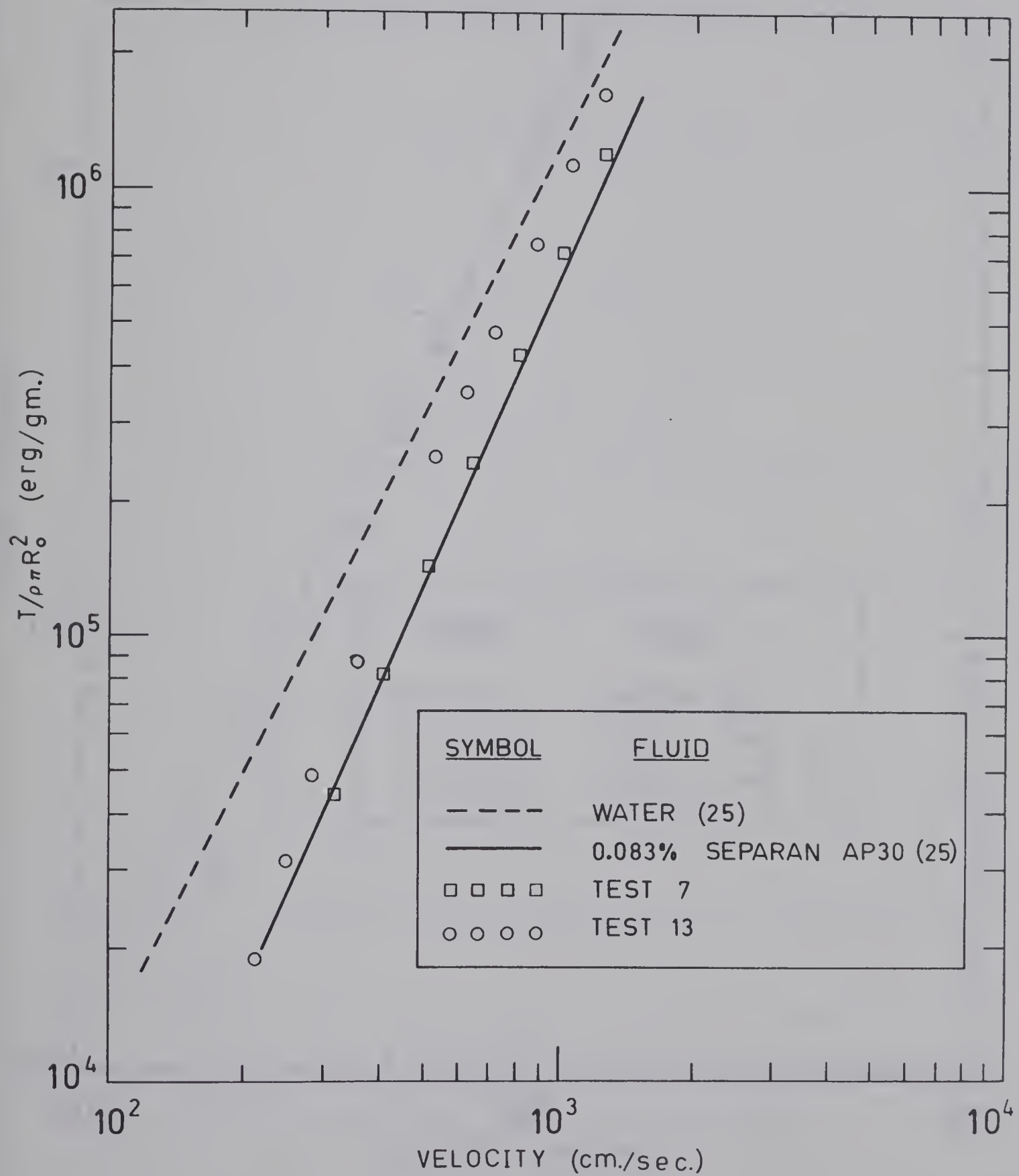


FIGURE (4.1)

THRUST-VELOCITY CURVES FOR WATER,
SEPARAN AP30 SOLUTIONS AND THE
MOST "ELASTIC" SUSPENSION

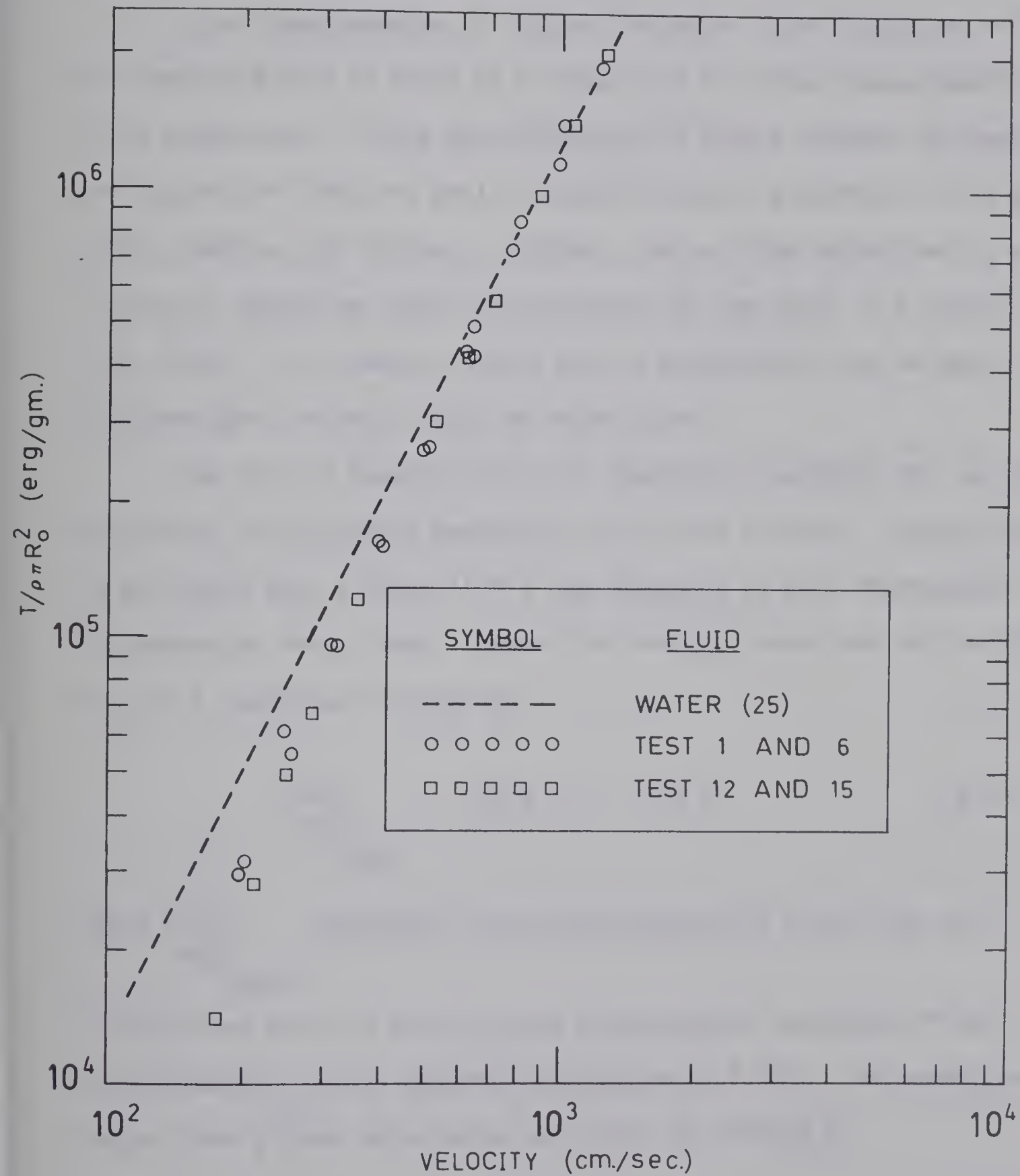


FIGURE (4.2)

THRUST-VELOCITY CURVES FOR WATER
AND SUGAR SOLUTIONS

Section (2.2)). The data presented in Figure (4.2) do not, however, distinguish the singular importance of surface tension from the overall thrust reduction in orifice jets.

Thrust measurements of viscous Newtonian flow through an orifice are presented here to serve as a comparison for thrust measurements of fibre suspensions. Since the difference in thrust between the Newtonian and suspension flows was small, they will not be presented in the form used by Metzner and Metzner. Instead, they will be normalized to an "averaged" Newtonian thrust and presented on the basis of a normalized thrust, T_N . However, before such a presentation can be made, some averaging criterion must be established.

The form of Equation (2.2.13) immediately suggests the use of a polynomial least-squares regression to fit the flowrate - thrust data. It was found that a Type III fit (see Appendix C) best represented the Newtonian thrust data. Hence, the average thrust per unit orifice area of a Newtonian is given by:

$$\left\langle \frac{T}{\pi R_o^2} \right\rangle_{\text{NEWT}} = [k_1] V_o^2 - [k_2] V_o \quad (4.2.1)$$

where $\left\langle \frac{T}{\pi R_o^2} \right\rangle_{\text{NEWT}}$ represents the averaged Newtonian thrust per unit

orifice area and $[k_1]$ and $[k_2]$ are least-squares estimates of the coefficients k_1 and k_2 defined by Equation (2.2.14). The normalized thrust, for a given data point, will then be defined by

$$TN = \frac{\frac{T}{\pi R_o^2}}{[k_1] V_o^2 - [k_2] V_o} \quad (4.2.2)$$

An averaged normalized thrust, for a given test, can be defined as

$$\langle TN \rangle = \frac{[k'_1] V_o^2 - [k'_2] V_o}{\left\langle \frac{T}{\pi R_o^2} \right\rangle_{\text{NEWT}}} \quad (4.2.3)$$

Where $\langle TN \rangle$ is simply a comparison of the smoothed thrust data, for a given test, to the best-fit curve of the Newtonian data. The parameters $[k'_1]$ and $[k'_2]$ were determined by a Type III fit for each test performed in this study. The Newtonian coefficients $[k_1]$ and $[k_2]$ were determined by a Type III fit on the combination of tests 1 and 6 for a pure 60% sugar solution (see Table 3.1)). It was found that the thrust per unit orifice area could be expressed as

$$\left\langle \frac{T}{\pi R_o^2} \right\rangle = 1.767 V_o^2 - 163.9 V_o \quad (4.2.4)$$

where $\left\langle \frac{T}{\pi R_o^2} \right\rangle$ is given in dyne/cm² and V_o in cm./sec. Similarly, the results of the combination of tests 12 and 15 showed that the thrust per unit orifice area for the 66-2/3% sugar solution could be expressed as

$$\left\langle \frac{T}{\pi R_o^2} \right\rangle = 1.8667 V_o^2 - 220.14 V_o \quad (4.2.5)$$

Figure (4.3) represents TN and $\langle TN \rangle$ for tests 12 and 15. The increased scatter in TN for lower velocities suggest that experimental

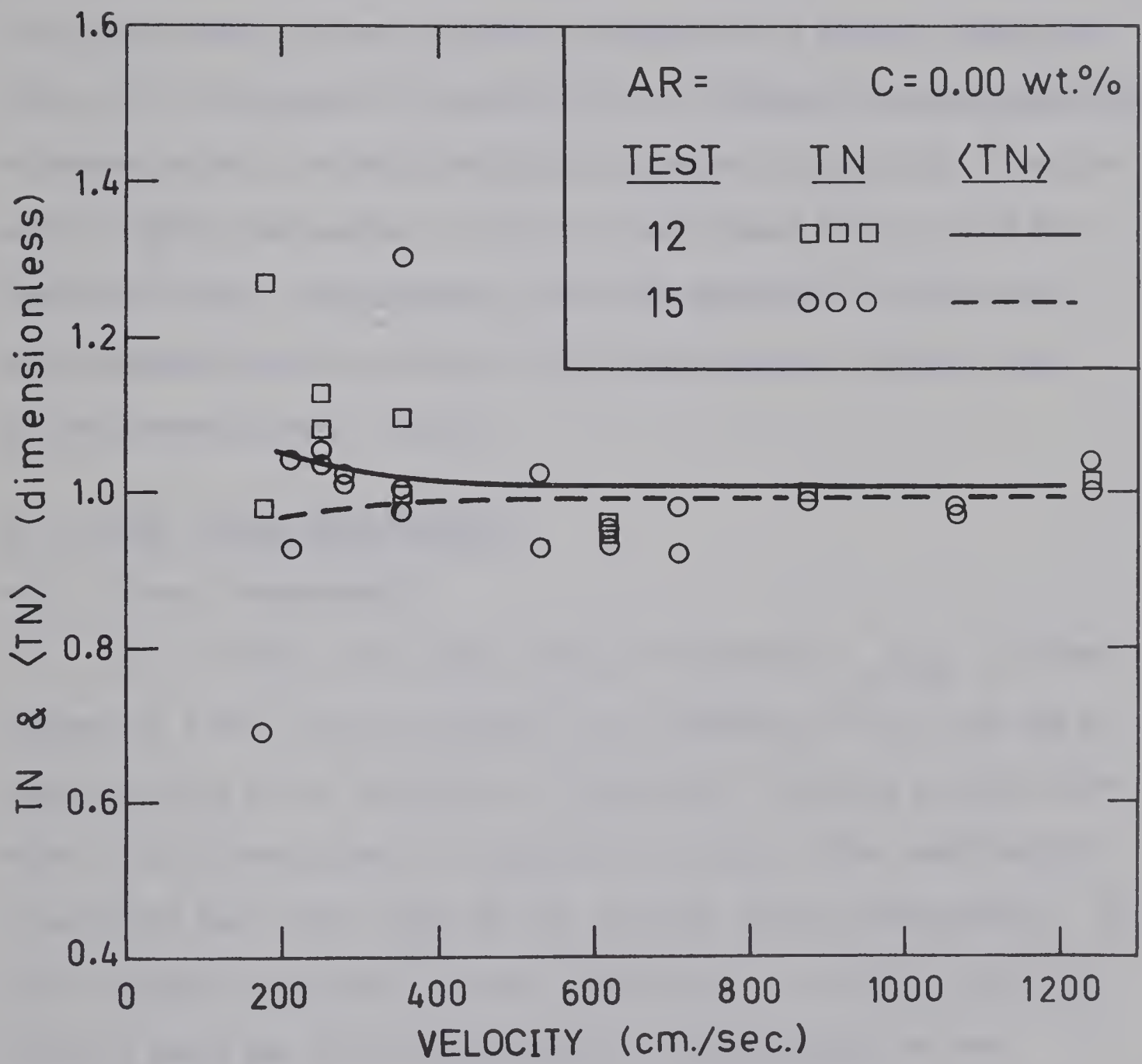


FIGURE (4.3)
NORMALIZED THRUST FOR TESTS 12 AND 15

uncertainty increases at lower velocities. This uncertainty was anticipated since the temperature sensitivity of the spring system made small measurements especially difficult. The apparent scatter in TN at high velocities, though regarded here as experimental uncertainty, can be qualified, in part, by the existence of an unusual behaviour which will be discussed in Section (4.4). Although the reproducibility of Newtonian data, at high velocities, appears to be within 1% on the basis of $\langle TN \rangle$, the scatter in TN is a less biased indicator of the reproducibility. Nevertheless, the close agreement of $\langle TN \rangle$ with unity demonstrates the utility of the least-squares smoothed data in the presentation of results.

4.3 FIBRE SUSPENSION BEHAVIOUR

4.3.1 Thrust Measurements

In principle, the normal stress difference, $S_{11} - S_{22}$, in fibre suspension flows can be calculated from Equations (2.2.8) and may be representative of an increase in elongational viscosity at high flowrates. Low flowrate data is essentially useless since experimental uncertainty masks the trends of the absolute thrust measurements. At high flowrates, the normal stress calculation is reliable only in a relative sense due to the uncertainty in the magnitude of the coefficient k_1' in Equation (2.2.14). In addition, the absence of deformation rate data leaves no convenient variable with which to correlate the normal stresses. Hence, the thrust data alone will qualitatively describe the increase in normal stress (or, equivalently, the elongational viscosity).

As noted in Section (4.2), the relatively small differences in thrust between Newtonians and fibre suspensions can be conveniently presented in terms of a normalized thrust, T_N . Since tests 2 to 6 were considered unreliable due to the uncertainty in sugar concentration, they will not be considered here except for test 3 which will serve as a comparison. The results of these tests have been normalized and appear, in normal form, in Appendix B. Test 8 was unsuccessful due to plugging. It was noted in Chapter III that the plugging itself was not a serious problem, however, a calibration change in the spring system resulted from the unplugging procedure. Tests 9 to 16 are considered reliable and will be discussed further.

Tests 9 to 16 and their least-squares representations were normalized with respect to Equation (4.2.5). Figures (4.4) to (4.9) depict T_N and $\langle T_N \rangle$ for tests 9 and 16, 10, 11, 13, 14 and 3 respectively. As in the case of the normalized Newtonian representation of Figure (4.3), the fibre results indicate increased scatter in T_N at lower velocities. The scatter is attributable to experimental uncertainty and to "partial-plugging" which was apparent only at the lower velocities. The "partial-plugging" became especially apparent for the longer fibres when the jet would not issue perpendicular to the orifice plate. This effect immediately disqualifies any correlation between "elastic" effects and behaviour of T_N or $\langle T_N \rangle$ at the lower velocities. The apparent scatter in T_N at higher velocities can, again, be qualified, in part, by an "unusual behaviour" which will be discussed later.

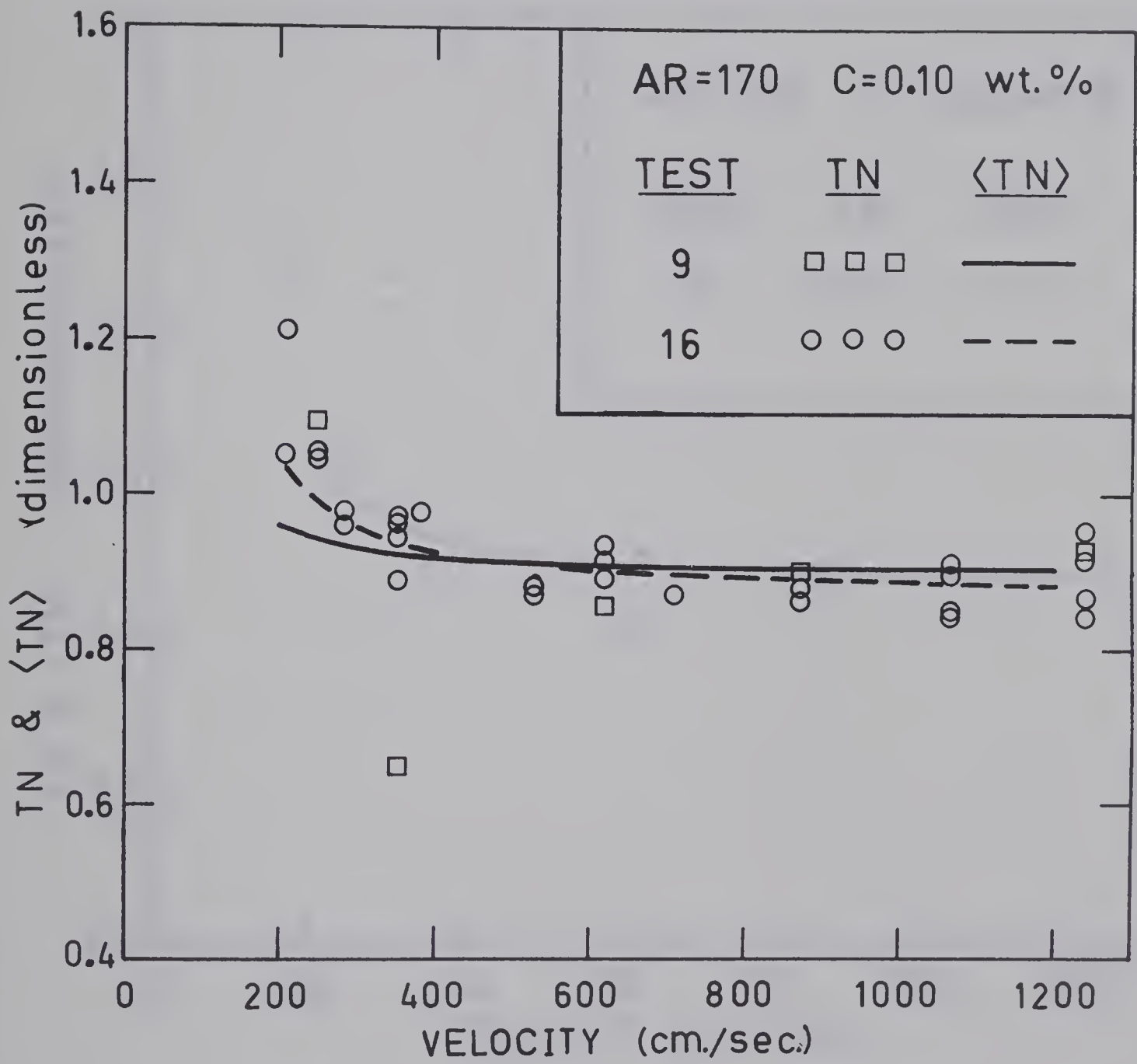


FIGURE (4.4)
NORMALIZED THRUST FOR TESTS 9 AND 16

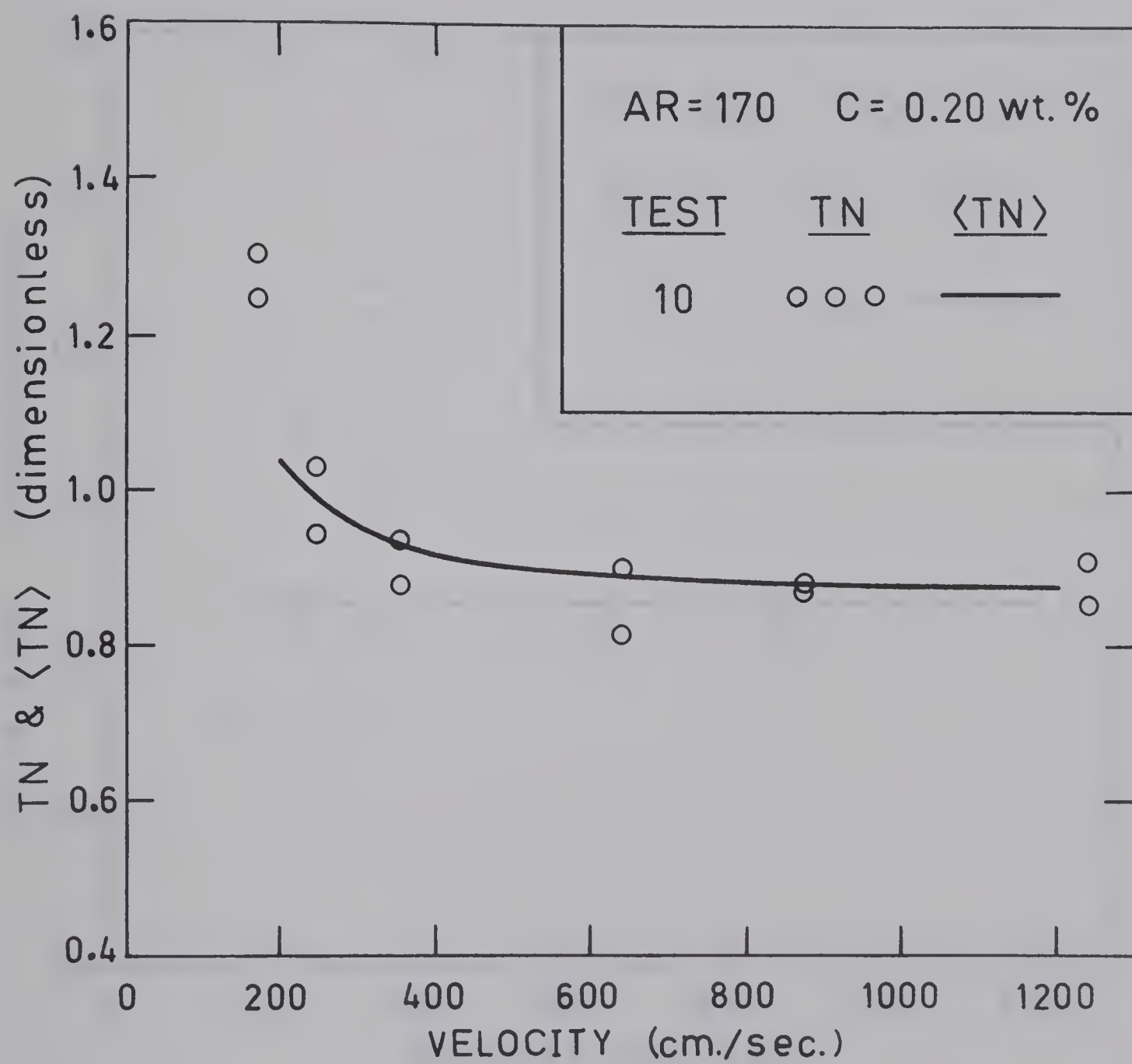


FIGURE (4.5)
NORMALIZED THRUST FOR TEST 10

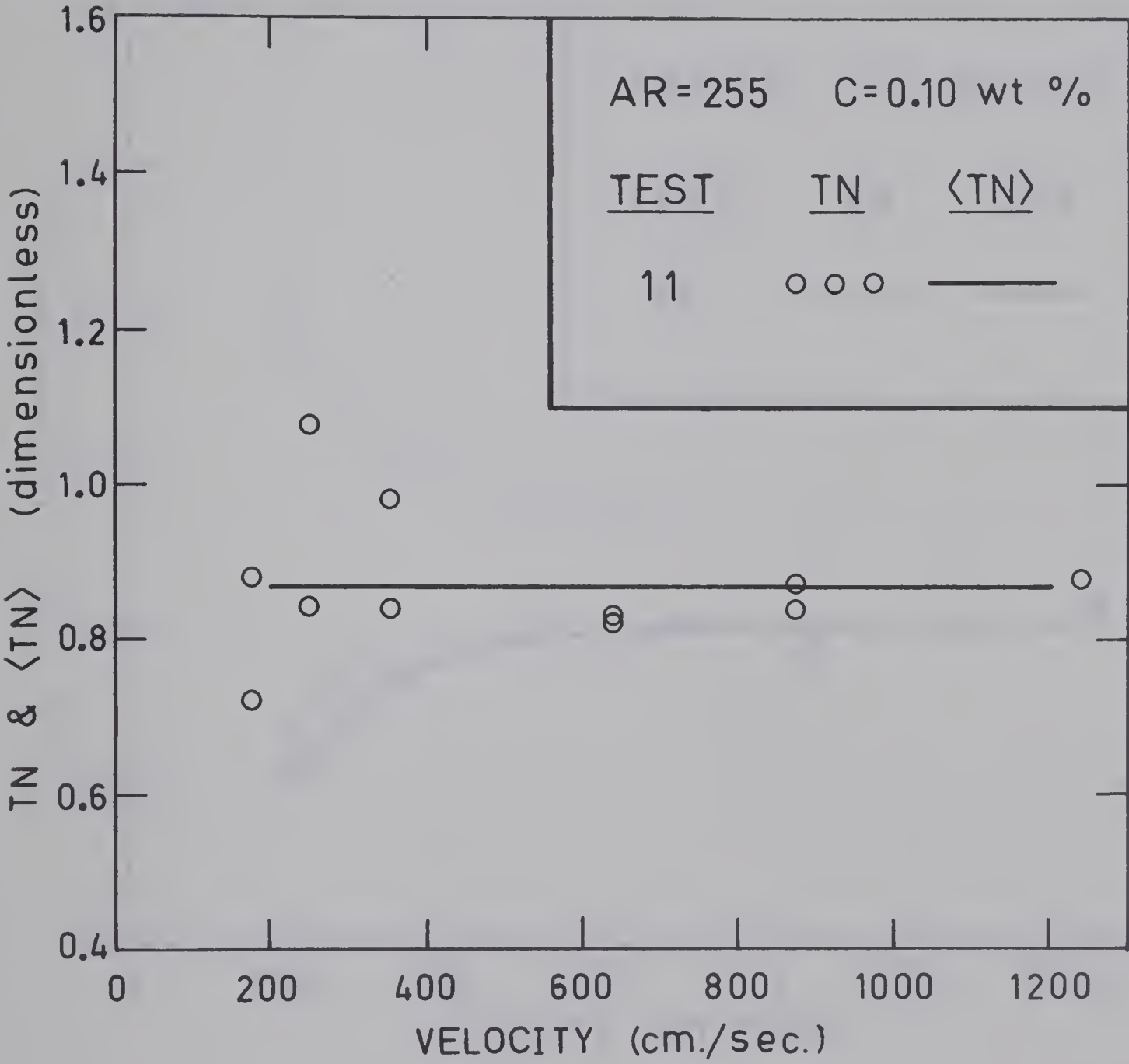


FIGURE (4.6)
NORMALIZED THRUST FOR TEST 11

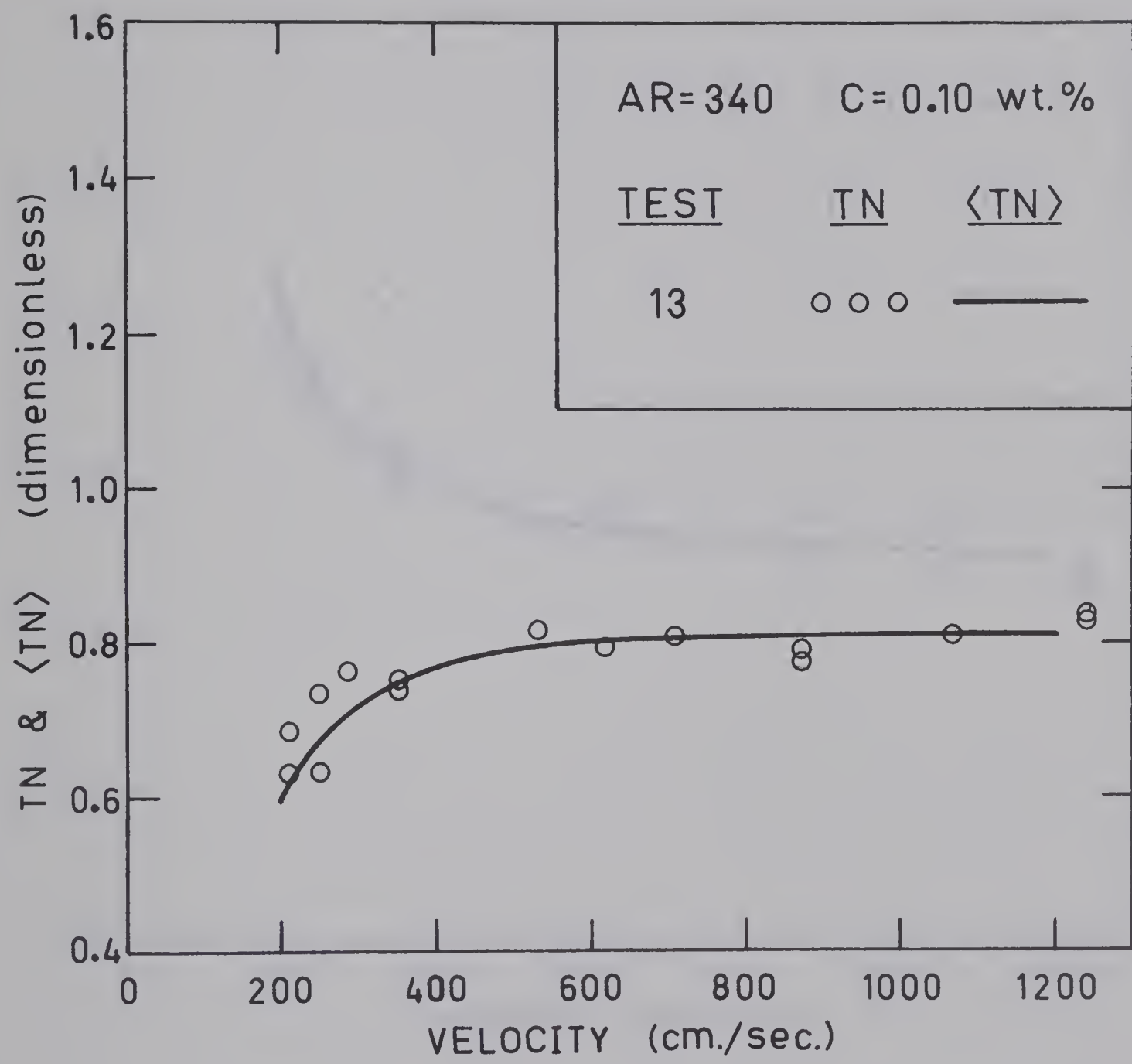


FIGURE (4.7)
NORMALIZED THRUST FOR TEST 13

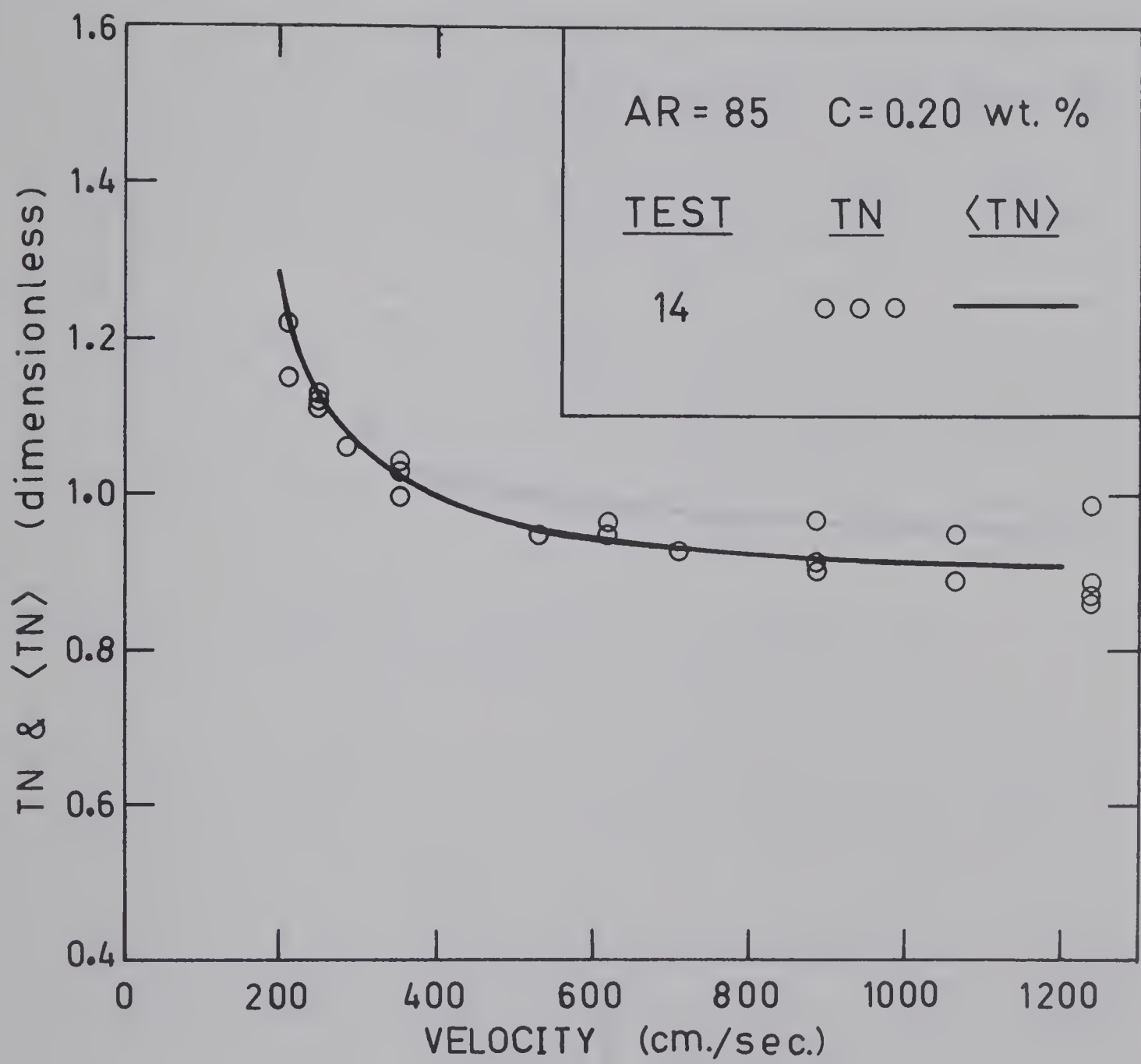


FIGURE (4.8)
NORMALIZED THRUST FOR TEST 14

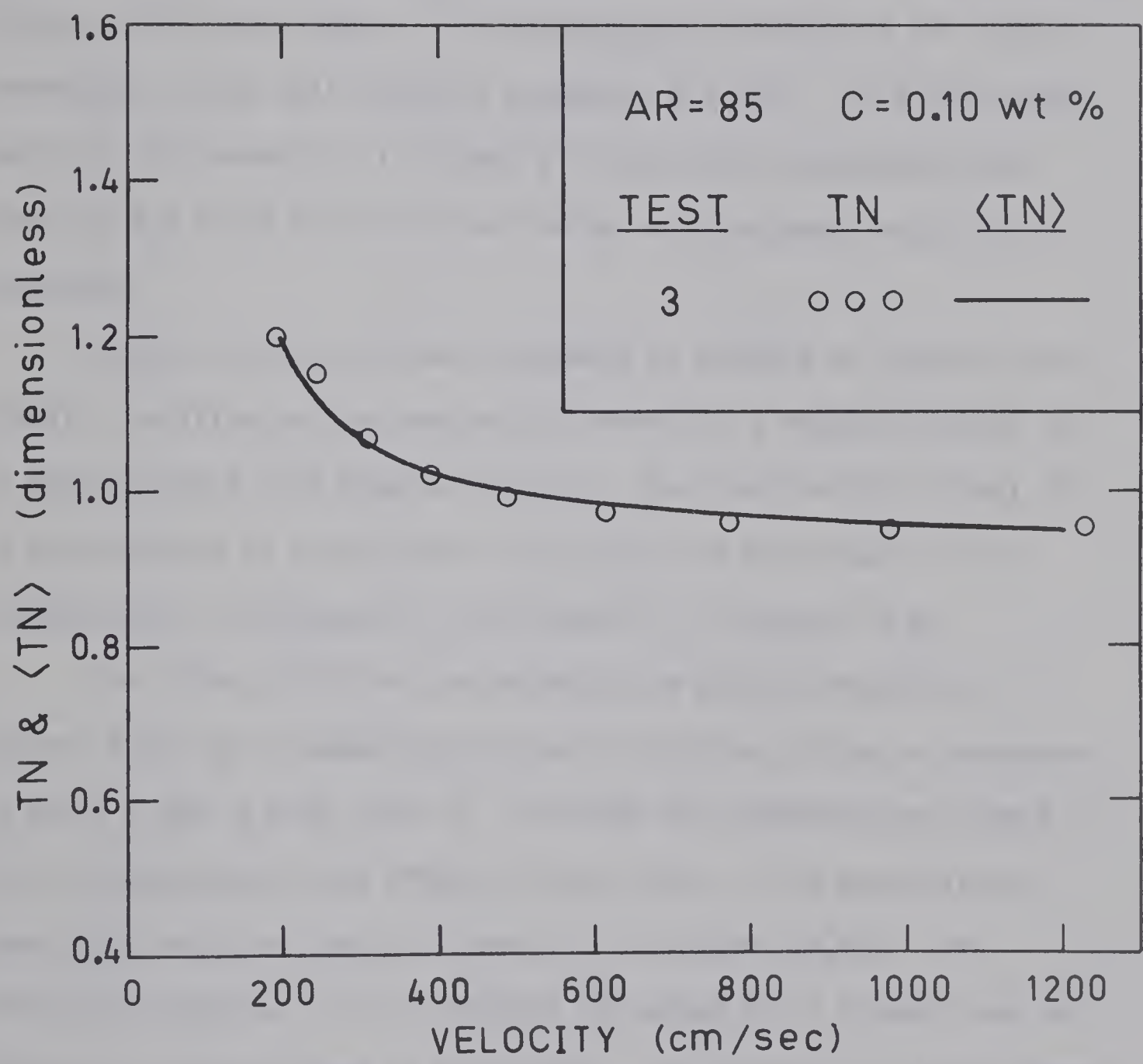


FIGURE (4.9)
NORMALIZED THRUST FOR TEST 3

Qualitatively, the data show a decrease in thrust, or, equivalently, increased normal stresses, with increasing fibre concentration and axis ratio, AR. The effect of AR on "elasticity" is depicted in Figure (4.10) with averaged normalized thrust curves from previous figures. Any bias inherent in the averaging criteria is of little consequence since only relative arguments are used. In other words, the bias (if present) will affect all the results essentially the same way and since only relative trends are expected, they will be preserved.

Except for test 16, which appears to exhibit an unusually low thrust, the effect of increasing axis ratio in a regular fashion is to reduce thrust in a regular fashion. The irregularity in test 16 is attributable to a consistent "unusually low behaviour". This irregularity is discussed, in more detail, in Section (4.4).

The effect of fibre concentration on $\langle TN \rangle$ is depicted in Figure (4.11) by a comparison of test 3 with test 14 and a comparison of tests 9 and 16 with test 10. Although the concentration effect is not as pronounced as the effect of axis ratio, it is qualitatively consistent with the theory of specific viscosity (39,40). In principle, Equation (2.2.14) defines the added axial stress (due to fibres) in orifice flows of suspensions. At present, it is not known whether the added stress is viscous or elastic in nature. This added stress, nevertheless, represents an increase in the elongational viscosity which, in terms of shear viscosity, is greater than the Newtonian value of 3μ . Estimates of elongational viscosities of the fibre suspensions are presented in the following section.

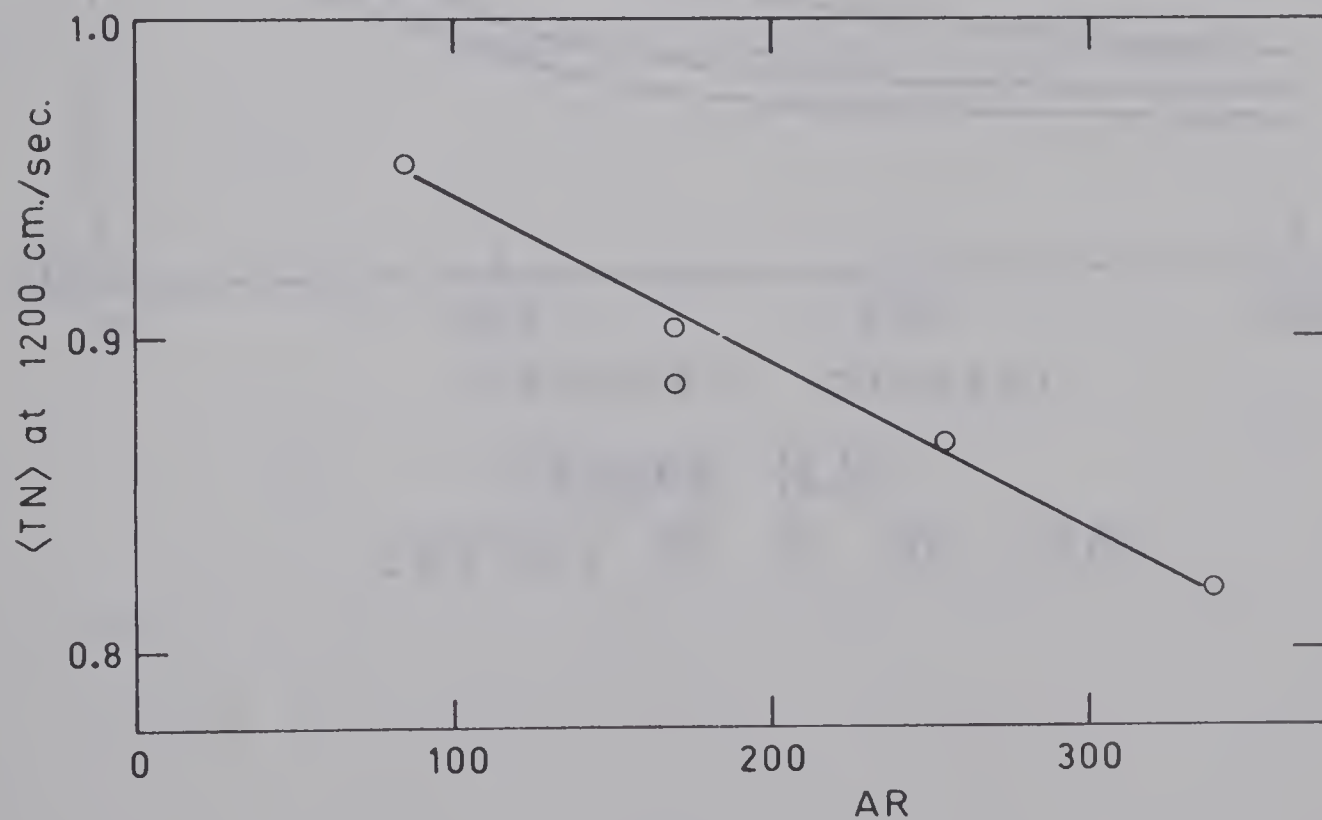
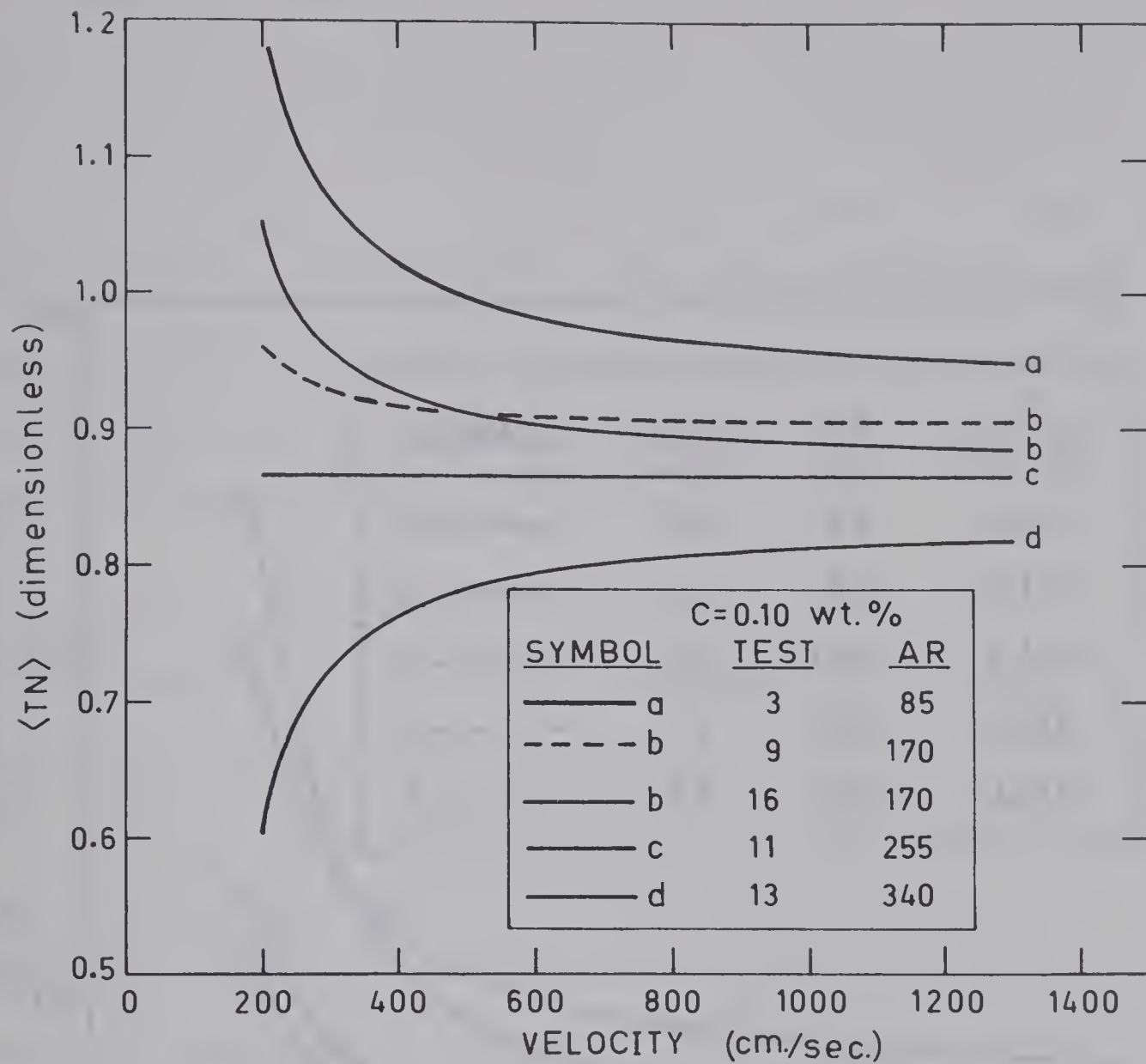


FIGURE (4.10)
EFFECT OF AR ON $\langle TN \rangle$

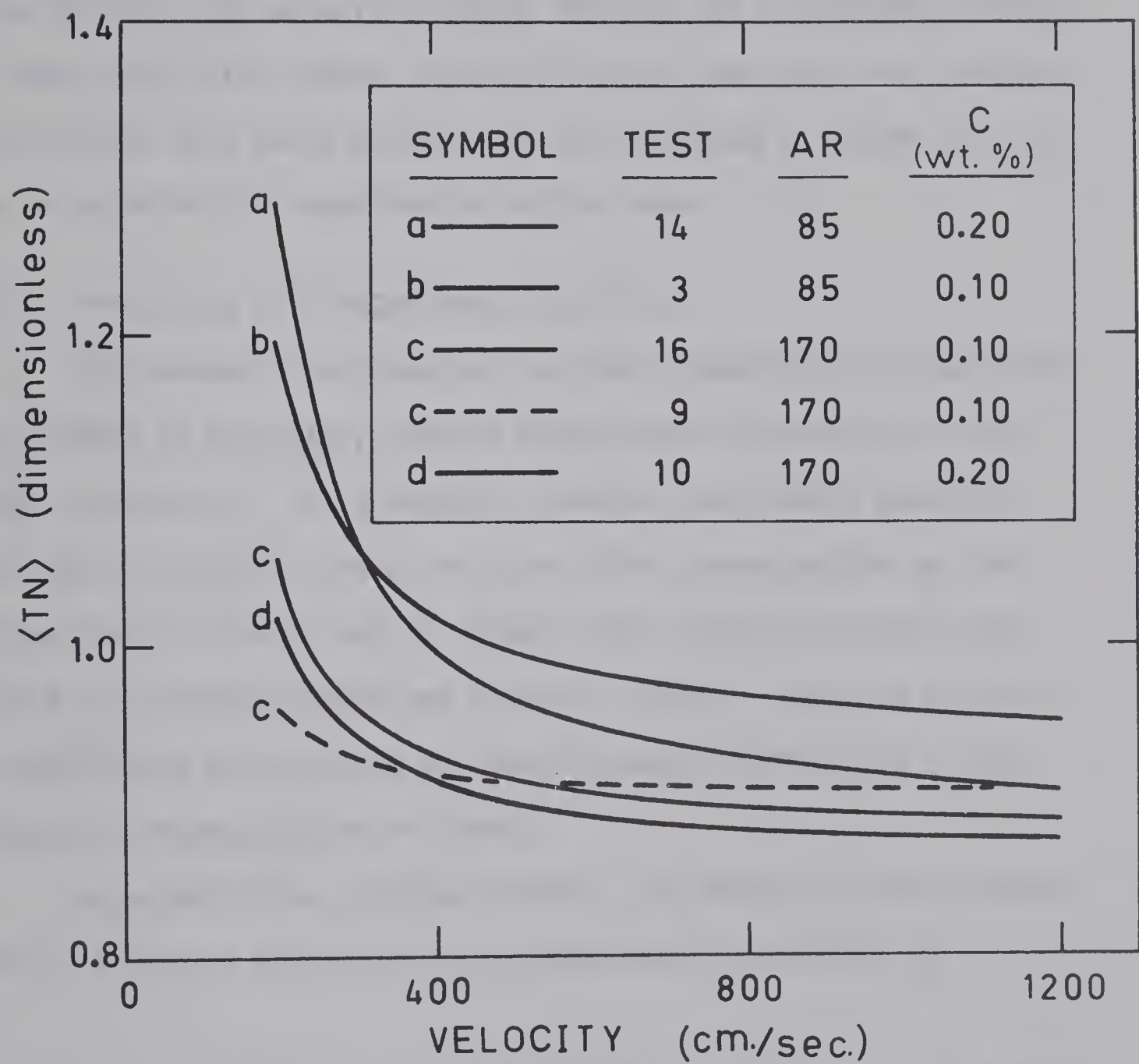


FIGURE (4.11)
EFFECT OF C ON <TN>

A comparison of the contraction coefficients for the fibre suspensions with the Newtonian suspending medium is depicted in Figure (4.12). The comparison merely indicates that the pressure drop for a given flowrate of suspension is approximately the same as the Newtonian value for the high velocities where the data are considered reliable. At lower velocities, where "partial-plugging" may have been present, the pressure drop would be too high (as indicated in Figure (4.12)), due to an effective reduction in orifice area.

4.3.2 Prediction of Elongational Viscosity

The absence of deformation rate data immediately disqualifies any attempt to accurately predict elongational viscosities of the fibre suspensions. It is possible, however, to crudely show the qualitative effects of axis ratio and fibre concentration on the elongational viscosity and to compare these effects to those predicted by Takserman-Krozer and Ziabicki (39,40). This can be done by numerically manipulating the least-squares coefficients of the polynomial representation of thrust.

As noted in the previous section, the thrust per unit orifice area of a viscous Newtonian can be adequately represented by

$$\frac{T}{\pi R_o^2} = [k_1] V_o^2 - [k_2] V_o \quad (4.3.6)$$

The equivalent thrust equation for a suspension of fibres is given by

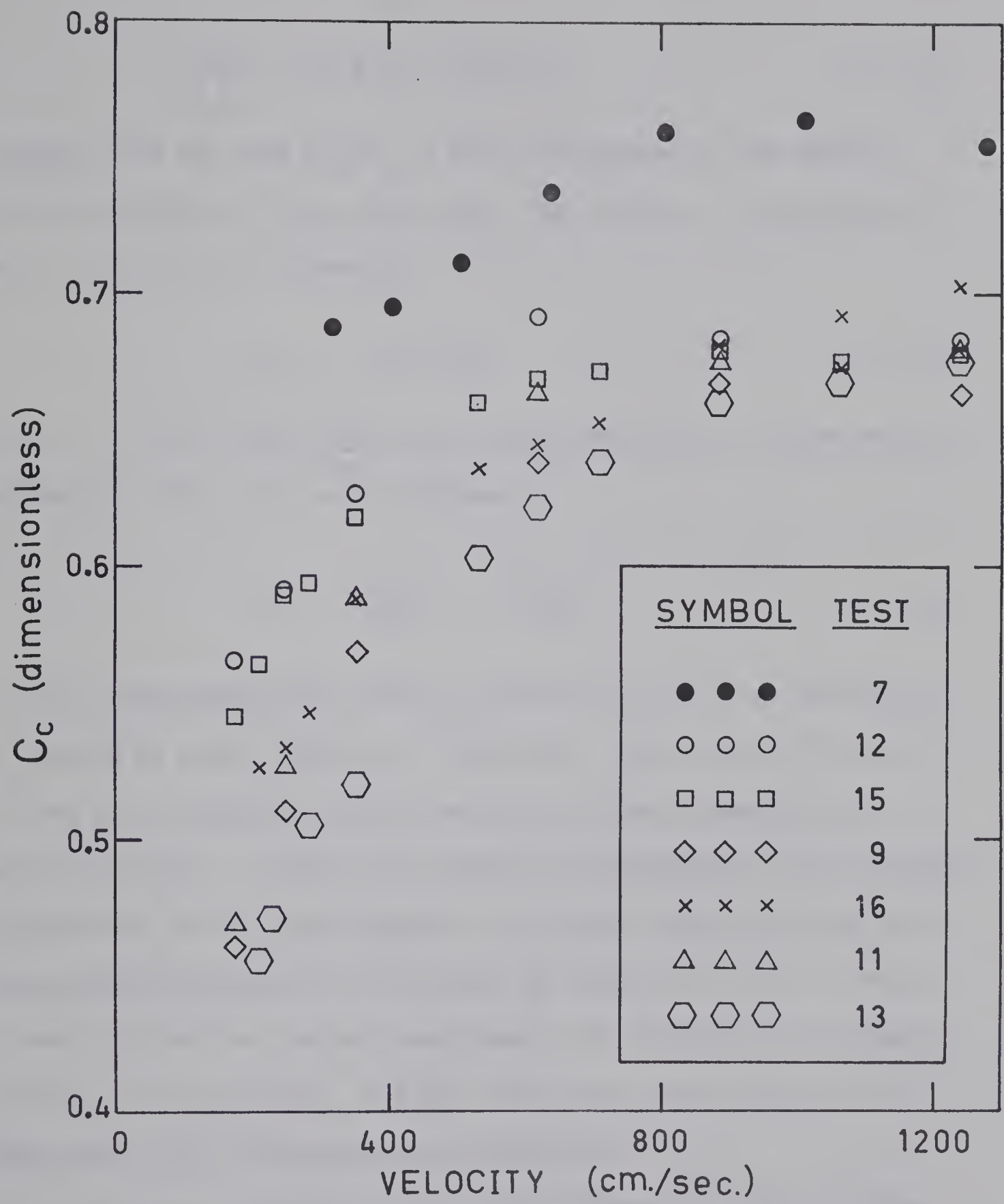


FIGURE (4.12)
COMPARISON OF CONTRACTION COEFFICIENTS

$$\frac{T}{\pi R_0^2} = [k_1'] V_0^2 - [k_2'] V_0 \quad (4.3.7)$$

Assuming that the term $[k_2]V_0$ is truly indicative of the tensile stresses developed in the extensional flow field, a "representative" axial stress $\{\tau_{11}\}$ is given by

$$\{\tau_{11}\} = [k_2] V_0 \quad (4.3.8)$$

Since $\eta = 3\mu$ for three-dimensional Newtonians (27), a "representative" deformation rate, $\{\dot{\epsilon}\}$, can be defined as

$$\{\dot{\epsilon}\} = \frac{\{\tau_{11}\}}{3\mu} = \frac{k_2 V_0}{3\mu} \quad (4.3.9)$$

The term "representative" refers to numerically relative quantities as opposed to actual physical quantities, since the coefficients of V_0^2 and V_0 in Equations (4.3.6) and (4.3.7) have essentially no analytical basis. In fact, the Newtonian deformation rates calculated via Equation (4.3.9) (see Appendix D) are much larger than the maximum possible deformation rate defined by Equations (2.2.4). Hence, in order to preserve further development from becoming an arithmetic exercise, it is necessary to place some severe restrictions on the magnitudes of the representative quantities.

As noted in Section (2.2.1), the deformation rates of fibre flows are expected to be somewhat lower than those of Newtonian flows. However, since the actual deformation rates are unknown, the most conservative estimates will be the "representative" Newtonian values

given by Equation (4.3.9). Qualitative examination of the unconstrained least-squares coefficients, $[k'_1]$ and $[k'_2]$ of all the reliable tests performed in this study (see Table (D-1)) indicate the following:

- i) $[k'_1]$ is a decreasing function of the fibre concentration and axis ratio as surmised in Section (2.2.2).
- ii) Numerically, the magnitude of $[k'_2]$ is very sensitive to the magnitude of $[k'_1]$.

Hence, in order to scale $[k'_2]$ to the order of the Newtonian representation, $[k_2]$, a constrained least-squares regression was performed by using the Newtonian $[k_1]$ to fit the fibre data in the form

$$\left[\frac{T}{\pi R_o^2} - [k_1] v_o^2 \right] = [k'_{2R}] v_o \quad (4.3.10)$$

In this case, a Type II fit, which weights points at high velocity, best represented the data and it was used rather than a Type III (see Appendix C). The "representative" elongational viscosity, $\{\eta\}$, of the suspensions can be calculated from

$$\{\eta\} = \frac{[k'_{2R}]}{[k_2]} (3\mu)_{\text{NEWT.}} \quad (4.3.11)$$

Results of these calculations are presented, in detail, in Appendix (D) and summarized in Figure (4.14).

The results depicted in Figure (4.14) indicate that the "representative" elongational viscosities are much lower than the limiting case of Takserman-Krozer et al for $\alpha = \infty$, which is expected

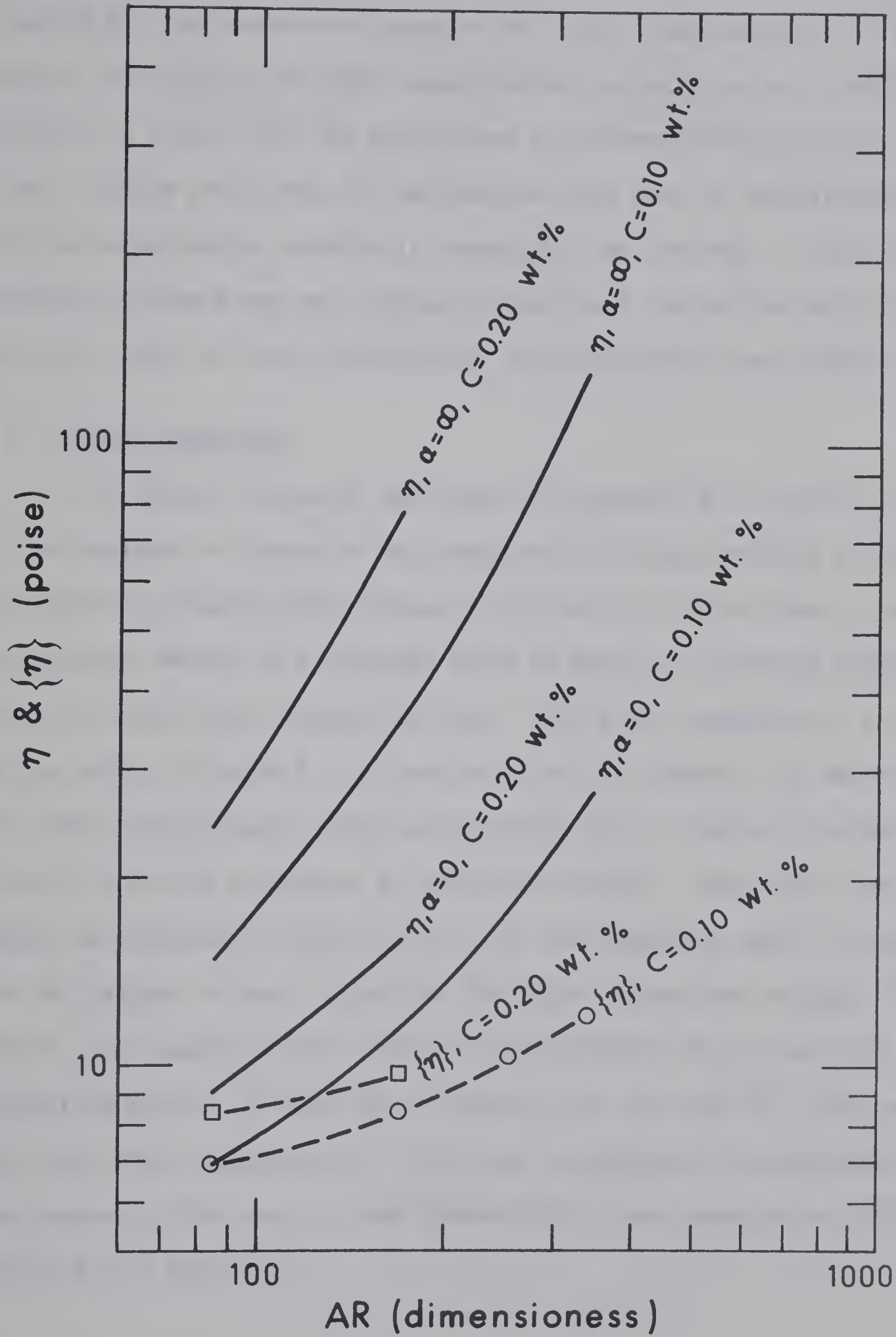


FIGURE (4.13)
COMPARISON OF "REPRESENTATIVE" AND
THEORETICAL ELONGATIONAL VISCOSITIES

to apply for the suspensions used in this study (see Section (1.2.3)). However, the effects of fibre concentration and axis ratio is qualitatively in accord with the predictions of Takserman-Krozer et al. It may also be noted that the deformation rate used in calculating $\{\eta\}$ from the experimental results is expected to be too high. A less conservative estimate may well define elongational viscosities which could be of the order of those predicted by Takserman-Krozer and Ziabicki.

4.4 UNUSUAL BEHAVIOUR

The unusual behaviour mentioned in Sections (4.1) and (4.2) refers to the apparent existence of two steady-state thrust profiles with two corresponding steady-state pressure profiles for orifice flows. Here, steady-state refers to a recorder trace of thrust or pressure which remains constant with respect to time. This effect appeared at random in the series of tests 6 to 16 and could not, in general, be duplicated. The "twin steady-state" effect was observed from a typical recorder trace of pressure and thrust at constant flowrate. This effect was noted, as depicted in Figure (4.14), for the Newtonian case in test 6, for the polymer in test 7, and for the fibre suspensions in tests 14 and 16. An example of this effect, when presented on the basis of a normalized thrust, is depicted in Figure (4.4) for test 16. The cases where the "twin steady-state" effect was experimentally encountered are denoted in the results (see Appendix B) by two consecutive entries labelled "LO" and "HI".

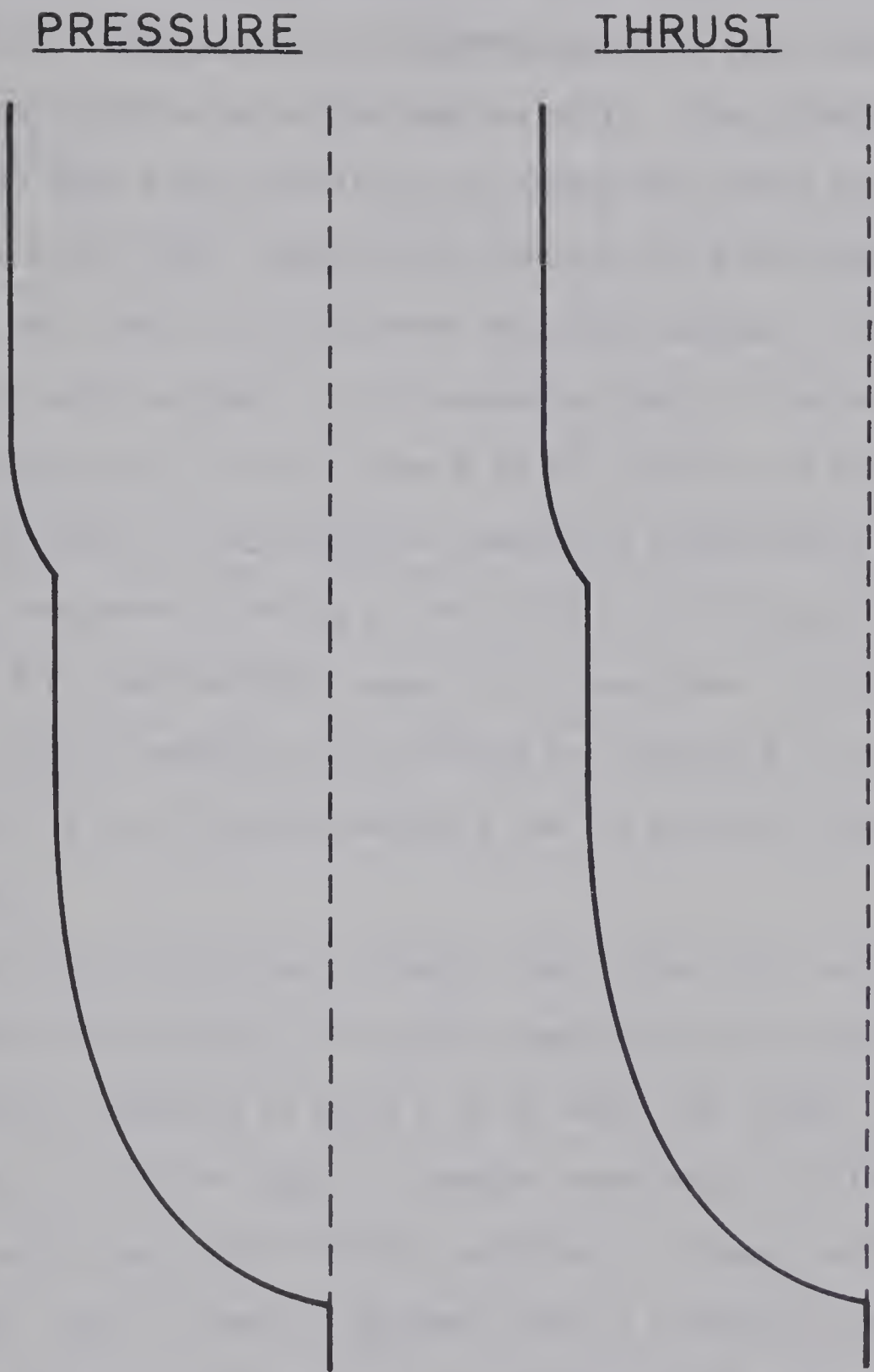


FIGURE (4.14)
TYPICAL RECORDER TRACE OF
"UNUSUAL BEHAVIOUR"

In terms of measured thrust, the lower steady-state value at a jet velocity of 1242 cm./sec. is approximately 14% lower than the higher steady-state value at the same velocity. The difference in $\langle TN \rangle$ between test 9 and test 16 can be explained on this basis. In test 9, where the "twin steady-state" behaviour did not appear, apparently only the high values were recorded, whereas, in test 16, both effects were recorded. It is suspected that this behaviour may have occurred in all the tests from 6 to 16, but did not display this behaviour directly by providing two concurrent steady-state pressure and thrust measurements during a particular run. The results depicted in Figure (4.8) qualitatively support this suspicion. Occasions where the unusual behaviour was observed are indicated in the data (see Appendix B) by LO and HI denoting the low and high values respectively.

The origin of the "twin steady-state" effect for orifice flows is presently not understood, hence the observations are noted. Since this effect was observed in tests 6 to 16 where the larger diameter (0.1477 cm.) orifice was used, a diameter dependence is evident. When the "twin steady-state" effect occurred, it always went from low to high. Also, it may be apparent that if a constant pressure feed device is used and flowrates are determined by sampling over a time interval, an observation of the "twin steady-state" effect is very unlikely. These observations may be useful in guiding future experimental study of this phenomena.

CHAPTER V

CONCLUSIONS AND RECOMMENDATIONS

5.1 CONCLUSIONS

Thrust measurements on orifice jets of viscous Newtonian showed abnormal thrust reduction at low orifice velocities. At higher velocities, the viscous thrust per unit area asymptotically approached the thrust per unit area of low viscosity Newtonians. An attempt to relate the abnormal thrust reduction to the high tensile stresses developed in orifice flows was not entirely successful. Although the profile relaxation-surface tension effect common to capillary flows may apply to orifice flows, the thrust reduction for Newtonians was not investigated in sufficient detail to verify this argument.

The viscous Newtonian thrust data were used as a basis for comparison with the suspension thrusts. Orifice jets of fibre suspensions exhibited significantly lower thrusts than the viscous Newtonian at a given velocity. This thrust reduction became more pronounced with increasing axis ratio and/or fibre concentration. If thrust reduction is regarded as an increase in the axial stresses developed in orifice flows, the increased axial stress, due to the presence of fibres, can be related to the elongational deformation rate by means of an elongational viscosity. Conservative estimates of the elongational viscosities are qualitatively consistent with the specific elongational viscosity theory of Takserman-Krozer and Ziabicki. Stronger statements than this are presently impossible owing to the uncertainty in the velocity field.

Qualitative observations have been made of a twin steady-state behaviour in orifice flows. At present, no explanation is available for this phenomena. Although the twin steady-state behaviour, as well as the need for local velocity measurements complicate the analysis of orifice jet thrust measurements, the orifice jet thrust technique may become a useful tool in non-shearing rheological studies.

5.2 RECOMMENDATIONS

The most important recommendations are those directed towards improving the equipment used in this study. The suggested improvements include the following:

- i) Temperature sensitivity of the spring system could be reduced by minimizing the bulk of the orifice reservoir. If this modification does not reduce the temperature sensitivity appreciably, it may be necessary to rebuild the entire spring system. In case reconstruction is required, it is suggested that only one material, preferably mild steel, be used throughout.
- ii) Overall noise in the spring system (vibrations) could be reduced by separating the spring leaves to a distance in the order of 9 inches. Small torsional displacements in the axis of the spring leaves were noted with the present (heavy) reservoir and leaf separation of 5-3/4 inches. Addition of a damping system, which is more sophisticated than the present viscous dashpot, would complete the task

of reducing the noise level.

- iii) A reservoir with a flush-mounted pressure transducer would eliminate the present bother with bleeding the pressure transducer signal line.

The recommendations for future study of suspensions in orifice flows are:

- i) Plugging or fibre aggregation is directly related to fibre concentration, fibre axis ratio, and absolute particle size, and inversely related to orifice size, suspending medium viscosity and fluid velocity. Hence, problems with plugging or fibre aggregation, at a given fibre axis ratio and concentration can be minimized by observing the following guidelines:
 - (a) using fibres of minimum thickness
 - (b) increasing orifice size
 - (c) increasing viscosity of suspending medium
 - (d) increasing fluid velocity
- ii) The use of sugar solutions as a suspending medium for fibres provides a convenient method for suspension preparation since the fibres can be easily dispersed in water, and viscosity can be adjusted by addition of sugar after dispersion is complete. At high sugar concentrations, however, the suspending medium viscosity is very sensitive to small changes in sugar concentration. It is suggested, therefore, that viscosity measurements be made to ensure reproducibility.

- iii) Since orifice flows of viscous media are prone to a twin steady-state behaviour, the use of a positive displacement pump is imperative.

BIBLIOGRAPHY

1. Aude, T.C., Cowper, N.T., Thompson, T.L. and Wasp, E.J., Chem. Eng. J., June, 74, (1971).
2. Bagley, E.B. and Duffy, H.J., Trans. Soc. Rheol., 14:3, 409, (1970).
3. Ballman, R.L., Rheol. Acta, 4, 137, (1965).
4. Beckett, R. and Hurt, J., "Numerical Calculations and Algorithms", Chapter 8, McGraw-Hill Book Company, New York, 1966.
5. Bird, R.B., Stewart, W.E. and Lightfoot, E.N., "Transport Phenomena", Chapter 7, John Wiley and Sons Inc., New York, 1966.
6. Blakney, W.R., J. Col. and Int. Sci., 22, 324, (1966).
7. Bugliarello, G. and Daily, J.W., TAPPI, 44, No. 7, 497, (1961).
8. Bugliarello, G. and Daily, J.W., TAPPI, 44, No. 12, 881, (1961).
9. Carter, T.R., Ph.D. Thesis, Dept. of Chem. Eng., The University of Utah, 1969.
10. Deletko, P.J., Ph.D. Thesis, The Graduate School of Maine, 1969.
11. Einstein, A., "Investigations on the Theory of Brownian Movement", Methuen and Co. Ltd., London, 1926.
12. Forgacs, O.L. and Mason, S.G., J. Col. Sci., 14, 457, (1959).
13. Forgacs, O.L. and Mason, S.G., J. Col. Sci., 14, 473, (1959).
14. Fredrickson, A.G., "Principles and Applications of Rheology", Chapter 9, Prentice-Hall Inc., New Jersey, 1964.
15. Goldsmith, H.L. and Mason, S.G., in "Rheology", Vol. IV, Chapter 2, Eirich, Ed., Academic Press, New York, 1967.
16. Graessly, W.W., Glasscock, S.D. and Crawley, R.L., Trans. Soc. Rheol., 14:4, 519, (1970).
17. Han, C.D. and Charles, M., Trans. Soc. Rheol., 14:3, 409, (1970).
18. Hlavacek, B., Private Communication.
19. Jeffrey, G.B., Proc. Roy. Soc. (London), A102, 161, (1922).

20. Jenson, V.G., and Jeffreys, G.V., "Mathematical Methods in Chemical Engineering", Chapter 10, Academic Press Inc. (London), 1963.
21. Kerekes, R.J.E., Ph.D. Thesis, Department of Chem. Eng., McGill University, Montreal, 1970.
22. Lamb, H. "Hydrodynamics", page 99, First American Edition, Dover, 1945.
23. Metzner, A.B., A.I.Ch.E. J., 13, 316, (1967).
24. Metzner, A.B., Trans. Soc. Rheol., 13, 467, (1969).
25. Metzner, A.B. and Metzner, A.P., Rheol. Acta, 9, 174, (1970).
26. Metzner, A.B., Uebler, E.A. and Chan Man Fong, C.F., A.I.Ch.E. J., 15, 750, (1969).
27. Middleman, S., "The Flow of High Polymers", Interscience Publishers, New York, 1968.
28. Middleman, S. and Gavis, J., Phys. Fluids, 4, No. 3, 355, (1961).
29. Nawab, M.A. and Mason, S.G., J. Phys. Chem., 62, 1248, (1958).
30. Perry, R.H., Chilton, C.H. and Kirkpatrick, S.D., "Chemical Engineers Handbook", Fourth Edition, Chapter 3, McGraw-Hill Book Company, New York, 1963.
31. Robertson, A.A. and Mason, S.G., TAPPI, 40, No. 5, 326, (1957).
32. Rollin, A.L., Ph.D. Thesis, Department of Chem. and Pet. Eng., University of Alberta, 1971.
33. Roscoe, R., J. Fluid Mech., 28, Part 2, 273, (1967).
34. Rudd, M.J., Private Communication.
35. Seyer, F.A., Ph.D. Thesis, The University of Delaware, 1967.
36. Seyer, F.A. and Metzner, A.B., Can. J. Chem. Eng., 45, 121, (1967).
37. Seyer, F.A. and Metzner, A.B., A.I.Ch.E. J., 15, 426, (1969).
38. Sokolnikoff, I.S. and Redheffer, R.M., "Mathematics of Physics and Modern Engineering", Chapter 10, Second Edition, McGraw-Hill Book Company, New York, 1966.

39. Takserman-Krozer, R. and Ziabicki, A., J. Polymer Sci., 1, 491, (1963).
40. Takserman-Krozer, R. and Ziabicki, A., J. Polymer Sci., 1, 507, (1963).
41. Uebler, E.A., Ph.D. Thesis, Department of Chemical Engineering, The University of Delaware, 1966.
42. Wang, Y.T. and Longwell, P.A., A.I.Ch.E. J., 10, 323, (1964).
43. Weast, R.C., Selby, S.M. and Hodgman, C.D., "Handbook of Chemistry and Physics", 41st Edition, Chemical Rubber Company, Ohio, 1959.
44. Whitaker, S., "Introduction to Fluid Mechanics", Chapter 8, Prentice-Hall Inc., New Jersey, 1968.

APPENDIX A

CALIBRATIONS

FLOWRATE CALIBRATION

Since both pumping systems used in this study were positive displacement and could be set at discrete speeds, flow calibration was a simple matter of relating flowrate to pump speed. For both systems, calibration was accomplished by direct weighing of a fluid sample over a known time interval. For the Instron pumping system, flowrates could also be calculated since both piston speed and cylinder diameter were accurately known. Results for the Zenith metering pump system are tabulated in Table (A-1) and plotted in Figure (A-1). Figure (A-1) shows that the deviation of individual flowrates from their linear representation is typically less than $\pm 1\%$. Calculated and calibrated flowrates for the Instron pumping system are tabulated in Table (A-2). The calibrated flowrates are consistently 1% lower than the calculated flowrates, probably as a result of inaccuracies in the calibration procedure. The calculated flowrates were arbitrarily used in determining the velocities for tests 8 to 16 where the Instron pumping system was used.

TABLE A-1ZENITH PUMP FLOWRATE CALIBRATION

Fluid: 64% sugar solution

Density: 1.30 gm./cc.

<u>Run</u>	<u>Pump Speed</u>	<u>Delivery Pressure (kdyne/cm²)</u>	<u>Fluid Mass (gm.)</u>	<u>Time (sec.)</u>	<u>Flowrate (cc./sec.)</u>
1	11.38	107	200	140.3	1.097
2	14.33	161	194	102.8	1.452
3	18.04	226	198	87.1	1.749
4	22.71	339	208	73.1	2.190
5	28.60	484	218	61.3	2.737
6	36.00	709	204	45.4	3.458
7	45.32	1060	609	107.4	4.364
8	45.32	1060	210	37.0	4.368
9	57.06	1610	658	92.2	5.492
10	71.83	2380	699	77.4	6.950
11	90.43	3490	749	66.2	8.707

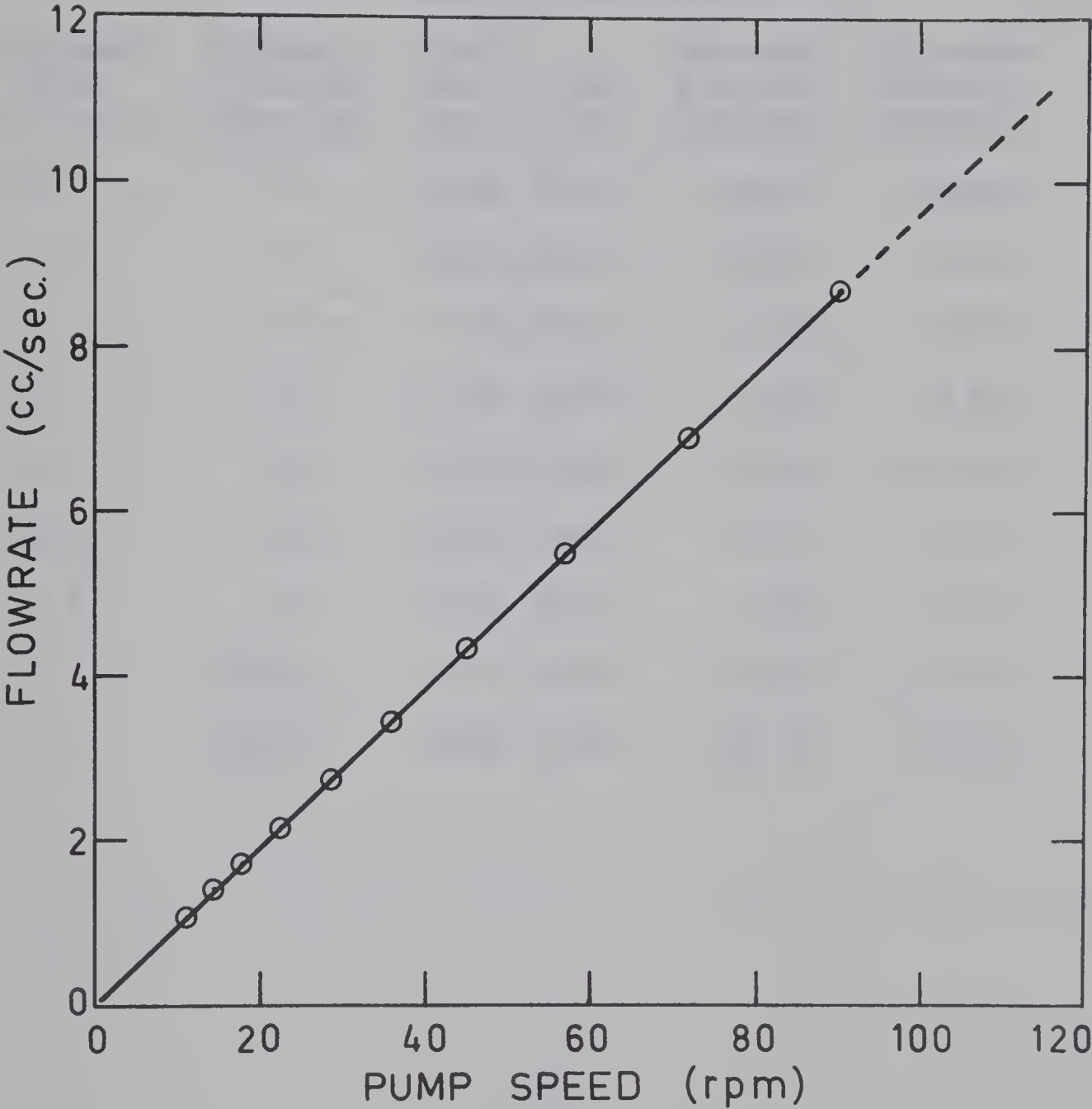


FIGURE (A-1)
ZENITH GEAR PUMP FLOWRATE CALIBRATION

TABLE (A-2)INSTRON FLOWRATE CALIBRATION

Fluid: Water
Density: 0.997 gm./cc.

Run	Crosshead Speed (cm./min.)	Delivery Pressure ₂ (kdyne/cm. ²)	Fluid Mass (gm.)	Time (sec.)	Measured Flowrate (cc./sec)	Calculated Flowrate (cc/sec)
1	10	0	3374	112.0	30.21	30.40
2	5	0	3033	201.2	15.12	15.20
3	2	0	1108	184.6	6.02	6.08
4	1	0	1124	374.6	3.01	3.04
5	7	0	3167	150.1	21.16	21.28
6	3.5	0	2082	198.0	10.54	10.64
7	1.4	0	1247	296.7	4.24	4.26
8	7	7000	2515	119.0	21.19	21.28
9	5	7000	2500	165.4	15.16	15.20

PRESSURE TRANSDUCER CALIBRATION

Pressure transducer calibration was accomplished by comparing amplifier output of the pressure transducer signal, to manometer reading. In order to cover the entire range of pressures encountered experimentally, two manometers were used; one containing mercury (S.G. = 13.53) (30), and one containing water (S.G. = 0.997) (30). Tables (A-3) and (A-4) represent the mercury and water data respectively. These results, which represent three ranges in transducer response, appear graphically in Figures (A-3), (A-4) and (A-5). For each range, the pressure can be expressed as a linear function of amplifier output. These linear expressions and their ranges of applicability are as follows:

$$\begin{array}{ll} P = 5.215 V & (0 \leq V \leq 40) \\ P = 9.00 + 4.96 V & (40 \leq V \leq 180) \\ P = 5.05 V & (180 \leq V \leq 600) \text{ (A-1)} \end{array}$$

where P is the pressure in kdyne/cm^2 , and V is amplifier output in arbitrary units.

TABLE A-3
PRESSURE TRANSDUCER CALIBRATION

Run	Pressure (inches Hg)	Pressure (kdyne/cm ² .)	Voltage (arbitrary units)
1	79.0	2665	528
2	76.8	2590	512
3	72.8	2460	486
4	67.2	2270	454
5	61.9	2090	414
6	59.1	1993	394
7	57.0	1923	382
8	48.0	1620	324
9	44.6	1503	300
10	41.5	1400	280
11	39.6	1337	268
12	37.4	1262	252
13	35.4	1194	238
14	33.4	1127	223
15	29.4	992	196
16	27.2	918	183
17	24.5	826	165
18	23.35	787	157
19	22.30	753	150
20	19.60	661	133
21	18.10	611	119
22	16.80	567	112
23	15.65	528	103
24	12.85	434	85.5
25	12.40	418	82.5
26	11.30	381	75.5
27	10.35	349	68.5
28	9.25	312	62.0
29	8.10	273	52.8
30	7.65	258	49.6
31	6.30	212	41.4
32	5.50	185.4	36.6
33	4.60	155.2	30.4
34	3.95	133.2	25.6
35	2.65	89.5	17.2

TABLE A-4
PRESSURE TRANSDUCER CALIBRATION

Run	Pressure (inches H ₂ O)	(kdyne/cm. ²)	Voltage (arbitrary units)
1	3.20	7.96	1.51
2	6.10	15.18	2.84
3	10.25	25.5	4.72
4	13.4	33.3	6.35
5	15.4	38.4	7.30
6	22.4	55.6	10.50
7	26.2	65.0	12.2
8	31.3	77.9	14.9
9	38.3	95.4	18.3
10	50.4	125.3	23.6
11	58.4	145.2	28.6
12	69.4	173	33.4
13	73.3	182	35.0
14	78.4	195	37.4
15	80.5	200	38.6

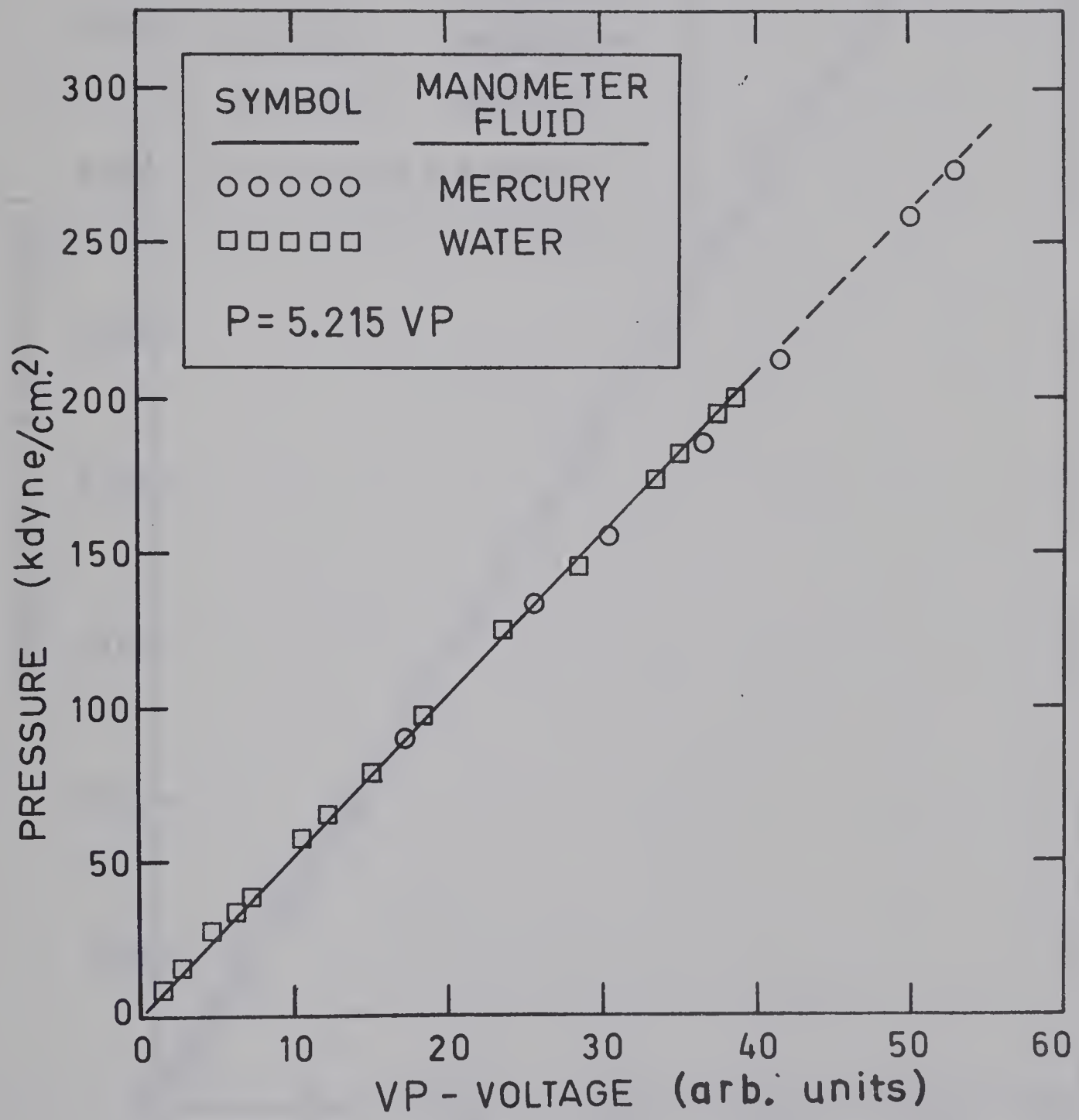


FIGURE (A-3)
PRESSURE TRANSDUCER CALIBRATION

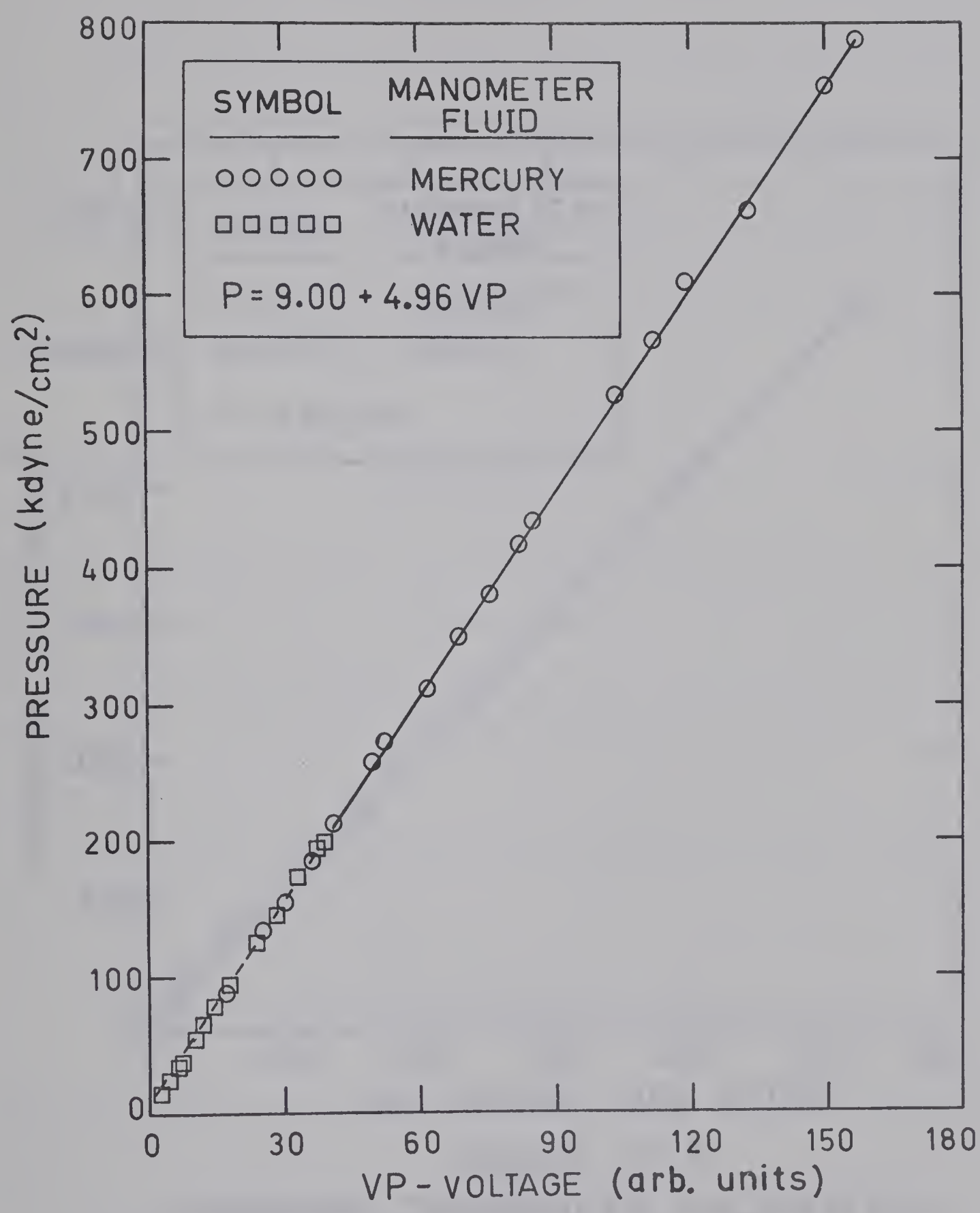


FIGURE (A-4)
PRESSURE TRANSDUCER CALIBRATION

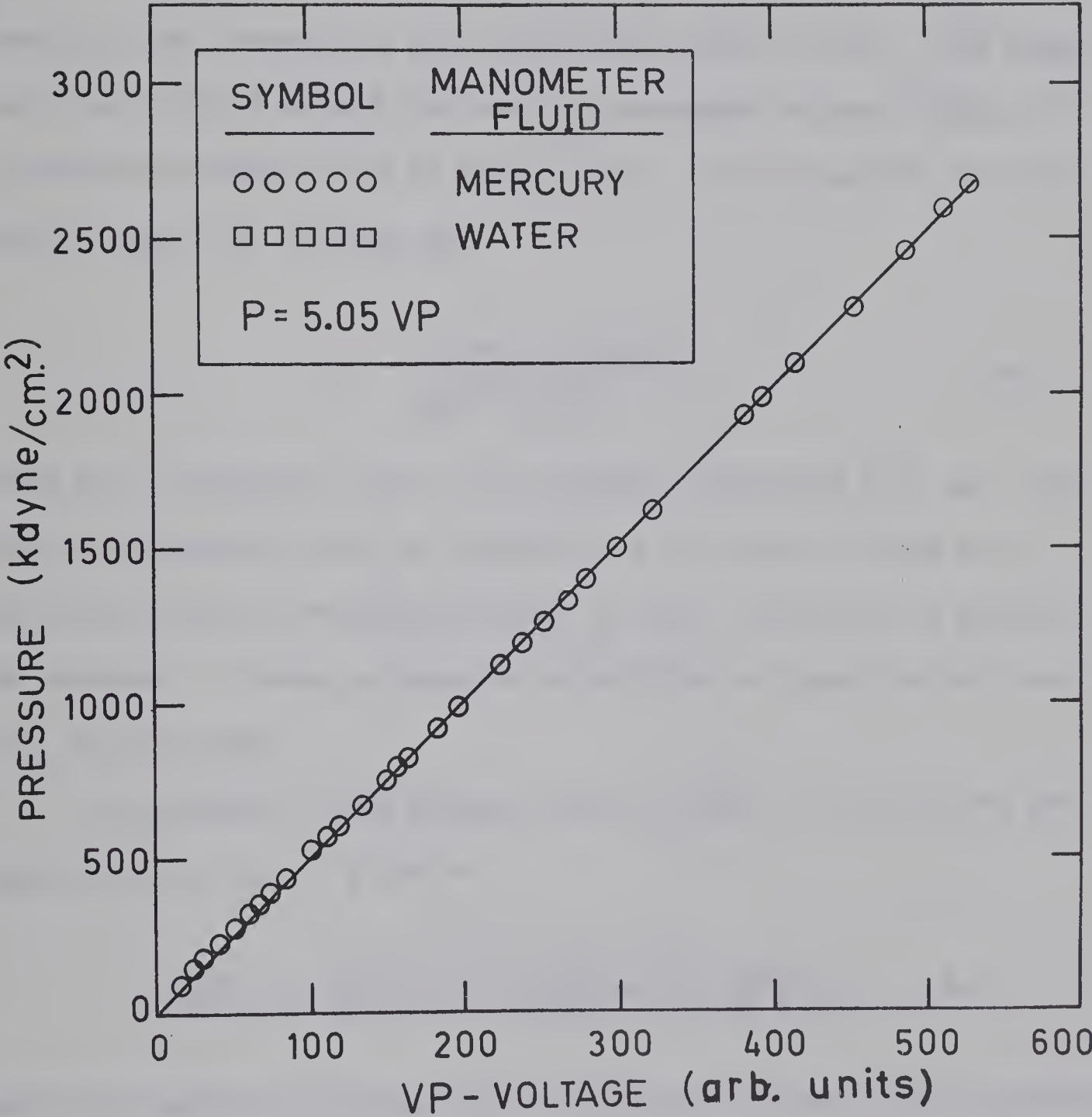


FIGURE (A-5)
PRESSURE TRANSDUCER CALIBRATION

THRUST CALIBRATION

Thrust calibration was accomplished by relating amplifier output of the displacement transducer signal to a known force applied normal to the spring face and in the axis of the orifice. The known force was applied through the use of a suspended balance weight, WT, as depicted schematically in Figure (A-6). For a given WT, the horizontal force, FH, is given by

$$F_H = \frac{(0.981) (WV)(WT)}{\sqrt{H^2 - (WV)^2}} \quad (A-2)$$

where WT is expressed in gm., FH in kdyne, and WV and H in cm. The thrust calibrations were not reproducible from test to test due to the sensitivity of the spring system to small variations in mounting the reservoir. Hence, a separate calibration was required for each test in this study.

An estimate of the maximum possible error in calculating the applied force, FH, is given by

$$(\Delta F_H) \leq \left| \frac{\partial F_H}{\partial WT} \right| |\Delta WT| + \left| \frac{\partial F_H}{\partial WV} \right| |\Delta WV| + \left| \frac{\partial F_H}{\partial H} \right| |\Delta H| \quad (A-3)$$

where the quantities prefixed by Δ indicate the error in that quantity and

$$\frac{\partial F_H}{\partial WT} = \frac{(0.981) (WV)}{[H^2 - (WV)^2]^{1/2}}$$

$$\frac{\partial F_H}{\partial WV} = \frac{(0.981) (WT) (H^2)}{[H^2 - (WV)^2]^{3/2}}$$

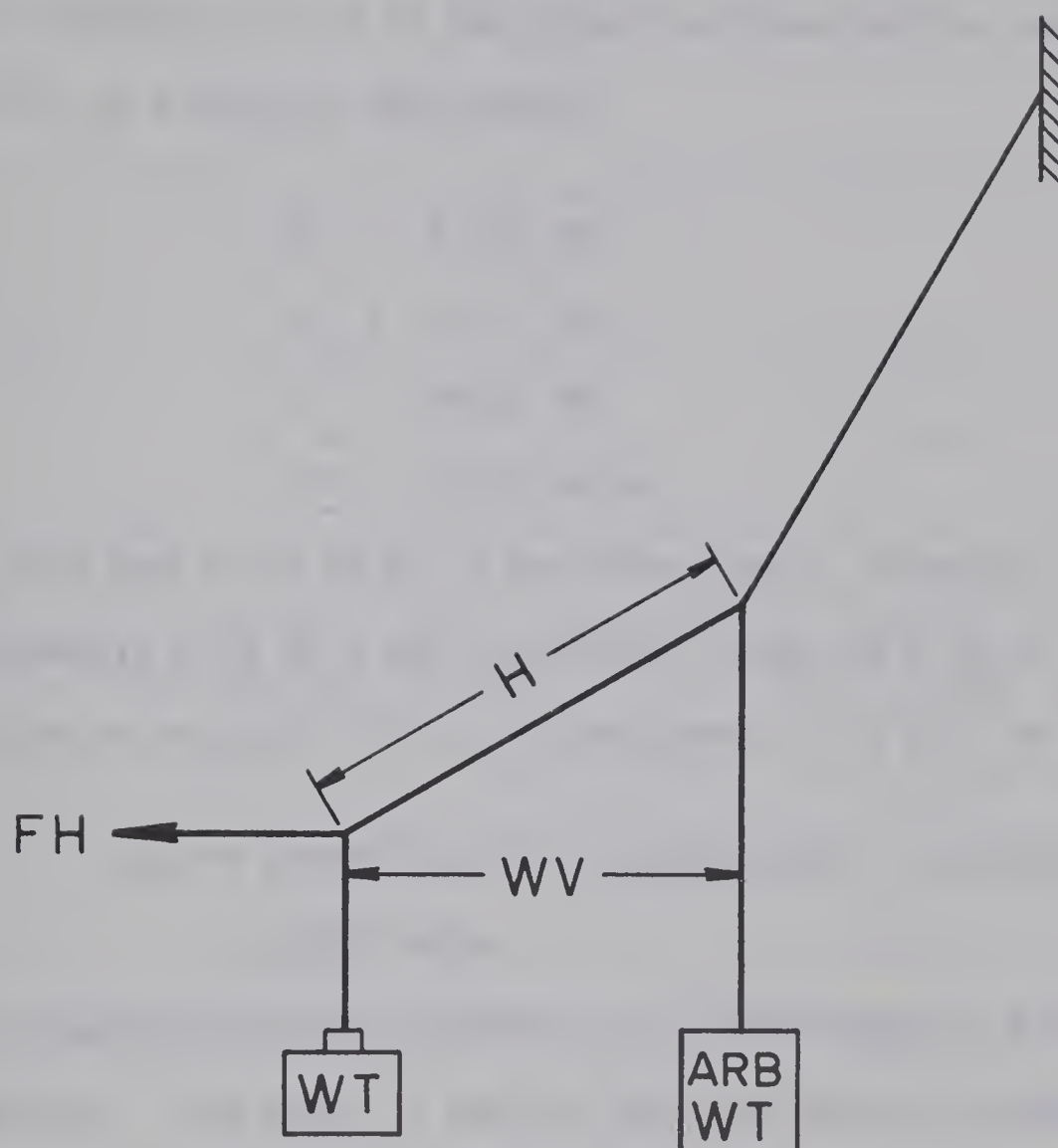


FIGURE (A-6)
THRUST CALIBRATION SCHEME

$$\frac{\partial FH}{\partial H} = \frac{-(0.981)(WT)(WV)(H)}{[H^2 - (WV)^2]^{3/2}} \quad (A-4)$$

Arbitrarily choosing run 2 of the thrust calibration for test 9 (see Table A-13), as a typical measurement,

$$WT = 5.452 \text{ gm.}$$

$$WV = 21.77 \text{ cm.}$$

$$H = 39.20 \text{ cm.}$$

$$FH = 3.572 \text{ kdyne}$$

Assuming that the error in WT is the thread mass, which was found to be approximately 0.06 gm., and the errors in WV and H to be the smallest division in the rule (0.1 cm.), the error in FH will be

$$\begin{aligned} \Delta FH &= (0.655)(0.06) + (0.237)(0.10) + (0.1313)(0.1) \\ &= 0.0761 \text{ kdyne} \end{aligned}$$

A typical (maximum) error, therefore, is 0.0761 kdyne or 2.1% of the applied force. This error is smaller than the error in reading the transducer signal on the recorder, which, among other things, is affected by the zero drift of the spring system.

The use of two different orifice sizes in this study required a change in the overall sensitivity of the transducer-carrier preamp system (or a change in the Cal Factor) to accommodate the maximum sensitivity of the transducer for each orifice size. Hence, in order to express the orifice thrust in terms of an amplifier output which would be equivalent for both sensitivities (or Cal Factors), an intermediate variable was defined, namely:

$$VSTAR = \text{Amplifier output in volts/Cal Factor} \quad (A-5)$$

The thrust, T, could then be represented as,

$$T = B \ VSTAR \quad (A-6)$$

where the constant B was determined from a first order TYPE-II least-squares regression of FH versus VSTAR.

Results of the thrust calibrations are presented in Tables (A-5) to (A-21) along with their respective least-squares representations. An example of a calibration change during a run is presented in Tables (A-18) and (A-19) which are a before and after calibration for test 14. Although the difference in the least-squares representations is small (less than 1%), the individual measurements of thrust are expected to vary from $\pm 3\%$ at the higher values to $\pm 10\%$ at the lower values of measured thrust. This error is expected to result mainly from the temperature sensitivity of the spring system.

TABLE (A-5)

THRUST CALIBRATION FOR TEST NO. 1

LENGTH OF HYPOTENUSE = 32.930 CM.
 CALIBRATION FACTOR * 1.000
 VSTAR = VT/CAL FACTOR

WT (GM)	WV (CM)	VT (VOLTS AT X1)	FH (KDYNES)	VSTAR
4.452	17.920	26.400	2.833	26.400
5.452	17.550	32.100	3.369	32.100
4.452	22.950	42.000	4.245	42.000
5.452	22.010	48.600	4.806	48.600
7.452	20.850	63.100	5.981	63.100
9.452	19.990	70.800	7.084	70.800
9.452	26.760	122.300	12.931	122.300
14.452	24.910	162.200	16.399	162.200

$$\text{THRUST (KDYNE)} = 0.10185 * \text{VSTAR}$$

TABLE (A-6)

THRUST CALIBRATION FOR TEST NO. 2

LENGTH OF HYPOTENUSE = 32.930 CM.
 CALIBRATION FACTOR * 1.030
 VSTAR = VT/CAL FACTOR

WT (GM)	WV (CM)	VT (VOLTS AT X1)	FH (KDYNES)	VSTAR
4.452	17.380	30.400	2.714	29.514
5.452	17.090	36.200	3.247	35.145
4.452	22.760	47.400	4.177	46.019
5.452	21.960	53.000	4.787	51.456
7.452	20.430	68.500	5.783	66.504
9.452	19.850	82.000	7.006	79.611
14.452	19.540	108.500	10.453	105.339
10.452	26.400	158.000	13.754	153.398
14.452	24.770	186.000	16.186	180.582
19.452	23.360	222.000	19.209	215.533
24.452	22.490	256.000	22.431	248.543

THRUST (KDYNE) = 0.09023 * VSTAR

TABLE (A-7)

THRUST CALIBRATION FOR TEST NO. 3

LENGTH OF HYPOTENUSE = 33.000 CM.
 CALIBRATION FACTOR * 1.030
 VSTAR = VT/CAL FACTOR

WT (GM)	WV (CM)	VT (VOLTS AT X1)	FH (KDYNES)	VSTAR
4.452	18.030	24.600	2.849	23.883
5.452	17.620	31.600	3.378	30.679
4.452	22.940	41.200	4.224	40.000
6.452	21.250	50.500	5.328	49.029
9.452	19.800	67.000	6.955	65.048
14.452	18.640	94.000	9.706	91.262
9.452	26.760	125.000	12.851	121.359
14.452	24.820	161.000	16.182	156.310
24.452	22.410	214.000	22.194	207.766
29.452	21.560	243.000	24.937	235.922

$$\text{THRUST (KDYNE)} = 0.10588 * \text{VSTAR}$$

TABLE (A-8)

THRUST CALIBRATION FOR TEST NO. 4

LENGTH OF HYPOTENUSE = 33.000 CM.
 CALIBRATION FACTOR * 1.030
 VSTAR = VT/CAL FACTOR

WT (GM)	WV (CM)	VT (VOLTS AT X1)	FH (KDYNES)	VSTAR
4.452	17.530	25.200	2.738	24.466
5.452	17.150	32.600	3.253	31.650
4.452	22.910	43.000	4.213	41.747
7.452	20.810	65.500	5.940	63.592
9.452	19.940	72.000	7.032	69.902
14.452	18.480	96.500	9.584	93.689
19.452	17.900	122.500	12.322	118.932
14.452	24.890	168.000	16.288	163.106
24.452	22.320	221.000	22.030	214.563
29.452	21.550	249.000	24.917	241.747

$$\text{THRUST (KDYNES)} = 0.10215 * \text{VSTAR}$$

TABLE (A-9)

THRUST CALIBRATION FOR TEST NO. 5

LENGTH OF HYPOTENUSE = 33.000 CM.
 CALIBRATION FACTOR * 1.030
 VSTAR = VT/CAL FACTOR

WT (GM)	WV (CM)	VT (VOLTS AT X1)	FH (KDYNES)	VSTAR
4.452	22.810	40.000	4.178	38.834
5.452	21.870	45.200	4.734	43.883
7.452	20.760	57.500	5.917	55.825
9.452	19.870	67.000	6.993	65.048
14.452	18.560	93.000	9.645	90.291
19.452	17.730	125.500	12.157	121.844
14.452	24.750	158.000	16.078	153.398
24.452	22.480	214.000	22.324	207.766
29.452	21.700	241.000	25.222	233.980

$$\text{THRUST (KDYNE)} = 0.10638 * \text{VSTAR}$$

TABLE (A-10)

THRUST CALIBRATION FOR TEST NO. 6

LENGTH OF HYPOTENUSE = 33.000 CM.
CALIBRATION FACTOR * 0.541
VSTAR = VT/CAL FACTOR

WT (GM)	WV (CM)	VT (VOLTS AT X1)	FH (KDYNES)	VSTAR
4.452	22.740	21.200	4.153	39.186
5.452	21.930	24.000	4.757	44.362
9.452	19.760	35.400	6.933	65.434
14.452	18.590	46.600	9.667	86.136
14.452	24.820	84.000	16.182	155.268
19.452	23.340	98.500	19.094	182.070
24.452	22.310	112.000	22.012	207.024
29.452	21.650	131.000	25.119	242.144
34.452	20.980	145.000	27.841	268.022
54.452	19.480	202.000	39.071	373.382

THRUST(KDYNE) = 0.10472 * VSTAR

TABLE (A-11)

THRUST CALIBRATION FOR TEST NO. 7

LENGTH OF HYPOTENUSE = 33.000 CM.
CALIBRATION FACTOR * 0.541
VSTAR = VT/CAL FACTOR

WT (GM)	WV (CM)	VT (VOLTS AT X1)	FH (KDYNES)	VSTAR
4.452	22.740	19.700	4.153	36.414
5.452	21.930	22.700	4.757	41.959
7.452	20.780	28.600	5.926	52.865
9.452	19.760	33.600	6.933	62.107
14.452	18.590	45.600	9.667	84.288
14.452	24.820	78.500	16.182	145.101
24.452	22.310	106.000	22.012	195.933
34.452	20.980	136.000	27.841	251.386
54.452	19.480	187.000	39.071	345.656

THRUST(KDYNE) = 0.11227 * VSTAR

TABLE (A-12)

THRUST CALIBRATION FOR TEST NO. 8

LENGTH OF HYPOTENUSE = 39.200 CM.
 CALIBRATION FACTOR * 0.541
 VSTAR = VT/CAL FACTOR

WT (GM)	WV (CM)	VT (VOLTS AT X1)	FH (KDYNES)	VSTAR
4.452	23.380	17.800	3.245	32.902
5.452	23.050	21.200	3.888	39.186
6.452	22.840	24.600	4.538	45.471
9.452	22.360	35.400	6.440	65.434
5.452	28.250	29.600	5.560	54.713
9.452	25.980	44.400	8.207	82.070
14.452	24.550	62.500	11.390	115.526
19.452	23.720	79.000	14.505	146.025
24.452	23.200	96.000	17.615	177.449
24.452	28.690	141.000	25.767	260.628
34.452	27.200	177.000	32.572	327.171
54.452	25.430	249.000	45.542	460.258
104.452	23.540	426.000	76.965	787.430
114.452	23.330	460.000	83.165	850.277

$$\text{THRUST (KDYNE)} = 0.09813 * \text{VSTAR}$$

TABLE (A-13)

THRUST CALIBRATION FOR TEST NO. 9

LENGTH OF HYPOTENUSE = 39.200 CM.
CALIBRATION FACTOR * 0.541
VSTAR = VT/CAL FACTOR

WT (GM)	WV (CM)	VT (VOLTS AT X1)	FH (KDYNES)	VSTAR
4.452	23.880	22.900	3.355	42.329
5.452	21.770	28.400	3.572	52.495
5.452	28.210	38.600	5.544	71.349
9.452	25.970	57.500	8.202	106.284
14.452	24.540	79.000	11.383	146.025
24.452	23.200	119.500	17.615	220.887
24.452	28.690	178.000	25.767	329.020
34.452	27.180	223.000	32.526	412.199
54.452	25.420	320.000	45.511	591.497
104.452	23.520	534.000	76.863	987.060

THRUST(KDYNE) = 0.07784 * VSTAR

TABLE (A-14)

THRUST CALIBRATION FOR TEST NO. 10

LENGTH OF HYPOTENUSE = 39.200 CM.
 CALIBRATION FACTOR * 0.541
 VSTAR = VT/CAL FACTOR

WT (GM)	WV (CM)	VT (VOLTS AT X1)	FH (KDYNES)	VSTAR
4.452	23.330	21.600	3.235	39.926
5.452	22.950	25.800	3.863	47.689
5.452	28.210	37.200	5.544	68.761
9.452	25.960	55.500	8.196	102.587
14.452	24.520	76.000	11.368	140.480
24.452	23.190	119.500	17.603	220.887
34.452	22.530	162.000	23.741	299.445
24.452	28.710	177.000	25.806	327.171
34.452	27.220	222.000	32.618	410.351
54.452	25.440	310.000	45.573	573.012
104.452	23.540	522.000	76.965	964.879
94.452	23.790	480.000	70.763	887.245

$$\text{THRUST (KDYNE)} = 0.07967 * \text{VSTAR}$$

TABLE (A-15)

THRUST CALIBRATION FOR TEST NO. 11

LENGTH OF HYPOTENUSE = 39.200 CM.
CALIBRATION FACTOR * 0.541
VSTAR = VT/CAL FACTOR

WT (GM)	WV (CM)	VT (VOLTS AT X1)	FH (KDYNES)	VSTAR
4.452	23.390	22.700	3.247	41.959
5.452	22.980	26.800	3.870	49.537
5.452	28.220	37.400	5.548	69.131
9.452	25.960	59.000	8.196	109.057
14.452	24.530	81.000	11.375	149.722
24.452	23.200	123.000	17.615	227.356
34.452	22.560	168.000	23.788	310.536
24.452	28.650	182.000	25.690	336.414
34.452	27.130	230.000	32.411	425.138
54.452	25.400	328.000	45.449	606.284
84.452	24.050	460.000	64.376	850.277
104.452	23.530	548.000	76.914	1012.939

THRUST(KDYNE) = 0.07583 * VSTAR

TABLE (A-16)

THRUST CALIBRATION FOR TEST NO. 12

LENGTH OF HYPOTENUSE = 39.200 CM.

CALIBRATION FACTOR * 0.541

VSTAR = VT/CAL FACTOR

WT (GM)	WV (CM)	VT (VOLTS AT X1)	FH (KDYNES)	VSTAR
4.452	23.360	23.100	3.241	42.698
5.452	22.940	27.600	3.860	51.016
5.452	28.260	39.000	5.564	72.088
9.452	25.980	59.000	8.207	109.057
14.452	24.550	81.000	11.390	149.722
24.452	23.190	123.500	17.603	228.280
34.452	22.550	171.000	23.772	316.081
24.452	28.720	183.000	25.826	338.262
34.452	27.210	230.000	32.595	425.138
54.452	25.450	330.000	45.604	609.981
84.452	24.080	484.000	64.505	894.639
104.452	23.550	552.000	77.016	1020.332

THRUST(KDYNE) = 0.07452 * VSTAR

TABLE (A-17)

THRUST CALIBRATION FOR TEST NO. 13

LENGTH OF HYPOTENUSE = 39.200 CM.

CALIBRATION FACTOR * 0.541

VSTAR = VT/CAL FACTOR

WT (GM)	WV (CM)	VT (VOLTS AT X1)	FH (KDYNES)	VSTAR
4.452	23.360	19.200	3.241	35.489
5.452	22.950	22.900	3.863	42.329
5.452	28.410	33.800	5.626	62.476
9.452	25.960	48.600	8.196	89.833
14.452	24.300	69.000	11.201	127.541
24.452	23.190	105.500	17.603	195.009
34.452	22.560	145.000	23.788	268.022
24.452	28.700	167.000	25.787	308.687
34.452	27.190	197.000	32.549	364.140
54.452	25.440	280.000	45.573	517.560
84.452	24.050	394.000	64.376	728.280
104.452	23.540	464.000	76.965	857.670

THRUST (KDYNE) = 0.08875 * VSTAR

TABLE (A-18)

THRUST CALIBRATION FOR TEST NO. 14

LENGTH OF HYPOTENUSE = 39.200 CM.
CALIBRATION FACTOR * 0.541
VSTAR = VT/CAL FACTOR

WT (GM)	WV (CM)	VT (VOLTS AT X1)	FH (KDYNES)	VSTAR
4.452	23.390	20.200	3.247	37.338
5.452	22.960	23.700	3.865	43.807
5.452	28.190	35.000	5.536	64.695
9.452	25.940	53.500	8.185	98.890
14.452	24.520	72.500	11.368	134.011
24.452	23.200	109.500	17.615	202.402
34.452	22.560	150.000	23.788	277.264
24.452	28.680	163.000	25.748	301.293
34.452	27.160	205.000	32.480	378.927
54.452	25.520	294.000	45.821	543.438
84.452	24.050	410.000	64.376	757.855
104.452	23.520	484.000	76.863	894.639

THRUST(KDYNE) = 0.08537 * VSTAR

TABLE (A-19)

THRUST CALIBRATION FOR TEST NO. 14

LENGTH OF HYPOTENUSE = 39.200 CM.
 CALIBRATION FACTOR * 0.541
 VSTAR = VT/CAL FACTOR

WT (GM)	WV (CM)	VT (VOLTS AT X1)	FH (KDYNES)	VSTAR
4.452	23.330	20.600	3.235	38.077
5.452	22.940	23.300	3.860	43.068
5.452	28.260	34.600	5.564	63.955
9.452	25.980	49.800	8.207	92.051
14.452	24.540	71.500	11.383	132.162
24.452	23.180	110.500	17.591	204.251
34.452	22.540	152.000	23.756	280.961
24.452	28.700	165.000	25.787	304.990
34.452	27.200	207.000	32.572	382.624
54.452	25.440	296.000	45.573	547.134
84.452	24.090	408.000	64.548	754.158
104.452	23.540	486.000	76.965	898.336

$$\text{THRUST (KDYNE)} = 0.08520 * \text{VSTAR}$$

TABLE (A-20)

THRUST CALIBRATION FOR TEST NO. 15

LENGTH OF HYPOTENUSE = 39.200 CM.
 CALIBRATION FACTOR * 0.541
 VSTAR = VT/CAL FACTOR

WT (GM)	WV (CM)	VT (VOLTS AT X1)	FH (KDYNES)	VSTAR
4.452	23.350	21.000	3.239	38.817
5.452	22.980	24.300	3.870	44.916
5.452	28.220	36.200	5.548	66.913
9.452	25.970	54.500	8.202	100.739
14.452	24.540	76.000	11.383	140.480
24.452	23.200	114.000	17.615	210.720
34.452	22.540	156.000	23.756	288.354
24.452	28.700	171.000	25.787	316.081
34.452	27.200	213.000	32.572	393.715
54.452	25.410	306.000	45.480	565.619
84.452	24.070	428.000	64.462	791.127
104.452	23.520	508.000	76.863	939.001

$$\text{THRUST (KDYNE)} = 0.08164 * \text{VSTAR}$$

TABLE (A-21)

THRUST CALIBRATION FOR TEST NO. 16

LENGTH OF HYPOTENUSE = 39.200 CM.
CALIBRATION FACTOR * 0.541
VSTAR = VT/CAL FACTOR

WT (GM)	WV (CM)	VT (VOLTS AT X1)	FH (KDYNES)	VSTAR
4.452	23.290	20.900	3.226	38.632
5.452	22.900	24.000	3.850	44.362
5.452	28.160	35.600	5.523	65.804
9.452	25.940	51.400	8.185	95.009
14.452	24.500	73.000	11.352	134.935
24.452	23.150	112.000	17.556	207.024
34.452	22.510	155.000	23.709	286.506
24.452	28.640	168.000	25.671	310.536
34.452	27.120	211.000	32.388	390.018
54.452	25.380	300.000	45.388	554.528
84.452	24.050	418.000	64.376	772.643
104.452	23.490	498.000	76.710	920.517

THRUST(KDYNE) = 0.08309 * VSTAR

APPENDIX B

EXPERIMENTAL RESULTS

THRUST MEASUREMENTS

Experimental results are summarized in Tables (B-1) to (B-16). The heading of each table classifies the fluid according to the weight concentration of sugar, axis ratio and weight concentration of fibres, and gives the orifice size used. Occasions where an unusual behaviour (see Section 4.4) occurred are indicated by two consecutive entries at the same velocity marked LO and HI to the right of the column headed by "TN". LO and HI denote the low and high values, respectively, which characterize the "unusual behaviour".

TABLE (B-1)

RESULTS FOR TEST NO. 1

FLUID * 60.0 PER CENT SUCROSE SOLUTION
 DENSITY * 1.2810
 FIBRE CONCENTRATION * 0.000 PER CENT
 FIBRE AXIS RATIO *****
 ORIFICE DIAMETER * 0.08460 CM.

NOTE * TN IS CALCULATED ON BASIS OF TESTS NO. 1 AND NO. 6

FLOWRATE (CC/SEC)	VELOCITY (CM/SEC)	PRESSURE (KDYNE/CM ²)	C (*)	THRUST (KDYNE)	T/A (KDYNE/CM ²)	TN (*)
1.097	195.153	87.090	0.529	0.207	36.964	1.046
1.382	245.854	129.332	0.547	0.440	78.276	1.176
1.742	309.897	184.610	0.577	0.692	123.213	1.036
2.190	389.595	266.920	0.603	1.185	210.912	1.032
2.760	490.996	381.000	0.636	1.879	334.307	0.967
3.470	617.303	564.519	0.657	3.167	563.521	0.984
4.370	777.411	837.320	0.679	5.286	940.410	0.999
5.510	980.214	*****	0.000	8.209	1460.444	0.950
6.930	1232.828	1858.400	0.723	13.546	2409.914	0.970

* DIMENSIONLESS

TABLE (B-2)

RESULTS FOR TEST NO. 2

FLUID * 60.0 PER CENT SUCROSE SOLUTION
DENSITY * 1.2810
FIBRE CONCENTRATION * 0.050 PER CENT
FIBRE AXIS RATIO * 85
ORIFICE DIAMETER * 0.08460 CM.

NOTE * TN IS CALCULATED ON BASIS OF TESTS NO. 1 AND NO. 6

FLOWRATE (CC/SEC)	VELOCITY (CM/SEC)	PRESSURE (KDYN/CM ²)	C (*)	THRUST (KDYN)	T/A (KDYN/CM ²)	TN (*)
1.097	195.153	62.580	0.624	0.206	36.781	1.041
1.382	245.854	91.783	0.649	0.332	59.224	0.890
1.742	309.897	137.676	0.668	0.569	101.305	0.851
2.190	389.595	200.255	0.696	0.902	160.530	0.785
2.760	490.996	296.680	0.721	1.576	280.538	0.811
3.470	617.303	442.999	0.742	2.540	451.978	0.789
4.370	777.411	668.679	0.760	3.942	701.346	0.745
5.510	980.214	994.849	0.786	6.570	1158.910	0.760
6.930	1232.828	1515.000	0.801	11.476	2041.697	0.822

* DIMENSIONLESS

TABLE (B-3)

RESULTS FOR TEST NO. 3

FLUID * 60.0 PER CENT SUCROSE SOLUTION
DENSITY * 1.2810
FIBRE CONCENTRATION * 0.100 PER CENT
FIBRE AXIS RATIO * 85
ORIFICE DIAMETER * 0.08460 CM.

NOTE * TN IS CALCULATED ON BASIS OF TESTS NO. 1 AND NO. 6

FLOWRATE (CC/SEC)	VELOCITY (CM/SEC)	PRESSURE (KDYNE/CM ²)	C (*)	THRUST (KDYNE)	T/A (KDYNE/CM ²)	TN (*)
1.097	195.153	46.152	0.727	0.238	42.426	1.201
1.382	245.854	126.724	0.552	0.431	76.806	1.154
1.742	309.897	191.912	0.566	0.714	127.096	1.068
2.190	389.595	266.920	0.603	1.171	208.474	1.020
2.760	490.996	395.879	0.624	1.932	343.799	0.995
3.470	617.303	574.440	0.651	3.135	557.759	0.974
4.370	777.411	837.320	0.679	5.067	901.558	0.958
5.510	980.214	1227.150	0.708	8.233	1464.804	0.952
6.930	1232.828	1848.300	0.725	13.363	2377.335	0.957

* DIMENSIONLESS

TABLE (B-4)

RESULTS FOR TEST NO. 4

FLUID * 60.0 PER CENT SUCROSE SOLUTION
 DENSITY * 1.2810
 FIBRE CONCENTRATION * 0.150 PER CENT
 FIBRE AXIS RATIO * 85
 ORIFICE DIAMETER * 0.08460 CM.

NOTE * TN IS CALCULATED ON BASIS OF TESTS NO. 1 AND NO. 6

FLOWRATE (CC/SEC)	VELOCITY (CM/SEC)	PRESSURE (KDYN/CM ²)	C (*)	THRUST (KDYN)	T/A (KDYN/CM ²)	TN (*)
1.097	195.153	111.079	0.468	0.245	43.756	1.239
1.382	245.854	152.277	0.504	0.416	74.103	1.114
1.742	309.897	219.303	0.529	0.709	126.152	1.060
2.190	389.595	318.999	0.552	1.174	208.902	1.022
2.760	490.996	438.040	0.593	1.490	265.185	0.767
3.470	617.303	611.640	0.631	3.183	566.364	0.989
4.370	777.411	908.999	0.652	5.008	891.009	0.947
5.510	980.214	1343.300	0.676	8.093	1439.730	0.936

* DIMENSIONLESS

TABLE (B-5)

RESULTS FOR TEST NO. 5						
FLUID * 60.0 PER CENT SUCROSE SOLUTION						
DENSITY * 1.2810						
FIBRE CONCENTRATION * 0.200 PER CENT						
FIBRE AXIS RATIO * 85						
ORIFICE DIAMETER * 0.14770 CM.						
NOTE * TN IS CALCULATED ON BASIS OF TESTS NO. 1 AND NO. 6						
FLOWRATE (CC/SEC)	VELOCITY (CM/SEC)	PRESSURE (KDYN/CM ²)	C (*)	THRUST (KDYN)	T/A (KDYN/CM ²)	TN (*)
3.470	202.525	94.913	0.526	1.177	68.722	1.749
4.370	255.053	142.891	0.539	1.941	113.331	1.549
5.510	321.588	205.471	0.567	3.139	183.258	1.409
5.510	321.588	182.525	0.602	2.871	167.585	1.288
6.930	404.466	263.944	0.630	4.585	267.654	1.201
6.930	404.466	232.199	0.671	4.296	250.775	1.125
8.710	508.355	358.680	0.679	7.075	412.935	1.106
10.970	640.259	574.440	0.676	12.239	714.347	1.153
13.820	806.598	822.440	0.711	18.075	1054.944	1.036
13.820	806.598	979.700	0.652	21.276	1241.820	1.220
17.420	1016.710	1585.699	0.646	35.323	2061.662	1.242
21.900	1278.183	2464.399	0.651	56.394	3291.426	1.229

* DIMENSIONLESS

TABLE (B-6)

RESULTS FOR TEST NO. 6

FLUID * 60.0 PER CENT SUCROSE SOLUTION
 DENSITY * 1.2810
 FIBRE CONCENTRATION * 0.000 PER CENT
 FIBRE AXIS RATIO *****
 ORIFICE DIAMETER * 0.14770 CM.

NOTE * TN IS CALCULATED ON BASIS OF TESTS NO. 1 AND NO. 6

FLOWRATE (CC/SEC)	VELOCITY (CM/SEC)	PRESSURE (KDYNE/CM ²)	C (*)	THRUST (KDYNE)	T/A (KDYNE/CM ²)	TN (*)
3.470	202.525	55.018	0.691	0.692	40.446	1.029
4.370	255.053	85.004	0.700	1.209	70.611	0.965
5.510	321.588	128.810	0.717	2.071	120.886	0.929
6.930	404.466	206.514	0.712	3.464	202.230	0.907
8.710	508.355	323.960	0.714	5.807	338.933	0.907
10.970	640.259	485.160	0.735	9.388	547.942	0.884 - L0
10.970	640.259	564.519	0.681	10.936	638.324	1.030 - HI
13.820	806.598	979.700	0.652	18.776	1095.884	1.077
17.420	1016.710	1575.599	0.648	30.390	1773.751	1.068

* DIMENSIONLESS

TABLE (B-7)

RESULTS FOR TEST NO. 7

FLUID * 0.10 PER CENT SEPARAN AP30 SOLUTION
 DENSITY * 1.0000
 FIBRE CONCENTRATION * 0.000 PER CENT
 FIBRE AXIS RATIO *****
 ORIFICE DIAMETER * 0.14770 CM.

NOTE * TN IS CALCULATED ON BASIS OF TESTS NO. 12 AND NO. 15

FLOWRATE (CC/SEC)	VELOCITY (CM/SEC)	PRESSURE (KDYNE/CM ²)	C (*)	THRUST (KDYNE)	T/A (KDYNE/CM ²)	TN (*)
5.510	321.588	108.993	0.688	0.757	44.210	0.361
6.930	404.466	168.965	0.695	1.421	82.971	0.383
8.710	508.355	254.519	0.712	2.469	144.139	0.389
10.970	640.259	376.040	0.738	4.192	244.674	0.391
13.820	806.598	564.519	0.759	7.346	428.785	0.413
17.420	1016.710	886.919	0.763	12.451	726.754	0.426
21.900	1278.183	1434.199	0.754	20.753	1211.257	0.437

* DIMENSIONLESS

TABLE (B-8)

RESULTS FOR TEST NO. 8

FLUID * 66.67 PER CENT SUCROSE SOLUTION
 DENSITY * 1.3200
 FIBRE CONCENTRATION * 0.300 PER CENT
 FIBRE AXIS RATIO * 85
 ORIFICE DIAMETER * 0.14770 CM.

NOTE * TN IS CALCULATED ON BASIS OF TESTS NO. 12 AND NO. 15

FLOWRATE (CC/SEC)	VELOCITY (CM/SEC)	PRESSURE (KDYN/CM ²)	C (*)	THRUST (KDYN)	T/A (KDYN/CM ²)	TN (*)
3.040	177.428	121.509	0.413	0.838	48.910	2.482
4.250	248.633	189.826	0.463	1.641	95.809	1.579
6.080	354.856	314.039	0.514	3.373	196.912	1.254
10.640	620.998	723.240	0.593	11.064	645.789	1.107
15.200	887.141	1262.499	0.641	22.492	1312.752	1.030
21.280	1241.997	2383.600	0.653	47.524	2773.719	1.064

* DIMENSIONLESS

TABLE (B-9)

RESULTS FOR TEST NO. 9

FLUID * 66.67 PER CENT SUCROSE SOLUTION
DENSITY * 1.3200
FIBRE CONCENTRATION * 0.100 PER CENT
FIBRE AXIS RATIO * 170
ORIFICE DIAMETER * 0.14770 CM.

NOTE * TN IS CALCULATED ON BASIS OF TESTS NO. 12 AND NO. 15

FLOWRATE (CC/SEC)	VELOCITY (CM/SEC)	PRESSURE (KDYNE/CM ²)	C (*)	THRUST (KDYNE)	T/A (KDYNE/CM ²)	TN (*)
3.040	177.428	97.520	0.461	0.627	36.616	1.858
4.260	248.633	155.407	0.512	1.136	66.347	1.093
6.080	354.856	255.015	0.570	1.755	102.460	0.652
10.640	620.998	624.039	0.638	8.561	499.702	0.856
15.200	887.141	1166.550	0.667	19.641	1146.376	0.899
21.280	1241.997	2302.800	0.664	41.441	2418.729	0.928

* DIMENSIONLESS

TABLE (B-10)

RESULTS FOR TEST NO. 10

FLUID * 66.67 PER CENT SUCROSE SOLUTION
 DENSITY * 1.3200
 FIBRE CONCENTRATION * 0.200 PER CENT
 FIBRE AXIS RATIO * 170
 ORIFICE DIAMETER * 0.14770 CM.

NOTE * TN IS CALCULATED ON BASIS OF TESTS NO. 12 AND NO. 15

FLOWRATE (CC/SEC)	VELOCITY (CM/SEC)	PRESSURE (KDYNE/CM. ²)	C (*)	THRUST (KDYNE)	T/A (KDYNE/CM. ²)	TN (*)
3.040	177.428	105.864	0.443	0.421	24.581	1.247
4.260	248.633	165.837	0.496	0.979	57.157	0.942
6.080	354.856	281.800	0.543	2.385	139.240	0.887
10.640	620.998	648.839	0.626	8.173	477.026	0.817
15.200	887.141	1196.850	0.658	18.997	1108.763	0.870
21.280	1241.997	2242.200	0.673	38.141	2226.121	0.854
3.040	177.428	114.730	0.425	0.441	25.785	1.308
4.260	248.633	175.224	0.482	1.067	62.314	1.027
6.080	354.856	264.440	0.560	2.518	146.975	0.936
10.640	620.998	703.400	0.601	8.983	524.298	0.899
15.200	887.141	1227.150	0.650	19.144	1117.358	0.877
21.280	1241.997	2252.300	0.672	40.645	2372.237	0.910

* DIMENSIONLESS

TABLE (B-11)

RESULTS FOR TEST NO. 11

FLUID * 66.67 PER CENT SUCROSE SOLUTION
DENSITY * 1.3200
FIBRE CONCENTRATION * 0.100 PER CENT
FIBRE AXIS RATIO * 255
ORIFICE DIAMETER * 0.14770 CM.

NOTE * TN IS CALCULATED ON BASIS OF TESTS NO. 12 AND NO. 15

FLOWRATE (CC/SEC)	VELOCITY (CM/SEC)	PRESSURE (KDYNE/CM ²)	C (*)	THRUST (KDYNE)	T/A (KDYNE/CM ²)	TN (*)
3.040	177.428	94.913	0.467	0.297	17.344	0.880
4.260	248.633	148.106	0.524	0.876	51.134	0.842
6.080	354.856	240.136	0.588	2.256	131.723	0.839
10.640	620.998	566.999	0.669	8.270	482.713	0.827
15.200	887.141	1191.800	0.660	18.293	1067.697	0.838
21.280	1241.997	2221.999	0.676	39.250	2290.844	0.879
3.040	177.428	93.870	0.470	0.243	14.235	0.722
4.260	248.633	144.977	0.530	1.121	65.452	1.078
6.080	354.856	237.159	0.591	2.635	153.813	0.980
10.640	620.998	584.360	0.659	8.200	478.622	0.820
15.200	887.141	1141.300	0.674	19.064	1112.696	0.873
21.280	1241.997	2191.700	0.681	39.250	2290.844	0.879

* DIMENSIONLESS

TABLE (B-12)

RESULTS FOR TEST NO. 12

FLUID * 66.67 PER CENT SUCROSE SOLUTION
 DENSITY * 1.3200
 FIBRE CONCENTRATION * 0.000 PER CENT
 FIBRE AXIS RATIO *****
 ORIFICE DIAMETER * 0.14770 CM.

NOTE * TN IS CALCULATED ON BASIS OF TESTS NO. 12 AND NO. 15

FLOWRATE (CC/SEC)	VELOCITY (CM/SEC)	PRESSURE (KDYNE/CM ²)	C (*)	THRUST (KDYNE)	T/A (KDYNE/CM ²)	TN (*)
3.040	177.428	69.359	0.547	0.429	25.085	1.272
4.260	248.633	117.859	0.588	1.122	65.528	1.080
6.080	354.856	209.383	0.630	2.658	155.177	0.988
10.640	620.998	547.160	0.682	9.505	554.780	0.951
15.200	887.141	1105.950	0.685	21.903	1278.407	1.003
21.280	1241.997	2191.700	0.681	45.460	2653.298	1.018
3.040	177.428	64.666	0.566	0.330	19.296	0.979
4.260	248.633	114.730	0.596	1.170	68.342	1.126
6.020	354.856	212.360	0.625	2.948	172.062	1.096
10.640	620.998	514.920	0.703	9.643	562.820	0.965
15.200	887.141	1110.999	0.683	22.041	1286.447	1.009
21.280	1241.997	2171.499	0.684	45.460	2653.298	1.018

* DIMENSIONLESS

TABLE (B-13)

RESULTS FOR TEST NO. 13

FLUID * 66.67 PER CENT SUCROSE SOLUTION
DENSITY * 1.3200
FIBRE CONCENTRATION * 0.100 PER CENT
FIBRE AXIS RATIO * 340
ORIFICE DIAMETER * 0.14770 CM.

NOTE * TN IS CALCULATED ON BASIS OF TESTS NO. 12 AND NO. 15

FLOWRATE (CC/SEC)	VELOCITY (CM/SEC)	PRESSURE (KDYNE/CM ²)	C (*)	THRUST (KDYNE)	T/A (KDYNE/CM ²)	TN (*)
4.255	248.341	184.610	0.469	0.762	44.526	0.736
6.080	354.856	291.720	0.533	1.985	115.863	0.738
10.640	620.998	653.799	0.623	7.957	464.411	0.796
15.200	887.141	1186.749	0.661	16.898	986.276	0.774
21.280	1241.997	2232.100	0.675	37.242	2173.637	0.834
18.240	1064.569	1676.599	0.667	26.086	1522.504	0.809
9.120	532.284	512.440	0.604	5.742	335.142	0.814
3.647	212.855	146.020	0.452	0.442	25.853	0.685
3.647	212.855	142.891	0.457	0.410	23.938	0.634
4.864	283.885	201.299	0.514	1.033	60.325	0.685
12.160	709.713	812.519	0.639	10.828	631.982	0.806
15.200	887.141	1201.900	0.657	17.226	1005.427	0.789
6.030	354.856	321.480	0.508	2.034	118.736	0.756
4.255	248.341	183.567	0.470	0.656	38.301	0.633
21.280	1241.997	2232.100	0.675	37.078	2164.062	0.830
4.864	283.885	216.327	0.495	1.148	67.028	0.762

*DIMENSIONLESS

TABLE (B-14)

RESULTS FOR TEST NO. 14

FLUID * 66.67 PER CENT SUCROSE SOLUTION
DENSITY * 1.3200
FIBRE CONCENTRATION * 0.200 PER CENT
FIBRE AXIS RATIO * 85
ORIFICE DIAMETER * 0.14770 CM.

NOTE * TN IS CALCULATED ON BASIS OF TESTS NO. 12 AND NO. 15

FLOWRATE (CC/SEC)	VELOCITY (CM/SEC)	PRESSURE (KDYNE/CM ²)	C (*)	THRUST (KDYNE)	T/A (KDYNE/CM ²)	TN (*)
4.255	248.341	149.149	0.522	1.167	68.159	1.127
6.080	354.856	249.063	0.577	2.761	161.187	1.027
10.640	620.998	611.640	0.645	9.626	561.852	0.963
15.200	887.141	1146.350	0.673	19.726	1151.336	0.903
21.280	1241.997	2100.800	0.696	38.506	2247.409	0.862
18.240	1064.559	1616.000	0.580	28.721	1676.346	0.891
3.647	212.855	122.030	0.495	0.789	46.053	1.221
9.120	532.284	363.640	0.717	6.691	390.533	0.948
4.864	283.885	184.610	0.536	1.593	93.028	1.057
12.160	709.713	787.719	0.649	12.467	727.644	0.928
15.200	887.141	1181.699	0.662	19.884	1160.547	0.911
21.280	1241.997	2120.999	0.692	38.979	2275.041	0.872 - L0
21.280	1241.997	2252.300	0.672	44.187	2578.994	0.989 - HI
4.255	248.341	158.536	0.506	1.230	71.843	1.189

* DIMENSIONLESS

TABLE (B-14) (CONT'D)

RESULTS FOR TEST NO. 14

FLUID * 66.67 PER CENT SUCROSE SOLUTION
DENSITY * 1.3200
FIBRE CONCENTRATION * 0.200 PER CENT
FIBRE AXIS RATIO * 85
ORIFICE DIAMETER * 0.14770 CM.

NOTE * TN IS CALCULATED ON BASIS OF TESTS NO. 12 AND NO. 15

FLOWRATE (CC/SEC)	VELOCITY (CM/SEC)	PRESSURE (KDYNES/CM ²)	C (*)	THRUST (KDYNES)	T/A (KDYNES/CM ²)	TN (*)
4.255	248.341	142.891	0.533	1.159	67.698	1.119
6.080	354.856	245.095	0.582	2.793	163.029	1.038
10.640	620.998	609.160	0.646	9.468	552.641	0.947
15.200	887.141	1146.350	0.673	19.725	1151.336	0.903
21.280	1241.997	2090.700	0.697	39.453	2302.673	0.883
3.647	212.855	118.902	0.501	0.741	43.290	1.147
6.080	354.856	252.040	0.574	2.682	156.581	0.997
9.120	532.284	485.160	0.620	6.691	390.533	0.948
15.200	887.141	1171.600	0.665	21.146	1234.233	0.968
18.240	1064.569	1676.599	0.667	30.615	1786.874	0.949

* DIMENSIONLESS

TABLE (B-15)

RESULTS FOR TEST NO. 15

FLUID * 66.67 PER CENT SUCROSE SOLUTION
DENSITY * 1.3200
FIBRE CONCENTRATION * 0.000 PER CENT
FIBRE AXIS RATIO *****
ORIFICE DIAMETER * 0.14770 CM.

NOTE * TN IS CALCULATED ON BASIS OF TESTS NO. 12 AND NO. 15

FLOWRATE (CC/SEC)	VELOCITY (CM/SEC)	PRESSURE (KDYNE/CM ²)	C (*)	THRUST (KDYNE)	T/A (KDYNE/CM ²)	TN (*)
3.040	177.428	69.881	0.545	0.232	13.564	0.688
3.647	212.855	92.305	0.569	0.671	39.196	1.039
6.080	354.856	214.343	0.622	2.625	153.262	0.976
9.120	532.284	438.040	0.653	6.519	380.513	0.924
15.200	887.141	1131.200	0.677	21.732	1268.379	0.995
18.240	1064.569	1646.300	0.674	31.239	1823.296	0.969
4.255	248.341	117.859	0.587	1.071	62.538	1.034
10.640	620.998	564.519	0.671	9.658	563.724	0.966
21.280	1241.997	2191.700	0.681	44.973	2624.841	1.007
4.864	283.885	150.192	0.595	1.539	89.843	1.021
12.160	709.713	723.240	0.677	12.375	722.271	0.921
4.864	283.885	150.192	0.595	1.524	88.962	1.011
12.160	709.713	743.080	0.668	13.205	770.716	0.983
4.255	248.341	117.337	0.588	1.094	63.859	1.056

* DIMENSIONLESS

TABLE (B-15) (CONT'D)

RESULTS FOR TEST NO. 15

FLUID * 66.67 PER CENT SUCROSE SOLUTION
DENSITY * 1.3200
FIBRE CONCENTRATION * 0.000 PER CENT
FIBRE AXIS RATIO *****
ORIFICE DIAMETER * 0.14770 CM.

NOTE * TN IS CALCULATED ON BASIS OF TESTS NO. 12 AND NO. 15

FLOWRATE (CC/SEC)	VELOCITY (CM/SEC)	PRESSURE (KDYNES/CM ²)	C (*)	THRUST (KDYNES)	T/A (KDYNES/CM ²)	TN (*)
6.080	354.856	218.311	0.617	3.471	202.588	1.290
10.640	620.998	566.999	0.669	9.356	546.108	0.936
15.200	887.141	1136.249	0.676	21.581	1259.571	0.988
21.280	1241.997	2232.100	0.675	46.482	2712.923	1.040
21.280	1241.997	2211.900	0.678	44.671	2607.225	1.000
18.240	1064.569	1646.300	0.674	31.692	1849.720	0.983
9.120	532.284	418.200	0.668	7.244	422.793	1.026
3.647	212.855	95.956	0.558	0.596	34.792	0.922
6.080	354.856	220.295	0.614	2.686	156.785	0.999

* DIMENSIONLESS

TABLE (B-16)

RESULTS FOR TEST NO. 16

FLUID * 66.67 PER CENT SUCROSE SOLUTION
DENSITY * 1.3200
FIBRE CONCENTRATION * 0.100 PER CENT
FIBRE AXIS RATIO * 170
ORIFICE DIAMETER * 0.14770 CM.

NOTE * TN IS CALCULATED ON BASIS OF TESTS NO. 12 AND NO. 15

FLOWRATE (CC/SEC)	VELOCITY (CM/SEC)	PRESSURE (KDYNE/CM ²)	C (*)	THRUST (KDYNE)	T/A (KDYNE/CM ²)	TN (*)
3.648	212.913	109.515	0.522	0.783	45.721	1.211
6.080	354.856	235.175	0.594	2.611	152.403	0.971
9.120	532.284	462.839	0.635	6.144	358.596	0.870
18.240	1064.569	1555.400	0.693	27.341	1595.756	- L0
18.240	1064.569	1656.400	0.671	29.338	1712.300	- HI
15.200	887.141	1121.100	0.680	19.200	1120.615	- L0
21.280	1241.997	2060.400	0.702	37.478	2187.440	- HI
21.280	1241.997	2201.800	0.679	41.472	2420.528	- L0
4.255	248.341	146.020	0.527	1.090	63.650	- HI
10.640	620.998	614.120	0.643	9.369	546.860	- L0
21.280	1241.997	2050.300	0.704	38.707	2259.160	- HI
21.280	1241.997	2211.900	0.678	42.701	2492.248	- L0
4.864	283.885	173.138	0.554	1.474	86.063	- HI
12.160	709.713	757.960	0.662	11.904	694.781	- L0

* DIMENSIONLESS

TABLE (B-16) (CONT'D)

RESULTS FOR TEST NO. 16

FLUID * 66.67 PER CENT SUCROSE SOLUTION
DENSITY * 1.3200
FIBRE CONCENTRATION * 0.100 PER CENT
FIBRE AXIS RATIO * 170
ORIFICE DIAMETER * 0.14770 CM.

NOTE * TN IS CALCULATED ON BASIS OF TESTS NO. 12 AND NO. 15

FLOWRATE (CC/SEC)	VELOCITY (CM/SEC)	PRESSURE (KDYNES/CM ²)	C (*)	THRUST (KDYNES)	T/A (KDYNES/CM ²)	TN (*)
4.255	248.341	139.762	0.539	1.075	62.754	1.038
4.255	248.341	139.762	0.539	1.075	62.754	1.038
6.080	354.856	244.600	0.582	2.580	150.610	0.959
10.640	620.998	614.120	0.643	9.139	533.412	0.914
3.647	212.855	105.864	0.531	0.677	39.535	1.048
6.080	354.856	233.192	0.596	2.534	147.921	0.942
9.120	532.284	457.879	0.639	6.205	362.182	0.879
15.200	887.141	1126.150	0.679	18.739	1093.720	0.858
18.240	1064.569	1595.800	0.684	27.187	1586.791	0.843
18.240	1064.569	1646.300	0.674	28.877	1685.405	0.895
21.280	1241.997	2201.800	0.679	40.858	2384.669	0.915
6.080	354.856	244.103	0.583	2.380	138.956	0.885
10.640	620.998	619.079	0.641	8.908	519.965	0.891
4.864	283.885	180.439	0.542	1.474	86.063	0.978
12.160	709.713	772.839	0.655	11.596	676.851	0.863
4.864	283.885	179.396	0.544	1.443	84.270	0.958

- L0
- HI

* DIMENSIONLESS

APPENDIX C

SAMPLE CALCULATIONS AND LEAST-SQUARES REGRESSIONS

SAMPLE CALCULATIONS

All calculations, including the least-squares regressions, were performed with the aid of the IBM 1800 Real-Time computer of the DACS Centre. The sample calculations presented below are based on the first run of test 9.

Recorder signals of thrust and pressure were converted to the physical units given in Tables (B-1) to (B-16) by the procedure outlined in Appendix A. From Table (B-9)

$$Q = 3.040 \text{ cc./sec.}$$

$$T = 0.627 \text{ kdyne}$$

$$P = 97.52 \text{ kdyne/cm.}^2$$

The velocity of the orifice, V_o , is given by

$$V_o = \frac{3.040 \text{ cc/sec}}{\pi \left(\frac{0.1477}{2} \right)^2 \text{ cm}^2} = 177.428 \text{ cm./sec.}$$

The thrust per unit orifice area is given by

$$\frac{T}{\pi R_o^2} = \frac{T}{A} = \frac{0.627 \text{ kdyne}}{\pi \left(\frac{0.1477}{2} \text{ cm} \right)^2} = 36.616 \text{ kdyne/cm}^2$$

The normalized thrust, T_N , defined by Equation (4.2.2), is

$$T_N = \frac{36.616}{(1.8667)(10^{-3})(177.428)^2 - (0.22014)(177.428)} = 1.858$$

The averaged normalized thrust, $\langle T_N \rangle$, defined by Equation (4.2.3), is

$$\langle TN \rangle = \frac{(1.68)(10^{-3})(200)^2 - (0.189)(200)}{(1.8667)(10^{-3})(200)^2 - (0.22014)(200)} = 0.959$$

for an orifice velocity of 200 cm./sec. The contraction coefficient, C_c , is defined by Whitaker (44), and for a large contraction ratio (ratio of reservoir area available for flow to orifice area) is approximated by

$$C_c = V_{or} \sqrt{\frac{\rho}{2P}} \quad (C-1)$$

For the first run of test 9, C_c is

$$C_c = 177.428 \sqrt{\frac{1.32}{(2)(97.5)(1000)}} = 0.461$$

The results of the above calculations are given in Tables (B-1) to (B-16).

LEAST-SQUARES REGRESSION

If a function $y = f(x)$ can be adequately represented by a polynomial, then the well-known principle of least-squares (38) can easily be applied to obtain the "best-fit" polynomial which defines the function y . For example, data, (x_i, y_i) , which can be expressed as a second-order polynomial in x , will give the following system of "residual" equations:

$$\begin{bmatrix} n & \sum x_i & \sum x_i^2 \\ \sum x_i & \sum x_i^2 & \sum x_i^3 \\ \sum x_i^2 & \sum x_i^3 & \sum x_i^4 \end{bmatrix} \begin{bmatrix} a_0 \\ a_1 \\ a_2 \end{bmatrix} = \begin{bmatrix} \sum y_i \\ \sum x_i y_i \\ \sum x_i^2 y_i \end{bmatrix} \quad (C-1)$$

or, in matrix notation,

$$X A = Y \quad (C-2)$$

where $x_i, (i = 1, 2, 3, \dots, n)$ are the data points of the independent variable x , and $y_i, (i = 1, 2, 3, \dots, n)$ are the corresponding data points of the dependent variable, y . The solution to the system of Equations (C-1) is given by

$$y = a_0 + a_1 x + a_2 x^2 \quad (C-3)$$

such that the sum of the squares of the deviations of $y_i, (i = 1, 2, 3, \dots, n)$ from y will be a minimum. For convenience, the unconstrained least-squares polynomial defined by Equation (C-3) will be labelled as a Type I fit.

If apriori knowledge of the function y indicates that $y(0) = 0$, then Equation (C-2) can be constrained to force the coefficient a_0 in Equation (C-3) to zero without violating the least-squares principle. At least two approaches are possible:

1. Apriori specification of $a_0 = 0$ leads to the following system of residual equations (38)

$$\begin{bmatrix} \sum x_i^2 & \sum x_i^3 \\ \sum x_i^3 & \sum x_i^4 \end{bmatrix} \begin{bmatrix} a_1 \\ a_2 \end{bmatrix} = \begin{bmatrix} \sum x_i y_i \\ \sum x_i^2 y_i \end{bmatrix} \quad (\text{C-4})$$

The least-squares fit derived from Equation (C-4) will be labelled as a Type II fit.

2. A simple constraint is provided by transforming Equation (C-3) to

$$z = \frac{y}{x} = a_1 + a_2 x \quad (\text{C-5})$$

giving a Type I, first-order polynomial whose solution can be obtained from the "residual" system defined as

$$\begin{bmatrix} n & \sum x_i \\ \sum x_i & \sum x_i^2 \end{bmatrix} \begin{bmatrix} a_1 \\ a_2 \end{bmatrix} = \begin{bmatrix} \sum z_i \\ \sum x_i z_i \end{bmatrix} \quad (\text{C-6})$$

The least-squares fit available from the solution of (C-6) will be labelled as a Type III fit.

A solution to either system of Equations (C-4) or (C-6) will result in a polynomial of the form

$$y = a_1x + a_2x^2 \quad (C-7)$$

which requires that y pass through the origin. The difference between a Type II and a Type III fit can be qualitatively described on the basis of the difference in the order of x in the corresponding elements of (C-4) and (C-6). Since the order of x in an element of (C-4) is +2 greater than the order of x in a corresponding element of (C-6), a Type II fit will be more sensitive to higher values of x than a Type III fit. Basically, a Type II fit will provide a better fit at essentially high values of x , while a Type III fit may provide a better overall fit.

A statistical goodness-of-fit criterion, such as the correlation coefficient (4), will generally indicate that a Type I fit represents data better than a Type II or a Type III fit since the Type I fit is less constrained than the other two. However, apriori knowledge of a functional form often suggests a constraint which is based (from a statistical point of view) on personal judgement and is not taken into account by the goodness-of-fit criterion. Hence, goodness-of-fit was determined by personal judgement rather than statistical means.

A qualitative comparison of the Type II and Type III fits is given in Figures (C-1) and (C-2). Figure (C-1) depicts the "unconstrained" thrust-velocity data representation of test 13 by each fit. Figure (C-2) depicts the "constrained" data representation of test 13 by each fit. It is apparent that a Type III fit best represents the "unconstrained" thrust-velocity relationship while

a type II fit best represents the "constrained" version.



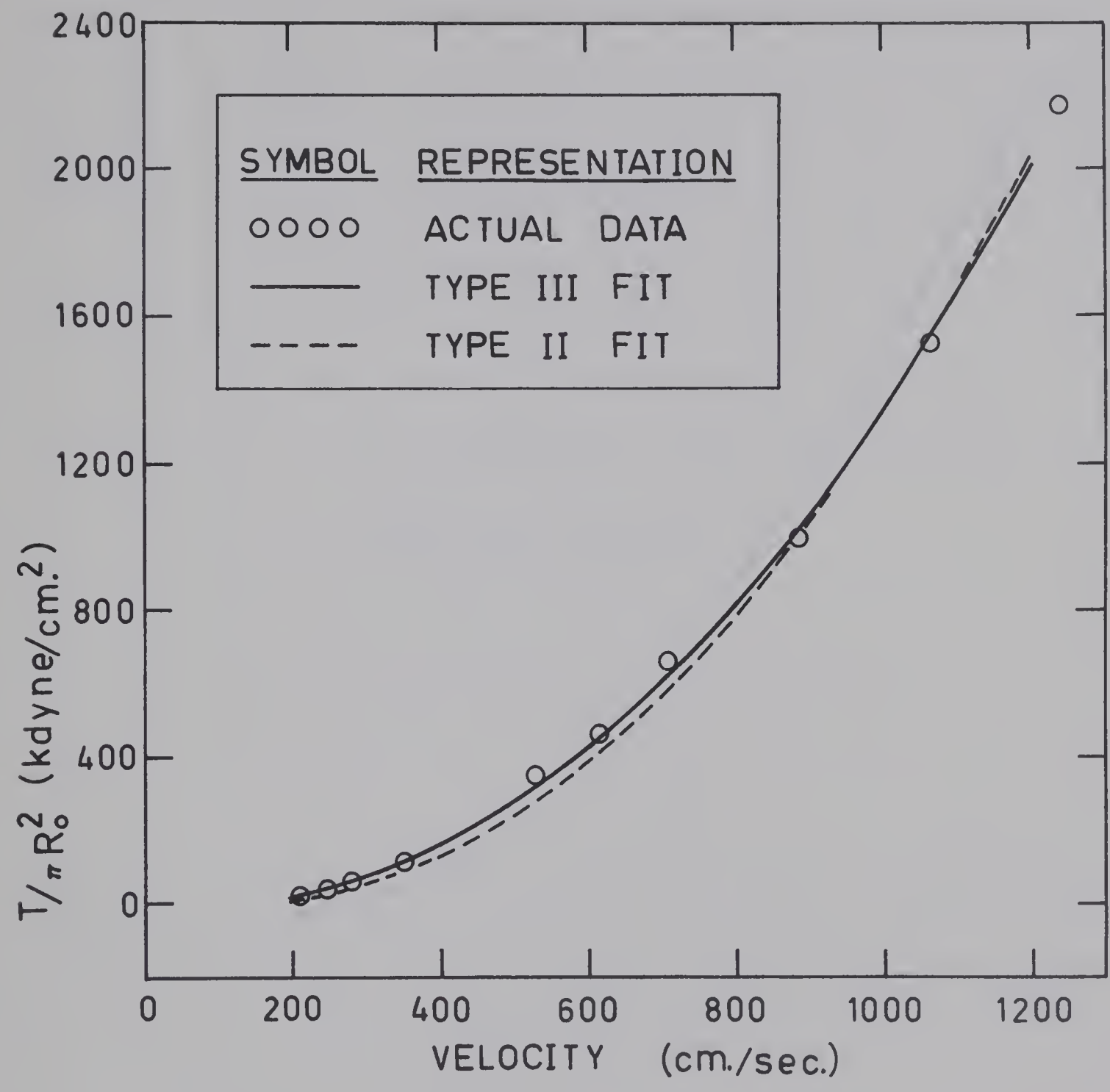


FIGURE (C-1)
UNCONSTRAINED REPRESENTATION OF TEST 13

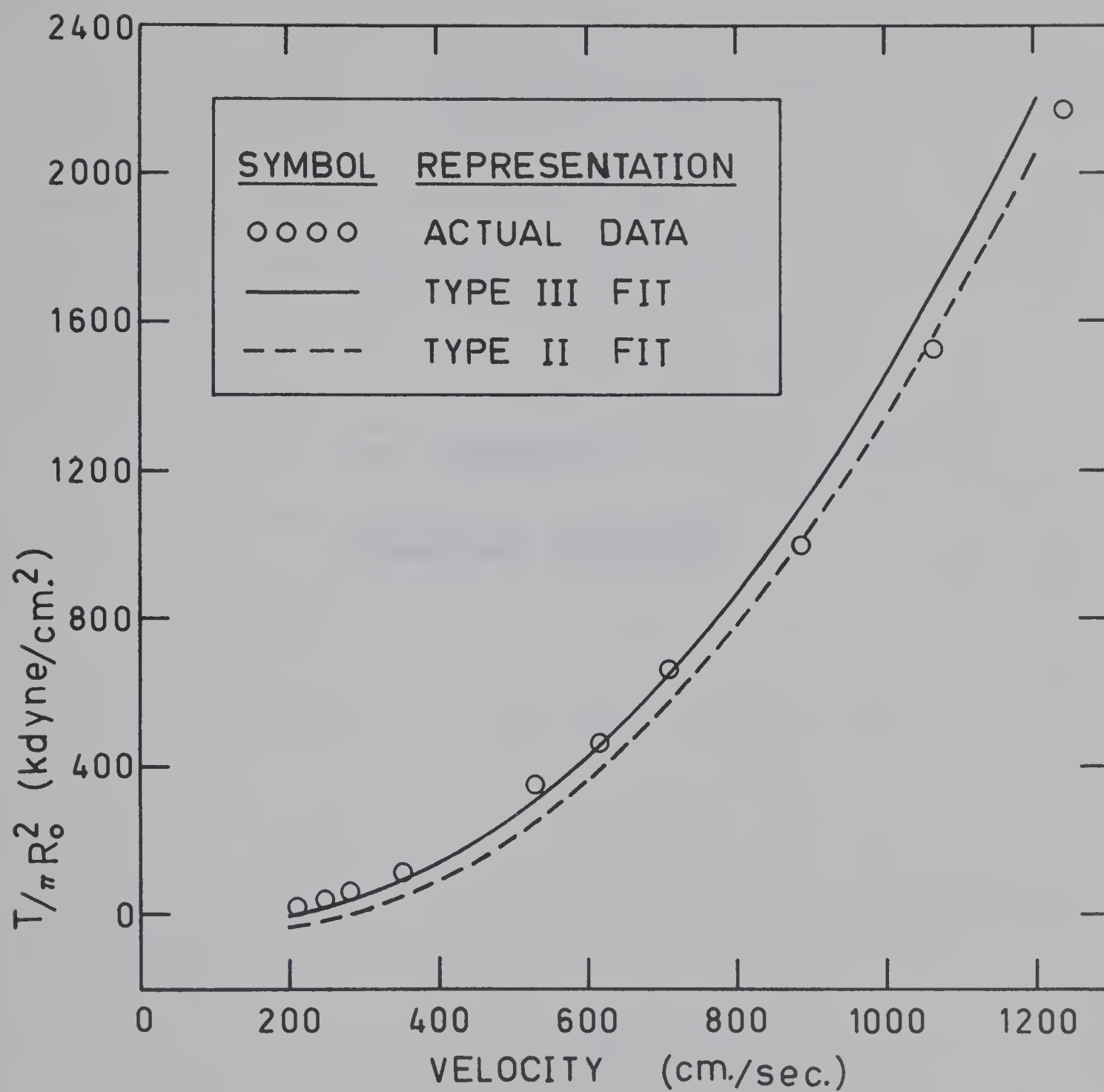


FIGURE (C-2)
CONSTRAINED REPRESENTATION OF TEST 13

APPENDIX D

APPENDIX D

ELONGATIONAL VISCOSITIES

"REPRESENTATIVE" ELONGATIONAL VISCOSITY

A more or less qualitative prediction of the elongational viscosity behaviour of fibre suspensions can be made via the development presented in Section (4.3.2). Accordingly, the least-squares representation of the thrust-flowrate data for the sugar solutions were used, in conjunction with the least-squares coefficients given in Table (D-1) to predict the "representative" elongational viscosity, $\{\eta\}$, of each suspension used in the reliable tests of this study.

Since the suspending medium for test 3 was a 60% sugar solution, $[k_2]$ is given by Equation (4.2.4), namely:

$$[k_2] = 0.1639$$

The shear viscosity, μ , of the 60% sugar solution is (43)

$$\mu = 0.52 \text{ poise}$$

The fibre concentration, given in Table (3.1) and the "constrained" least-squares coefficient, $[k'_{2R}]$, given in Table (D-1) are

$$C = 0.090 \text{ vol. \%}$$

$$[k'_{2R}] = 0.221$$

Hence, for test 3, $\{\eta\}$ is given by Equation (4.3.11), i.e.

$$\{\eta\} = \frac{0.221}{0.1639} (3)(0.52) = 2.10 \text{ poise}$$

In order to find what the elongational viscosity, $\{\eta\}_{66-2/3\%}$ would be for a volumetric concentration of 0.0926%, a fibre axis ratio of

85 and suspended in 66-2/3% sugar solution, Equation (1.2.6) is utilized, i.e.

$$\left(\frac{\{\eta\}_{sp}}{C}\right) = \frac{2.10 - 1.56}{(9.00)(10^{-4})(1.56)} = 385$$

Since

$$\eta = \eta_0(1 + C\eta_{sp})$$

then

$$\begin{aligned}\{\eta\}_{66-2/3\%} &= 5.1[1 + (0.000926)(385)] \\ &= 6.92 \text{ poise}\end{aligned}$$

It is now possible to compare $\{\eta\}_{66-2/3\%}$ with the elongational viscosities of the suspensions used in tests 9, 11, 13, and 16.

The "representative" elongational viscosities of the suspensions used in the reliable tests of this study were calculated as outlined above and appear in Table (D-2). Table (D-2) also lists the theoretically predicted (39,40) elongational viscosities, η'_0 and η'_∞ .

THEORETICAL ELONGATIONAL VISCOSITY

Rudd (34) defines a rotational diffusion constant, D , which is given by

$$D = \frac{3\kappa T[\ln(\frac{2l}{d}) - \frac{1}{2}]}{\pi \mu_0 l^3} \quad (D-1)$$

where κ is the Boltzman constant, T the absolute temperature, μ_0

the shear viscosity of the suspending medium, and l and d are the length and diameter, respectively, of the particle. For the fibres used in this study, D has a value of 10^{-12} sec. $^{-1}$ Since

$$\alpha = \dot{\epsilon}/D \quad (D-2)$$

the limiting case of $\alpha = \infty$ is expected to apply for the suspensions used in this study.

Equation (13) of Takserman-Krozer and Ziabicki (40) define v for the limiting cases of $\alpha = 0$ and $\alpha = \infty$ for a suspension of rigid rods, i.e.

$$\begin{aligned} v_0 &= \frac{1}{5}(2K + 7M + 12N) \\ v_\infty &= (2K + M) \end{aligned} \quad (D-3)$$

where

$$\begin{aligned} K &= \frac{\bar{\alpha}_0''}{\bar{\alpha}_0' \bar{\beta}_0''} \\ M &= \frac{1}{\bar{\alpha}_0'} \\ N &= \frac{1}{\bar{\beta}_0' [(AR)^2 + 1]} \end{aligned} \quad (D-4)$$

For rods,

$$\bar{\alpha}_0' = \frac{1}{4} \sigma [2(AR)^2 - 5 + \frac{3}{2}\lambda]$$

$$\begin{aligned}
\bar{\alpha}_0'' &= \sigma \left[\frac{1}{2} (AR)^2 + \frac{1}{4} + \frac{4(AR)^2 - 1}{8} \lambda \right] \\
\bar{\beta}_0' &= \sigma \left[\frac{2}{(AR)^2} + 1 - \frac{3}{2} \lambda \right] \\
\bar{\beta}_0'' &= \sigma \left[-3 + \frac{2(AR)^2 + 1}{2} \lambda \right]
\end{aligned} \tag{D-5}$$

where

$$\begin{aligned}
\lambda &= \frac{1}{AR\sqrt{(AR)^2 - 1}} \ln \frac{AR + \sqrt{(AR)^2 - 1}}{AR - \sqrt{(AR)^2 - 1}} \\
\sigma &= \frac{(AR)^2}{[(AR)^2 - 1]^2}
\end{aligned} \tag{D-6}$$

The intrinsic viscosities, v_0 and v_∞ , were calculated, as outlined above, for the fibres used in this study and the "limiting" elongational viscosities, η_0' and η_∞' were determined from Equation (1.2.9), namely:

$$v = \left(\frac{\eta_{sp}}{C} \right)_{C \rightarrow 0} \tag{D-7}$$

and Equation (1.2.6)

$$\eta_{sp} = \frac{\eta^i - \eta_0}{\eta_0} \tag{D-8}$$

The limiting elongational viscosities η_0' and η_∞' , for the suspensions used in tests 9, 10, 11, 13, 14 and 16 are presented in Table (D-2).

TABLE D-1
LEAST-SQUARES COEFFICIENTS OF
RELIABLE THRUST-VELOCITY DATA

<u>Test</u>	<u>[k₁']</u>	<u>[k₂']</u>	<u>[k_{2R}']</u>
3	0.00163	0.100	0.221
9	0.00168	0.189	0.361
10	0.00160	0.162	0.418
11	0.00161	0.191	0.433
13	0.00156	0.221	0.515
14	0.00163	0.130	0.363
16	0.00162	0.164	0.402

TABLE D-2
"REPRESENTATIVE" AND THEORETICAL
ELONGATIONAL VISCOSITIES

<u>Test</u>	<u>AR</u>	<u>Fibre Conc. (wt. %)</u>	<u>{η}</u> <u>(poise)</u>	<u>η'_0</u> <u>(poise)</u>	<u>η'_∞</u> <u>(poise)</u>
3	85	0.10	6.92	6.95	14.7
9	170	0.10	8.35	11.40	36.6
10	170	0.20	9.65	16.1	78.4
11	255	0.10	10.00	18.2	70.0
13	340	0.10	11.90	26.9	137.0
14	85	0.20	8.37	9.08	23.9
16	170	0.10	9.27	11.4	36.6

B30013